EXPERIMENTAL INVESTIGATION OF PRESSURE DISTRIBUTION OVER SURFACE AIRFOIL NACA 0012 TYPE

A THESIS
SUBMITTED TO THE DEPARTMENT OF MECHANICAL ENGINEERING TECHNIQUES OF POWER
IN PARTIAL FULFILLMENT OF THE REQUIREMENTS FOR THE TECHNICAL MASTER DEGREE IN THERMO MECHANICS ENGINEERING

BY

YOUSIF FAYEZ YOUSIF

Supervised by

ASST. PROF.DR. ZAID AL-DULAIMI

ASST. PROF.DR. MOHAMED AL-FAHHAM

October / 2021

سورة الضحى

بِسْمِ ٱللَّهِ ٱلرَّحْمَٰنِ ٱلرَّحِيمِ

وَٱلضُّحَىٰ ﴿١﴾ وَٱلَّيْلِ إِذَا سَجَىٰ ﴿٢﴾ مَا وَدَّعَكَ رَبُّكَ وَمَا قَلَىٰ ﴿٣﴾ وَلَلْآخِرَةُ
خَيْرٌ لَّكَ مِنَ ٱلْأُولَىٰ ﴿٤﴾ وَلَسَوْفَ يُعْطِيكَ رَبُّكَ فَتَرْضَىٰٓ ﴿٥﴾ أَلَمْ
يَجِدْكَ يَتِيمًا فَـَٔاوَىٰ ﴿٦﴾ وَوَجَدَكَ ضَآلًّا فَهَدَىٰ ﴿٧﴾ وَوَجَدَكَ عَآئِلًا
فَأَغْنَىٰ ﴿٨﴾ فَأَمَّا ٱلْيَتِيمَ فَلَا تَقْهَرْ ﴿٩﴾ وَأَمَّا ٱلسَّآئِلَ فَلَا تَنْهَرْ ﴿١٠﴾ وَأَمَّا
بِنِعْمَةِ رَبِّكَ فَحَدِّثْ ﴿١١﴾

Supervisor Certification

We certify that this thesis titled **" Experimental Investigation of pressure distribution over surface airfoil NACA 0012 type "** which is being submitted by **Yousif Fayez Yousif** was prepared under our supervision at the Department of Mechanical Engineering Techniques of Power, Engineering Technical College-Najaf, AL-Furat Al-Awsat Technical University, as a partial fulfillment of the requirements for the degree of Master of Technical in Mechanical Engineering.

Signature:

Name: Asst.Prof. Dr. Zaid al-dulaimi

(Supervisor)

Date: / / 2021

Signature:

Name: Asst.Prof. Dr. Mohamed Al-fahham

(Co-Supervisor)

Date: / / 2021

In view of the available recommendation, I/we forward this thesis for debate by the examining committee.

Signature:

Name: Asst.Prof. Dr. Dhafer M. Hachim

(Head of Power Mechanics Tech. Eng. Dept.)

Date: / / 2021

Committee Report

We certify that we have read this thesis titled " **Experimental Investigation of pressure distribution over surface airfoil NACA 0012 type**" which is being submitted by **Yousif Fayez Yousif** and as Examining Committee, examined the student in its contents. In our opinion, the thesis is adequate for award of degree of Master of Technical in Mechanical Engineering.

Signature:
Name: Asst.Prof. Dr. Zaid al-dulaimi
(Supervisor)
Date: / / 2021

Signature:
Name: Asst.Prof. Dr. Mohamed Al-fahham
(Co-Supervisor)
Date: / / 2021

Signature:
Name: Dr. Balasem Abdulameer Jabbar
(Member)
Date: / / 2021

Signature:
Name: Asst.Prof. Dr. Ahmed Hashim Yousif
(Member)
Date: / / 2021

Signature:
Name: Prof. Dr. Riyadh Sabah Al-Turaihi
(Chairman)
Date: / / 2021

Approval of the Engineering Technical College- Najaf

Signature:
Name: Asst.Prof. Dr. Hassanain G. Hameed
Dean of Engineering Technical College- Najaf
Date: / / 2021

Linguistic Certification

This is to certify that this thesis entitled **" Experimental Investigation of pressure distribution over surface airfoil NACA 0012 type"** was reviewed linguistically. Its language was amended to meet the style of the English language.

Signature :

Name :

Date : / / 2021

Abstract

The boundary layer separation from the airfoil surface has a large and direct effect on the aerodynamic characteristics of the airfoil, so that, the control of this separation will improve these characteristics.

The present work has dealt with the effect of rough surfaces models on the performance of airfoil which has been investigated experimentally.

experimental investigation will be carried out for selected airfoil model (symmetrical with four-digit NACA0012) and the flow is presented for six models of rough surface (Mo.1 ,2 ,3 ,4 ,5 and 6) as (40, 60, 80, 100, 120 and 200 holes per inches) respectively. Models were investigated for Pressure, lift and drag coefficients curves with different angles of attack (0°, 2°, 4°, 6°, 8°, 10°, 12°, 14°, and 16°) and investigated for mean velocity profile at zero angle of attack.

Experimental tests are conducted in open-typed wind tunnel at the chord Reynolds number numbers (1.39×10^5, 1.67×10^5 and 1.86×10^5) and the results indicate that the rough surface models are the key parameters for controlling the airfoil characteristic. The rough surface technique is able to alter the flow properties and thus to improve the aerodynamic characteristics performance. The most effective rough surface model is (Mo.6), by comparison to smooth surface, the results show an increment in lift slope curve about (8-17%) and a decrement in drag about (12-18%) for NACA0012 over the angles of attack range from (0° to 16°).

Acknowledgements

Praise be to Allah for his guidance that has enabled me to achieve this work.

I wish to express my deep thanks and sincere gratitude to my supervisors Asst. Prof. Dr. Zaid al-dulaimi and Dr.mohamed al-fahham for their available guidance, constant encouragement and support during the preparation of this thesis.

I would like to express my gratitude and thanks to Dean of Engineering Technical College- Najaf Asst.Prof. Dr. Hassanain G. Hameed and *Head of Power Mechanics Asst.Prof. Dr. Dhafer M. Hachim for there assistance and for all the staff of Mechanical Engineering especially for the staff of fluid laboratory.*

Special thanks are also presented to my dear family for their love and support.

youssif Fayez Youssif

M.s.c. Student

Thermo Mechanics Engineering

2021

DISCLAIMER

I confirm that the work submitted in this thesis is my own work and has not been submitted to another organization or for any other degree.

Yousif Fayez Yousif

Signature:

Date

CONTENTS

LIST OF TABLES

Table No. | **Title of the Tables** | **Page No.**

LIST OF FIGURES

Nomenclature

Latin Symbols		
Symbol	**Description**	**Units**
b	Span Length	m
C_f	Skin Friction Coefficient	---
C_d	Drag Coefficient	---
C_L	Lift Coefficient	---
C_L / C_d	Lift to drag ratio	
C_p	Pressure Coefficient	---
c	Chord Length	m
d	Pitot Static Tube external diameter	m
g	Acceleration due to Gravity	m/s^2
h	Hight	m
k	Turbulent Kinetic Energy	m^2/s^2
l	Lower Surface of airfoil	---
L	Lift force	N
P_{atm}	Atmosphere Pressure	N/m^2
P_d	Dynamic Pressure	N/m^2
P_s	Static Pressure	N/m^2
P_t	Total Pressure	N/m^2
p	Pressure	N/m_2
R_D	Skin Friction Drag Reduction	---
Re	Reynolds Number	---
R	Gases general constant	J/kg.K
s	Area of Wing	m^2

T_a	Air Temperature	K°
u_∞	Freestream Velocity	m/s
u	Upper Surface	---
Greek Symbols		
Symbol	**Description**	**Units**
α	Angle of Attack	degree
δ	Boundary Layer Thickness	m
θ	Momentum Thickness of Boundary Layer	m
μ	Dynamic Viscosity	N. s/m^2
ν	Kinematic Viscosity	m^2/s
ρ	Fluid Density	Kg/m^3
τ	Wall Shear Stress	N/m^2
Δ	Difference in Quantity	---

CHAPTER ONE

INTRODUCTION

CHAPTER ONE

INTRODUCTION

1.1 Research background

The measurement of the pressure distribution across the chord of an aircraft wing in flight is often carried out during flight testing on new aircraft designs or any scale wind tunnel testing that has been carried out. The four main forces acting on an aircraft are lift, drag, thrust and weight. During steady-state flight, the weight force of an aircraft will be balanced by the lift generated, while for a powered aircraft the drag of the aircraft will be balanced by the thrust produced. The relationship between the forces is shown in Figure (1.1).

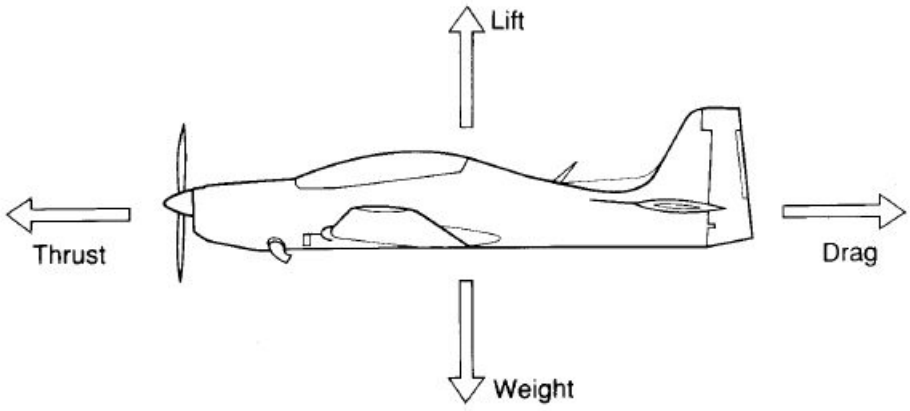

Figure (1.1) : Forces on an aircraft in flight [1]

The distribution of pressure over an airfoil creates a net resultant force that is typically broken up into components; lift and drag forces relative to the free stream direction or normal and axial forces relative to the airfoil.

The distribution of pressure is characterized by pressures much lower than atmospheric pressure over the upper leading edge of the wing. This is associated with the area of largest surface curvature and as the air is accelerated around the leading edge the static pressure is lowered. As the air travels towards the trailing edge over the upper surface the pressure recovers toward atmospheric pressure. The airflow over the lower surface is characterized by a stagnation point on the lower leading-edge surface, where the kinetic energy of the air is converted completely to static pressure. This point is the point of highest absolute pressure. The air pressure over the lower surface is typically higher than atmospheric pressure, with the pressure reducing towards the trailing edge. See Fig (1.2) where Red lines represent pressures lower than atmospheric while blue lines represent pressures higher than atmospheric [1]

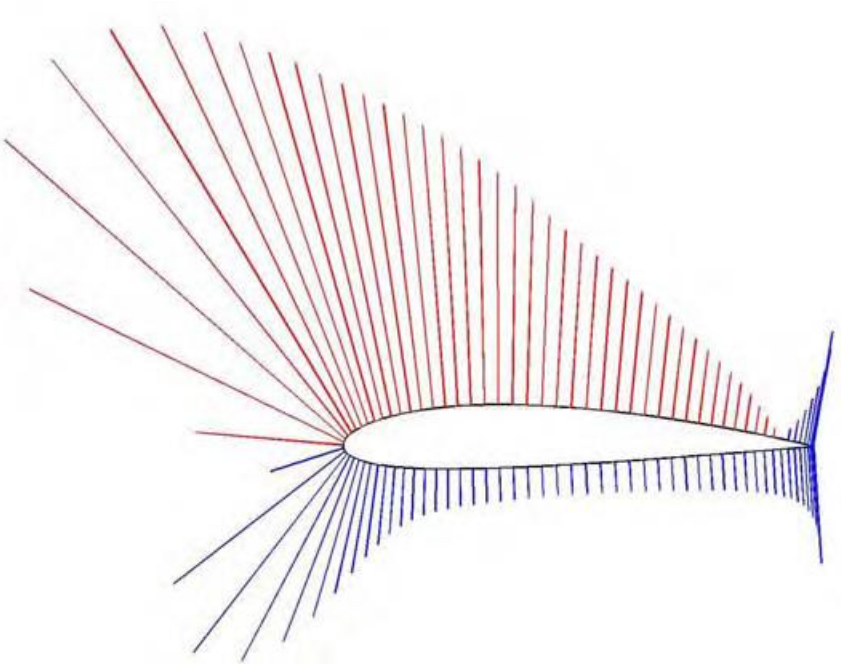

Figure (1.2): Typical distribution of pressure over an airfoil [1]

1.2 Develop pressure distribution on airfoil

Various methods have been developed for measuring the pressure over an airfoil in flight. The most common method involves wrapping small diameter tubes around the airfoil section. The tubes are used to pipe the air pressure from discrete points on the airfoil section to a pressure sensor. On another side, drag reduction is considered an important parameter to develop the pressure distribution on surfaces bodies exposed to a fluid flow. Fish swimming, for example, can be very instructive in exploring the mechanism of drag reduction because it has developed as a result of many millions of years of evolution. However, this is not the only form used by sharks to be fast. They have a slippery form that reduces pressure drag, and their specialized skin layer (dermal denticles) helps reduce skin friction drag, which is what inspired the riblets. There is limited accurate data on the velocities of pelagic sharks because of inherent difficulties dealing with predatory animals and because of problems simulating their environment [2]. According to [3], the swift hammerhead shark can fly at a maximum speed of 72 kilometers per hour (about 45 miles per hour). One of the ways in which fast-swimming sharks reach such incredible speeds is due to the scales they have. These scales have fine grooves running in a streamline pattern, designed to create a graceful motion figure (1.3).

Figure (1.3) photo: scales of great white shark [4].

The topic of riblets has addressed numerous international conferences, both from the perspective of basic fluid mechanics as well as various practical applications. Because of the reduction in drag on civil transport aircraft, the efficiency of civil aircraft is affected, but also of course, expense, and the atmosphere. Around 22% of the direct operating cost for a standard long-range transport aircraft is made up of fuel consumption, for large transport aircraft, even a 1% drag reduction will lead to a 0.2% cost decrease. It's found a 1% of drag reduction may results in involving an extra 10 passengers or an additional 1.6 tons on empty weight [5]. Drag reduction is a major task, but skin or viscous friction drag accounts for around 40-50% of the overall drag under cruise conditions. estimated fuel saving of 1 – 2 percent for the A320 experimental aircraft with riblet film added to the surface, fig (1.4). In addition, the German airplane manufacturer used riblet surface fuselage. This approach helps planes save 8% on fuel by contrasting covered plane techniques.

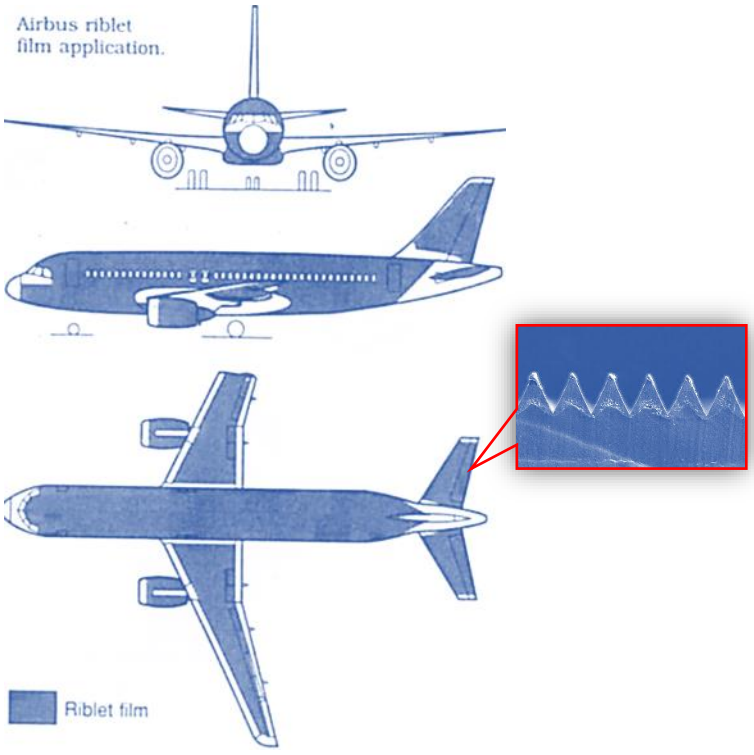

Figure (1.4) 1% -2% reduction in fuel if 70% of airplane covered with riblet film - French Airbus [5].

1.3 NACA Airfoil

The airfoil is the cross-section of the aircraft wing or the turbine blade or any engineering application that requires a high lift and low drag. Airfoils have the potential for use in the design of aircraft, propellers, rotor blades, wind turbines, and other applications of aeronautical engineering. Accordingly, the airfoil is designed with an appropriate geometry to achieve that purpose.

There are many types of airfoils based on geometry of cross section. The NACA airfoil used in this work is the NACA 0012 airfoil which is classified within a family of the symmetric four-digit series. The first digit specifies the maximum camber (m) in percentage of the chord (airfoil length), the second indicates the position of the maximum camber (p) in tenths of chord, and the last two numbers provide the maximum thickness (t) of the airfoil in percentage of chord.[6]

The various terms related to airfoils are defined below

- The suction surface (upper surface) is generally associated with higher velocity and lower static pressure.

- The pressure surface (lower surface) has a comparatively higher static pressure than the suction surface. The pressure gradient between these two surfaces contributes to the lift force generated for a given airfoil.[7]

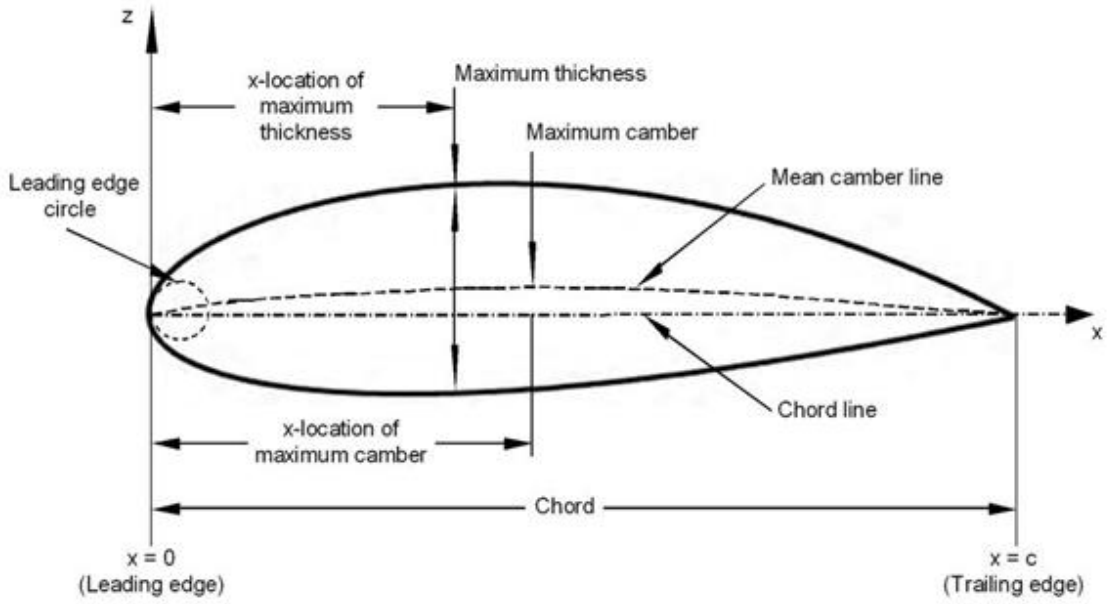

Figure (1.5) Airfoil-section geometry and it is nomenclature[7]

The geometry of the airfoil is described with a variety of terms :

- The leading edge is the point at the front of the airfoil that has maximum curvature (minimum radius).
- The trailing edge is defined similarly as the point of maximum curvature at the rear of the airfoil.
- The chord line is the straight line connecting leading and trailing edges.
- The mean camber line or mean line is the locus of points midway between the upper and lower surfaces

1.4 Background of boundary layer

The phenomenon of boundary layer is a layer near to a surface where viscous effects are prominent. When real fluid flows over a solid body or a solid plate, the fluid particles adhere to the boundary of the stationary surface and the phenomenon of no slip condition occurs. This results that the velocity of fluid near to the boundary will be same as that of boundary. If the boundary is stationary, the velocity of fluid at the boundary will be zero. Further away from the boundary, the velocity will be increase gradually and as a result of this variation of velocity, the velocity gradient will exist. The velocity of fluid increases from zero velocity on the stationary boundary to the free stream velocity of the fluid in the direction normal to the boundary. The boundary layer can be divided according to nature and structure of the flow into laminar (LBL) and turbulent (TBL) and there is a very short region between them which is known as the transition region from LBL to TBL, this is shown in the figure (1.6). In the laminar region, the fluid molecules flow at low velocities, in straight and parallel lines. For the flow around the airfoil, this region occurs close to the leading edge of airfoil and develops towards the downstream. In the turbulent region, strong vortices are developed, the layer thickness increases and the flow becomes a rough. For the flow around the airfoil at low angles of attack, the turbulent region occurs after the maximum thickness of the airfoil and develops towards the downstream. On the other hand, at high attack angles, the turbulent region approaches the leading edge of the airfoil.[8]

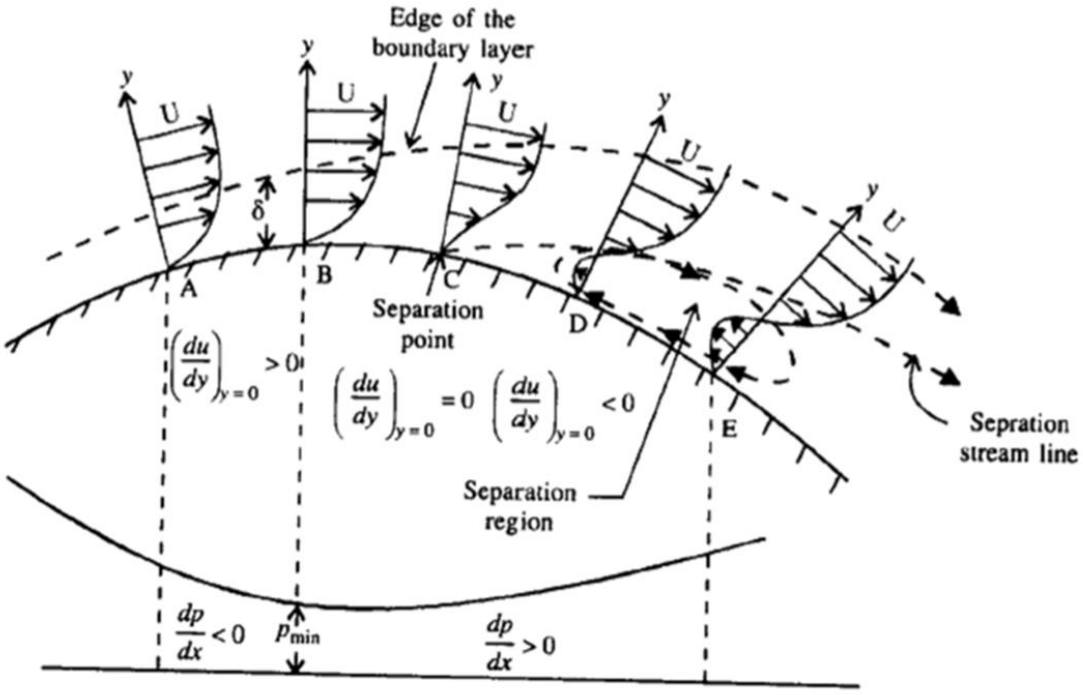

Figure (1.6) Boundary layer velocity profile [9]

In the aerodynamic applications such as the wings of aircrafts, due to the nature of the airfoil geometry, the flow starts as laminar then converts to turbulent, thus the layer thickness grows. This is shown in figure (1.6). When the attack angle increases, the boundary layer near the surface becomes sluggish and the local velocity in this location approaches to zero. Accordingly, adverse pressure gradients are generated on the airfoil surface which forcing the air to flow in the opposite direction therefore, its separation from the surface. As the attack angle increases, the flow separation point approaches the airfoil leading edge. Thus, the separation bubble size will increase as shown in figure (1.3). This will lead to the occurrence of the stall condition which means a reduction of the lift force and hence the airfoil efficiency. So that, the boundary layer separation from the body surface in these applications is considered undesirable.

1.5 Boundary layer Separation Control

Passive or active separation control can be defined as a form of control. Passive flow control is usually applied by changes to boundary conditions, such as adjusting the pressure gradient or free-stream turbulence level by introducing passive devices, such as spoilers, riblets, or large break-up devices (LEBO). However, it appears that the amount of improvement that can be made in passive flow control methods is small, but even for growing consumer demand on economically efficient aerodynamic devices, such as wings, blades, combustion chambers, and transportation vehicles. Active flow management provides the best prospect of meeting improved aerodynamic performance demands. tables (1.1) and (1.2) compare between the benefits and drawbacks of passive and active method of Separation. [10]

Table 1.1 Benefits and drawbacks of Passive Flow Control methods.[9]

Advantages	Disavantages
Easy to implement	*Re* dependent
No external energy source	Off-design sensitivity
No mechanical or electro-mechanical parts	Often associated drag penalty

Table 1.2: Benefits and drawbacks of Active Flow Control methods.[9]

Advantages	Disavantages
Adjustable	Technically more complex
Adaptability to variable flow conditions	External energy source necessary
Separation management for off-design performance	
Closed-loop feedback possible	

The functional significance of the issue of laminar to transition and transition to turbulent flow in boundary layers is important. In order to comprehend these physical problems, Transitional experiments need to be coupled with the principle of control and reduction. For example, the high skin friction drag associated with laminar boundary layer flow is attractive to those who want to build high performance vehicles and airplanes. However, in some situations, such as with combustion, mixing and heat transfer is useful for the turbulent boundary layer. Reattachment and separation of laminar and turbulent flows occur in many real-world engineering applications, particularly in external flows including around airfoils and buildings. Internal flow systems such as diffusers, combustors, and channels with sudden expansions.

We can use the Boundary Layer prototype model to build our design. In the working section of the wind tunnel, we put a model. The aspect ratio of a model should be equal to the original, to ensure accuracy. In the low-speed wind tunnel, there is some speed limitation. Classification of the wind tunnel is very important for the observation point of view [10].

1.6 Problem Statement

Whenever there is relative movement between a fluid and a solid surface, whether externally round a body, or internally in an enclosed passage, a boundary layer exists with viscous forces present in the layer of fluid close to the surface. Boundary layers can be either laminar or turbulent. A reasonable assessment of whether the boundary layer will be laminar or turbulent can be made by calculating the Reynolds number of the local flow conditions.

Flow separation or boundary layer separation is the detachment of a boundary layer from a surface into a wake. When the boundary layer separates, its remnants form a shear layer and the presence of a separated flow region between the shear layer and surface modifies the outside potential flow and pressure field. In the case of airfoils, the pressure field modification results in an increase in pressure drag, and if severe enough will also result in stall and loss of lift, all of which are undesirable. For internal flows, flow separation produces an increase in the flow losses, and stall-type phenomena such as compressor surge, both undesirable phenomena.

Another effect of boundary layer separation is regular shedding vortices. Vortex shedding produces an alternating force which can lead to vibrations in the structure. If the shedding frequency coincides with a resonance frequency of the structure, it can cause structural failure

1.7 Objectives of study

The main aim of this research is to improve the NACA 0012 airfoil aerodynamic characteristics (increasing the lift, reducing the drag, and improving the airfoil performance) by using the technique of the cover the airfoil surface with woven wire.

Therefore, this study embarks on the following objectives while achieving the aim of this research:

1. To experimentally investigate the turbulent flow, lift, and drag properties of symmetrical airfoil surface NACA 0012 with six models of rough surfaces in an open circuit low-speed wind tunnel.
2. Studying the effect of the grid dimensions of rough surface models on the characteristic of airfoil NACA 0012.
3. To compare the results over the rough surfaces with the baseline test results conducted with the smooth surface under the same conditions.

4. he rough surface introduced on the wall of the airfoil. It has been shown that a small change in the dimensions of these surfaces can alter the response of the system for the lift and drag.

1.8 Scope of the Present Work

The present work is characterized by the following:

1. The airfoil NACA 0012 was adopted with span and chord of 300 mm, 150 mm respectively.
2. A new kind of rough surface (woven wire) with six models of rough based on grid size.

3. The experimental work was carried out in lab field at low speed wind tunnel in order to obtain flow behavior and aerodynamic characteristic
4. The working fluid is air at turbulent, incompressible, viscous, steady flow for two dimensional.
5. Inlet operation parameters at a different range of Reynolds numbers, 1.39×10^5, 1.67×10^5 and 1.86×10^5
6. The performance of pressure distribution on airfoil surface was evaluate in terms of lift coefficient, drag coefficient, and pressure coefficient

1.9 Thesis outline

The thesis will be structured as follows:

- Chapter 1: The first chapter has outlined the background to the research project. The origin and objectives of the thesis have also been outlined.
- Chapter 2: The second chapter will present a review of literature relevant to the problem of measuring the pressure distribution on an airfoil section
- Chapter 3: The third chapter will outline the development of the pressure distribution measurement system. The details of the system will be described. also describe the testing that was carried out.
- Chapter 4: The fourth chapter describes the testing that was carried out and the experimental results that were gathered.
- Chapter 5: This chapter will present conclusions from the project and recommendations for future research work.

CHAPTER TWO

LITERATURE REVIEW

CHAPTER TWO

LITERATURE REVIEW

The boundary layer has to be analyzed before we can think about velocity profiles. So many papers have been published on boundary layer growth that it is hard to keep track of them all. The analysis of the boundary layer is just about making something. The definition of relative velocity is very important in this relative world, as the study of relative motion helps with the stabilization of moving and stationary parts. When it comes to high-velocity vehicles or aircraft, it is important to understand the boundary layer. Some research papers about different objects are contained in the working section of the wind tunnel, and in this chapter, we define the following parameters: inclination, roughness, velocity, and pressure gradient.

2.1 Definition of Airfoil

Airfoil is known as a sold body with a wing cross-section view which is designed with a curve in the surface. when an airfoil moving in fluid produces a force called aerodynamic force, one component is the lift which is perpendicular to the line of motion, and drag which is parallel to the line of motion. There are two types of airfoil, symmetrical airfoil wish has the same upper and lower surfaces and the cord with the camber lines are the same, the second type is non-symmetrical airfoil which has different upper and lower surfaces, this type has different cord and chamber lines.

2.2 Type of Aerodynamic surfaces

There are many types of Many Aerodynamic surfaces that include flat plate and airfoil surfaces, studies concerning the experimental analysis for those surfaces in this chapter.

2.2.1 Flat plate surfaces

An experimental investigation is conducted by **Vivek Gupta [11]** This research was performed in a low-speed wind tunnel in the laboratory. studying the boundary layer's impact on flat plates with 50cm width and 100cm length with varying surface roughness. In this analysis, four different surface roughness grades (40, 50, 60, and 120) are employed. For grains in the 40, 50, 60, and 120 Grades, the numerical value is 375 micrometers, 345 micrometers, 290 micrometers, and 125 micrometers respectively. Velocity measurement is obtained on rough flat plate (different grade emery papers stacked on wood surface) at defined locations. In the experiment, the flat plate is being tilted to create negative pressure. The boundary layer developed to clarify how fluid moves over a flat surface. The result shows that raising the incline from horizontal would increase the boundary layer thickness. Also, the impact of roughness on the boundary layer will contribute to an increase in the boundary layer thickness.

Experimental investigation for the characteristics of a turbulent flow field over a riblet surface plate models and compared with a smooth surface is done by **Noor H. Al-Fatlawie [12]**. Several experiments were conducted in a low-speed open-type wind tunnel. With a steady air flow of 20 m/s and a Reynolds number of 4.9×10^5 based on the length of the flat plate.

Two models, sinusoidal and straight riblets with two different values of a/λ ratio are studied to learn about drag reduction in turbulent flow over a riblet-covered surface, as seen in figures (2.1) and (2.2).

The cross-section of all riblets are rectangular cross-section with the same wetted area. The parameters selected 12 kinds for the sinusoidal model and 12 kinds for the straight model, in order to investigate the details of drag reduction for the shape and dimensions of riblet. Different nature of the flow over sinusoidal and straight riblet surfaces as well as on the smooth flat plate is noticed by looking at mean velocity, shear stress and turbulent skin friction coefficient in the near-wall flow field. The research showed that the form, width, and height of the riblet, as well as the lateral spacing, are key factors in reducing drag. There has been a 10–14% skin friction drag reduction obtained with straight rivets, and the best dimensions are (s=1mm, h=0.25mm, and w=1mm). Riblets displaying sinusoidal effects minimize the drag coefficient by 19%. Dimensions that produce the greatest drag reduction for this Riblet model are (h=0.125mm, and w=2mm, and s=2mm). It has been indicated that surface geometry variations which change the near-wall structure of the flow have been effective in drag reduction.

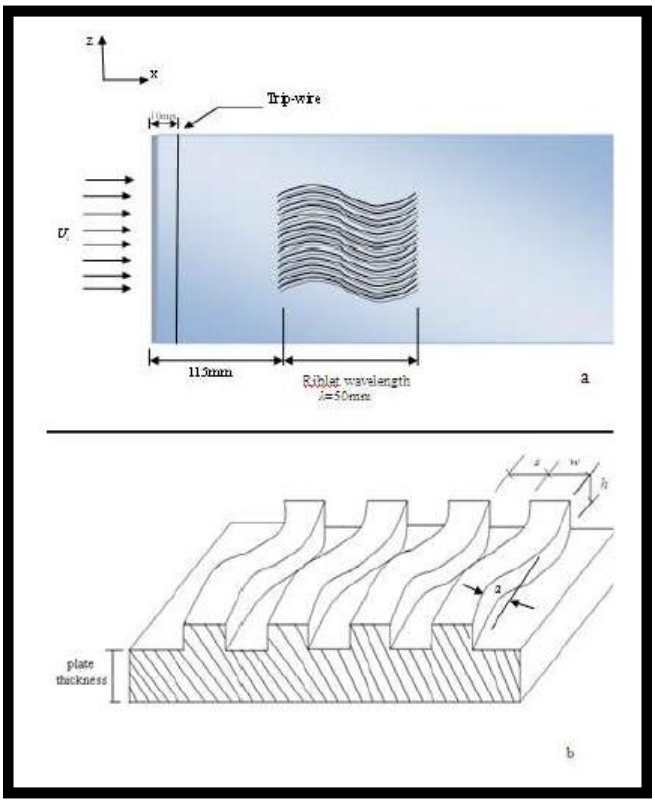

Figure (2.1)
a- test plate diagram
b- sinusoidal riblet Cross-section [12]

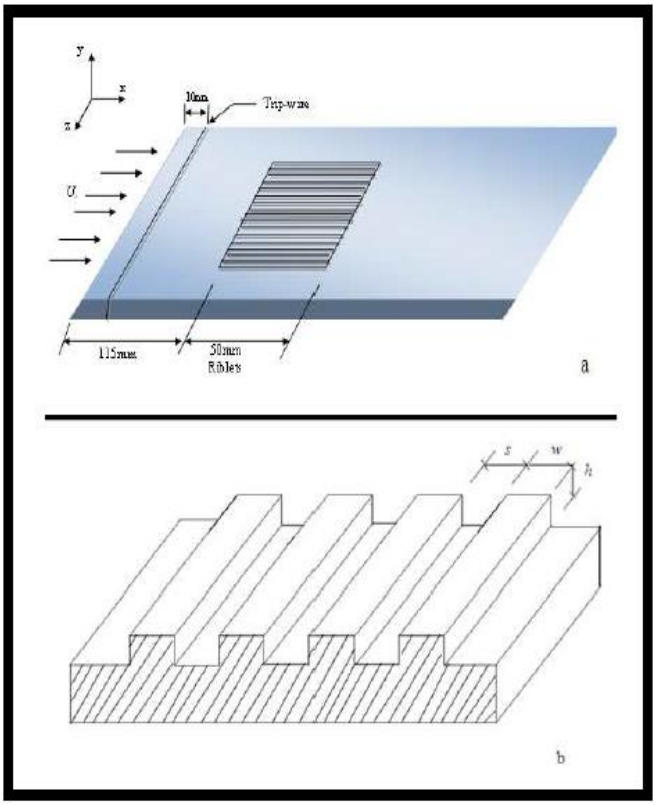

Figure (2.2)
a- test plate diagram
b- straight riblet Cross-section [12]

Rzuqe [13] conducted an analysis to discover how riblets affect drag reduction. The riblet was made up of an adhesive tape of varying thickness (h = 6.5, 13, and 19.5), width (w = 93, and 186), and spacing (s = 93, and 186). 13 different surfaces are tested (including the smooth one). To obtain the velocity distribution on each surface, and to measure the momentum thickness, a free-stream velocity of 35 m/s was used. The data show that manipulated surfaces such as riblets (h=6.5, w=93, s=186) minimize drag by 10%, but the other surfaces normally increase drag.

An experiments study on riblets were performed by **Walsh [14]**. The rectangular, V-groove, and semicircular groove riblets shown in Figure (2.3) are all being tested to find out which form aligns with the flow the best, the drag reduction occurred when the geometric condition of $s^+ < 30$ and $h^+ < 25$, $s^+ = s\ u\ \tau/\nu$ and $h^+ = h\ u\ \tau/\nu$, for a symmetric V – groove riblet was found. Also, the drag reduction was 8% for the symmetric V-groove riblet with $h^+ (= s^+) = 12$, and for the riblet with broad valley curvature and sharp peaks, which has $h^+ = 8$ and $s^+ = 16$.

Additional experimental evidence supports the finding that reduced drag occurs in adverse pressure gradients at slower speeds are shown by **Debisschop [15]** for a flat plate boundary layer of applied adverse pressure gradients. Both V-groove (h=s) and trapezoidal groove (h=0.5s) riblets used a specially-designed skin friction drag balance for their experiments. The reduced skin friction drag achieved in the range of 12-13% was calculated. Also, in adverse pressure gradients, riblets become more effective. The increased effectiveness appears to be common, and is not restricted to V-grooves with h=s.

Parker[16] applied the V-rivet-produced surfaces having unique dimensions (h/s=0.22 and 1) to a smooth plate, machining in a longitudinal direction, in order to lower the viscous drag on a body. After the riblet was applied, the resulting effect on skin friction drag force was measured and tests have shown that the plate could minimize turbulent skin friction drag by up to 7 percent, depending on the size of the riblet. According to the boundary layer study of the turbulent flow characteristics on a smooth surface and the riblet surfaces, the laminar sublayer increased in thickness on the riblet surfaces. At a Reynolds number of (1.17×10^5), a 6.83% drag reduction was observed for the surface covered with the symmetric riblet (h/s=1).

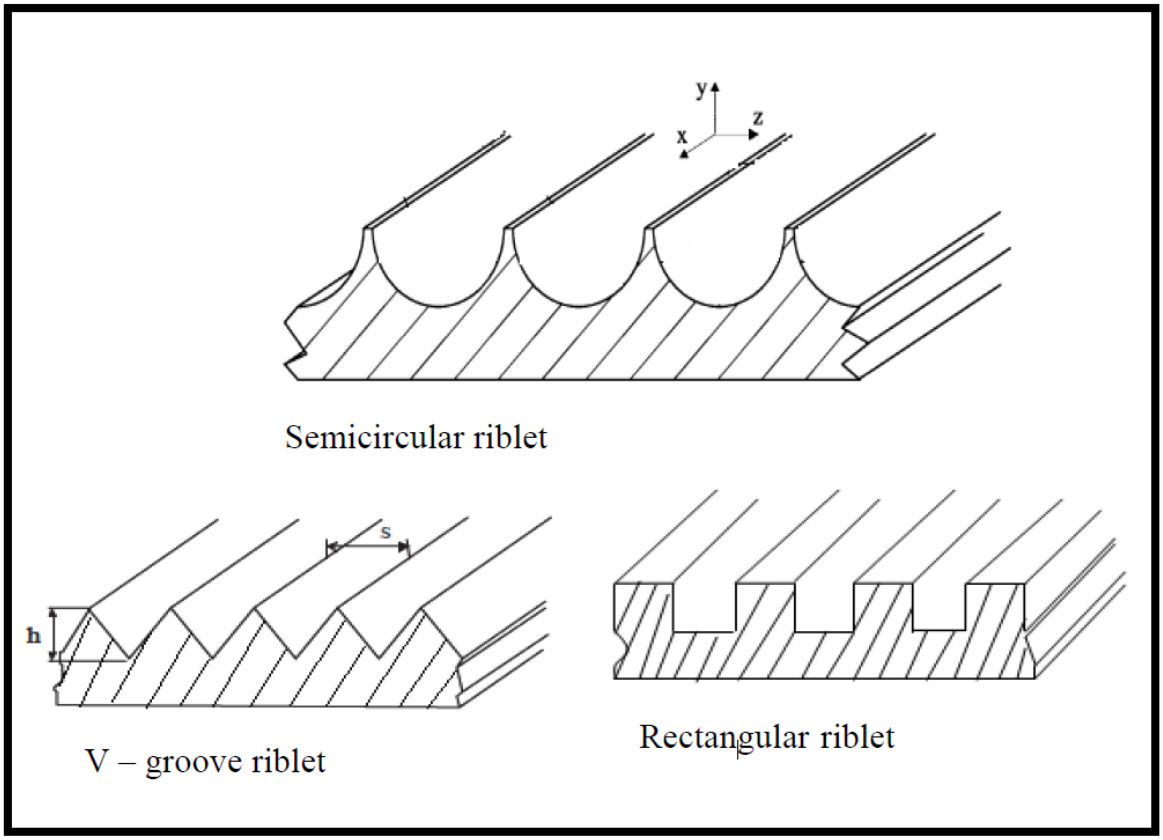

Figure (2.3) Some Riblet Configurations [14]

2.2.2 Airfoils surfaces

Yan Zhang [17] Investigated the effect of distributed-leading-edge roughness on performance of low-Reynolds-number airfoils. This was achieved using a closed-circuit low-speed wind tunnel. The tunnel test section was 1.0 ft by 1.0 ft (30 cm by 30 cm) cross-section. Leading-edge roughness was simulated by using thin plastic strips with roughness components. The hemi-spherical shapes were

developed to be the rough models. Four different roughness patterns (two distribution patterns and two roughness heights) were designed to explore different variables that could potentially influence the results. A substantial reduction in lift coefficients is observed for all cases of roughness. Large roughness caused the aerodynamic stall to be substantially advanced, while small roughness appears to delay the stall angle.

An experimental study is carried out by **Michael F.Kerho [18]** to establish how boundary layer formation and transition are influenced by the presence of a large distributed roughness, experimentally by placing a large distributed roughness close to the leading edge of an airfoil. This study included the use of the NACA 0012 airfoil model, which is a two-dimensional model that was placed vertically in the tunnel, At Re numbers of $0.75 * 10^6$, $1.25 * 10^6$, and $2.25 * 10^6$, the airfoil had a span of 0.8573 m, with a chord of 0.5334 m. Distributed roughness was developed by molding hemispherical forms in staggered rows into plastic strips of 0.5 inches wide by 4 inches long. A controlled experiment has found that the transitional boundary layer formed by high dispersed roughness varies significantly from the smooth model. There were no completely formed turbulent boundary layers found near the roughness region. In comparison, it was found that a transitional boundary layer was formed when the roughness was found to be spread over a wide area. The strength levels of streamwise turbulence in the transitional zone, caused by roughness, were found to be significantly lower than in the smooth region.

An experimental investigation is conducted by **Diane R. Bloch [19]** To find out the impact of distributed roughness on the boundary layer, aerodynamic characteristics, and efficiency of the Wortmann FX 63-137 airfoil, tests were

performed to discover this knowledge. Consideration needs to be provided to the extra roughness added to the airfoil's leading edge, as well as the suction peak. Reynolds numbers of 80,000, 100,000, and 200,000 are considered along the chord. Measurements involving force balance, pressure distribution, and flow visualization were used. When the distributed roughness was applied, the separation bubble moved forward. The direction of the suction peak roughness had a substantially greater effect on the stability and performance of the aircraft. the lack of difference in roughness height did not have a significant effect. The application of roughness became more and more harmful as Reynolds number increased. It was found that the distributed roughness height prediction method to correct the transition position was ineffective.

Walid Chakroun [20] investigated the effects of surface roughness on the aerodynamic characteristics of the airfoil by varying the roughness position and size. NACA 0012 were carried out on the Samples, where the Reynolds number was set at $1.5*10^5$ based on chord, with symmetrical airfoils. They ran different roughness size and roughness position in experiments with various attack angles. Velocity and pressure profiles were measured, as well as drag coefficients and lift, for the grid 36 (500 μm) roughened and smooth versions.As Roughness on the surface increases, which results in a reduction in lift and an improvement in minimum drag due to an increase in skin friction. Roughness on the surface can be seen to cause a decrease in the stall angle, as well as adding lift in the stall area. Compared to other cases of roughness, the airfoil model has a minimum drag and maximum lift up to the stall angle, whereas the roughness is situated at the trailing edge.

Adel Ahmed [21] experimentally investigated the effect of surface roughness on a NACA 0012 airfoil. The experiments include measurements for the drag coefficients, lift coefficients and pressure distribution. Two different rough surfaces (P80 and P120) (80 μm and 120 μm) are analyzed, and their data are compared to the smooth surface. The angles of attack range of-15° to 30° with 3° steps with two Reynolds numbers 3.4×10^5 and 1.7×10^5. It is found that the roughness has a large effect on the flow over the airfoil. With increasing roughness size on the surface, the minimum value for the drag coefficient increases. The lift over angles of attack from 0° up to around 10° decrease. In the stall region (beyond $\alpha = 10°$), the lift of the rough surface is seen to increase corresponding to value for the smooth surface, with a higher increase for the larger roughness size. The separation mechanism is also affected by the presence of surface roughness, where roughness is found to delay the separation.

An experimental investigation is carried out by **Mahbubur Rahman [22]** To detect the effect of integrating the vortex generator (VG) on a NACA0012 airfoil at zero to twenty-degree angle of attack with flow separation control. A rise in lift coefficient and a decrease in drag coefficient occur as the vortex generator is introduced at large incident angles (VG). This paper found that the fluid flow and aerodynamic forces that act on the airfoil are affected by VG. This experimental investigation is using vortex generator methods to investigate modern passive flow control. This group of methods is generally used to accomplish lift enhancement, drag reduction, flow separation control. Using a wind tunnel with a 1m×1m test section, a test speed of 25m/s, and an inclination of 0-20 degrees, an experiment was performed in which an airfoil was tested both with and without a vortex generator.

The test results of this study indicated a significant increase in lift coefficient and a significant decrease in drag coefficient. In order to obtain these results, vortex

generators were used by Comparison of lift coefficient, drag coefficient, and pressure coefficient of airfoil between one that has a vortex generator and one that does not.

Nibras Mohammed [23] investigated numerically and experimentally the effect of longitudinal riblet surface models on the performance of straight and swept wings. Numerical investigation involves solving the covering equations (Continuity and Navier-Stokes equations) for examining drag reduction by using the known package FLUENT version (6.1). Two selected airfoil models (symmetrical with four-digit NACA0012 and unsymmetrical with five-digit NACA23015) will be carried out for numerical solution .the solution of the flow equations is presented for seven models of riblet three models (Mo.1, 2 and 3) as U, V and semi-Circular riblets and four models (Mo.4, 5, 6 and 7) as U-riblet with fillet with taking into account the effect of riblet height (h=0.1, 0.15, 0.2 and 0.25mm). Models were investigated at chord Reynolds number (3.56×105) with different angles of attack (0°, 5°, 10°, 12°, 15° and 17°). Pressure coefficient, kinetic energy, streamlines, velocity vectors, shear stress, lift and drag coefficient are presented as a result.

Open-typed wind tunnel is separately conducted the experimental tests and flow visualization at the chord Reynolds number (3.56×105) and smoke tunnel at chord Reynolds number of (1×104). The results indicate that the key parameters for controlling the boundary layer characteristic is the riblet surface models. The riblet surface technique is able to alter the flow properties and thus to improve the aerodynamic characteristics performance. The most effective riblet surface is U-riblet with fillet model (Mo.4, h=0.1mm).

by compare to smooth models, the results show a small increment in lift slope curve about (3-7%) and a decrement in total drag about (5-9%) for NACA0012 and lift increase (3-8%) and total drag decrease (6-11%) for

NACA23015 over the angles of attack range from (0° to 17°). For the swept wing, the U riblet with fillet (Mo.4) has shown the greatest drag reduction in comparison with a smooth model for all measurements, max reduction was (6.7%) at (a=0°). Results also show that the computational and experimental works give fair agreements in improving the solutions and the analysis.

To test the lift force induced by the wake of a NACA 0012 Airfoil, an experimental analysis is done by **Md. Mahbub [24]** are tested the 0 to 90-degree angle of attack and the Reynolds number, 5.3 to 5.1×10^4, to study the near wake of the airfoil with low to ultra-low Reynolds number. The lift force is measured by a load cell, the laser-Doppler anemometry, is used to monitor detailed flow structure, particle image velocimetry, and laser-induced fluorescence flow visualization. The airfoil stall is observed at $Rec > 1.05 \times 10^4$ and is characterized by a decrease in lift energy, but it decayed at $Rec = 5.3 \times 10^3$.This result connected to the position where the bubbles are separated, which can be seen at the high values of Rec.

Zambri Harun [25] An experimentally-investigated flow features, including converging-diverging riblets, were applied to an airfoil in order to explore their effect. For use on the NACA 0026 airfoil, the Riblet sheets are added to the surface. When the yaw angle is zero, ±10 the Riblet height and spacing of h are one millimeter, and the distance between the Riblet is two millimeters. Using a Reynolds number of 200, the riblets strip has an approximate chord percentage of 7.5%, when the differential pressure parameter, β, has a value of 0.5 to 0.8. If no riblets are presented, a pronounced wake will be shown in the velocity profile. The flow's logarithmic area is underlain by a very thin layer of vortices that have a large-scale size of approximately 20d (d is the boundary layer thickness). The

spectral analysis shows that all forms of riblets split these 20d features into smaller features between 3d and 4d away from the near wall.

An experiment was performed to investigate the impact of Reynolds numbers from 1×106 to 10×106 on clean and rough airfoils by **K. Kaiser [26]** The final concept was tested using a wind tunnel and by simulations using the Navier-Stokes solver. The overall dimensions of the two-dimensional wind tunnel physical model are 2400 mm in span and 500 mm in chord. Increasing the performance is illustrated by the rough surface configurations, which include the use of zig-zag tape for transition fixing and carborundum-based dispersed roughness around the nose. However, on the other hand, no severe reduction in the maximum lift occurs in a clean surface configuration. An rise in drag has caused the lift-to-drag ratio to drop from around 95 to about 85.

Coustols[27] Dragged findings on an LC100D airfoil with riblets were seen for low-speed applications. where only the upper (or suction) surface of the airfoil is covered with riblets. wake survey was used to make measurements of drag varying from 0° to 6°. At α=0° and 2°, overall drag reduction was approximately 2%, and no drag reduction was observed at high α; the corresponding viscous drag reduction was calculated to be approximately 7%. Riblets did not perform well at higher angles because boundary layer separation was postulated to be a major cause.

Raju [28] performed an experimental work in a low-speed wind tunnel on a (13.6% thick) GAW (2) airfoil model, with trailing edge thickness ratio of (0.5%) with V-riblet films applied between (0.1 and 0.96 c) on both the top and bottom surfaces. Three micro manometers were used to measure the free stream

dynamic pressure, model surface, and the base pressure. complete drag was measured using pitot and static measurements in the wake. The use of a hot wire anemometer to find vortex shedding behind the base proved the presence of the vortex. the data presented here shows that drag reduction is sustained to an airfoil incidence of (6°) and it is only within these results (7 percent).

Viswanath [29] conducted an in-depth study of the various applications for ribs on airfoil, wings, and wing-body or aircraft configurations at different speed regimes, as well as effects including pressure gradients and three-dimensionality. Tests on wind tunnels and flight tests have provided convincing evidence to show that riblets from low-speed to moderate supersonic Mach numbers are effective. optimized riblets have demonstrated skin friction drag reduction in the range of 5-8% at low incidence and in moderate adverse pressure gradients. Good evidence is found at low speeds to suggest that riblets are more effective in adverse pressure gradients. As long as the local angle between surface streamlines and riblet orientation is small (approximately 10°), riblet remain effective providing drag reduction comparable to two dimensional airfoils. Restricted data available on wing-body configurations indicates that a drag reduction of 2-3% is possible.

Riblets on a swept wing can be influenced by two variables: the flow's pressure gradient and the amount of yaw angles that occurs between the flow's surface streams and direction of grooves. **Mclean et al. [30]** The records indicated that skin friction drag reduction can be obtained on a T-33 jet trainer with riblet film glued on the upper layer over one wing, with a swept angle of about 9°. This means that the testes were produced in the flight Mach number range of 0.35 to 0.70. Seven percent to 83 percent of the local wing chord is filled by Riblets with groove height of 0.033 and 0.076mm. Results from the tests showed that, when

under zero pressure gradient conditions, riblets with h=0.033 and 0.076mm resulted in skin friction drag reduction of approximately 6 – 7 percent. **McLean et al** performed a flight evaluation of two significant facets: gradients of pressure that can impact effectiveness and yaw angle on riblets. On the T–33, a smooth plastic film was mounted instead of the conventional riblets of x/c=0.5, which was roughly where the adverse pressure gradients started. Measurement has shown a slightly lower friction drag reduction (about 2% to 3%) relative to what was found when riblets extended all the way up to x/c=0.83, providing evidence that riblets are very effective in adverse pressure gradients. In a different flight, the riblets were oriented at 15° to the flight direction, and the results showed a lower drag reduction (about 3%) which indicates that the riblet effectiveness degrades relatively strongly when the yaw angle is different under flight conditions.

The effectiveness of riblets of different sizes on an airfoil was tested experimentally by **Squire & Savil [31]** at subsonic and transonic Mach numbers. In a wind tunnel at Reynolds and Mach numbers of 0.50 and 0.88, the experiments were performed. riblets decreased the overall skin friction drag by 5% for zero pressure gradient flows at both Mach numbers. the corresponding mean h+ range was 10-15. They discovered that for transonic Mach numbers, riblets perform almost as well as at lower speeds when no adverse pressure gradient conditions occur. In addition, it's likely that the drag can still be minimized by increasing the number of grooves, while also decreasing their size.

In 2017, **Luo et al [32],** controlled the boundary layer separation on the NACA 0012 airfoil numerically using a micro-cylinder close to the leading edge. At Reynold number equals 600,000 and high attack angles (16˚ to 23˚). It was

found that the micro-cylinder can delay the flow separation hence, it can improve the airfoil efficiency.

The aerodynamic characteristics of NACA 0012 airfoil with and without dimple were simulated numerically by **Amit K. Saraf et al** [33] in 2017. The study was carried out using an inward single dimple at different positions (75%, 50%, 25% and 10%) of the chord from the leading edge. This was at a constant air speed of 7.3 m/s and a variable attack angle. It was concluded that the dimple at the position of 75%c increases the lift by 7% and reduces the drag by 3% as compared with the smooth airfoil.

In an experimental study, vortex-generators were used to improve the aerodynamic performance of the NACA 63_2217 and NACA 23012 airfoils in 2015 by **Simão Ferreira et al** [34]. The results indicated that using this technique in case of the NACA 23012, the maximum lift coefficient increases approximately by 14% comparing with the smooth airfoil. In addition, the drag coefficient remains approximately constant for 2° attack angle. Whereas, in the case of the NACA 63_2217, the increase in the maximum lift is 9% and the drag does not increase for about 3° attack angle.

In 2016, **Gildersleeve et al** [35] studied experimentally an effect of cylindrical pins on the NACA 0012 flapped airfoil aerodynamic behaver at different Reynolds numbers. For delaying the flow separation on the upper surface and enhancing the airfoil performance. The results showed that the cylindrical pins technique can reduce the separation region and increase the lift coefficient, therefore it can improve the airfoil performance.

Domel et al [36], in 2017, examined experimentally the NACA 0012 airfoil performance without and with shark skin-inspired denticles at Reynolds number of 40,000, a variable attack angle from 0˚ to 24˚ and airfoil chord length of 68

mm. The results demonstrated that using this technique reduces the drag, increases the lift and largely improves the aerodynamic performance of the airfoil.

The aerodynamic efficiency of NACA 0012 airfoil without and with dimples was studied experimentally in 2017 by **Rasal et al [37].** The study was carried out by adding dimples on the airfoil surface at 30%c from the trailing edge at conditions of 6 and 10 m/s air velocity, 30 cm chord length, 0 to 23-degrees range of the attack angles and 1%c, 2%c and 3%c size of the dimpled surface. It was found that the airfoil aerodynamic efficiency is improved by using the dimples specially with the 3%c size.

Leknys et al [38] in 2018 investigated experimentally an effect of tripwires on the NACA 0012 airfoil performance. The investigation was carried out by using the tripwires at the airfoil leading edge with different diameters (2, 1.6, 1.2, and 0.95) mm at 20,000 Reynold number and different attack angles. The results showed that the tripwires technique improves the airfoil efficiency for a wide range of attack angles, but it becomes ineffective after the stall angle.

2.3 Summary

In this chapter, it is noticed that there are many experimental works into the analysis of pressure distribution and drag reduction by longitudinal riblets over different surfaces (flat plate, airfoil, wing and flying body) as well as the effectiveness of longitudinal riblets of varying shapes including triangular, rectangular and semi-circular at different speed regimes were studied experimentally.

In this study experiments were carried out using stainless steel wire mesh as six different rough surfaces (Mo.1, Mo.2, Mo.3, Mo.4, Mo.5 and Mo.6) and a smooth surface of airfoil for comparison. The tests have been achieved for two dimensional, steady, turbulent, incompressible, viscous flow. All cases were used for the pressure measurement in the low-speed wind tunnel at Reynolds numbers (1.39×10^5, 1.67×10^5 and 1.86×10^5) based on the mean velocity and airfoil chord length. Rough surfaces were applied on 50% of the airfoil area, and pitot tube was utilized to measure the dynamic pressure in the working suction of wind tunnel. The experimental results included pressure, mean velocity profile, lift, drag coefficients curves for the airfoil.

Comparisons between the results of the present experimental work for the rough surfaces models (Mo.1, Mo.2, Mo.3, Mo.4, Mo.5 and Mo.6) and others researches are presented in this paragraph. It is found that the results for rough module (Mo.6) of computational work agree well with the results obtained by [23] Nibras Mohammed wish is investigated experimentally the effect of longitudinal riblet surface models on NACA 0012. For other surfaces module (Mo.1, Mo.2, Mo.3, Mo.4 and Mo.5) the results obtained agree with [13] W. Chakroun, and [20] A.A. Abdel-Rahman which is show that the smooth surface is more efficient than other modules (Mo.1, Mo.2, Mo.3, Mo.4 and Mo.5).

CHAPTER THREE

EXPERIMENTAL WORK

CHAPTER THREE

EXPERIMENTAL WORK

This chapter involves the experimental work of this study for investigating the aerodynamic performance of NACA 0012 airfoil with and without a rough surface experimentally. This would be carried out by adding that rough surface (woven wire) on the airfoil surface

The experiments were conducted in the Al-Furat Al-Awsat Technical University / Engineering Technical College- Najaf in the Fluid Mechanics laboratory. The tests were performed in an open circuit wind tunnel at low speed. The ultimate aim of the experimental research in the present work is to investigate the impact of roughness and flow characteristics over the test surfaces. The experiments are repeated a significant number of times for various rough surface cases.

3.1 Testing Equipment

In the following section, the equipment used in the experimental work are described by means of the work theory and suitable figures.

3.1.1 Wind Tunnel

In this section the main overview for wind tunnel design and its properties are explained.

Mainly, a wind tunnel contains three structure part, which are the contraction, test section, and diffuser, see figure (3.1). The first component is the contraction (effuse) which has two general functions turbulence reduction and near-isentropic flow acceleration. It has multiple flow devices; these devices are a screen and honeycomb. There are different shapes of the honeycomb cross-section area. rectangular, circular, and hexagonal are the most popular shapes. Plastic or metal is usually used to made honeycomb. Wind tunnel usually has only a single honeycomb section. The flow then enters the test section or working suction where the model is fixed. The test section length is 600 mm, width is 305 mm, and height is 305 mm in which an airfoil is mounted horizontally. In order to perform and give full visibility, the upper and sidewalls of the test section are made from acrylic. There are two holes located on the working section of the upper body of the machine, which house two pitot devices and two wall taps used to measure the static pressure upstream of the working section. The test section is used to simulate the flight environment and to get uniform flow as accurately as can. Working section can be an open or close loop. The air then goes through a grille and a diffuser, which is designed to re-expand and slow the flow, and then to an axial fan. Loose objects are stopped from damaging the fan due to the grille. The air goes through a silencer unit, passes through the fan, and then is discharged out into the atmosphere, see figure (3.2). The air mean velocity at the test section was (15,18 and 20 m/s), the Reynolds number is based on the mean velocity and airfoil chord length was (1.39×10^5, 1.67×10^5 and 1.86×10^5) respectively

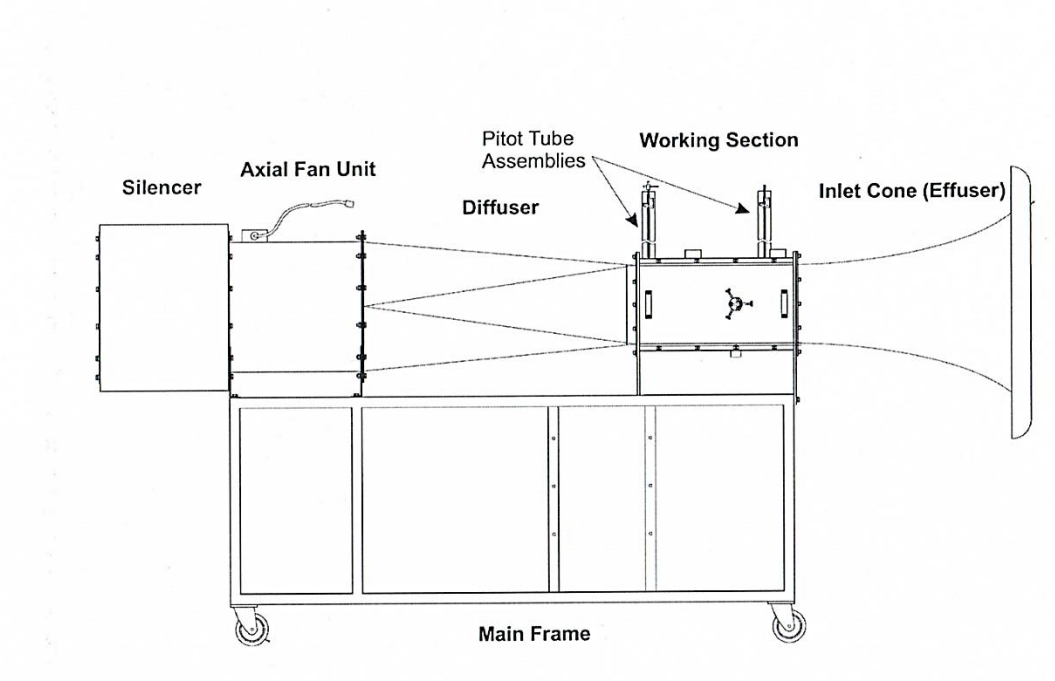

Figure (3.1) General layout for Wind Tunnel

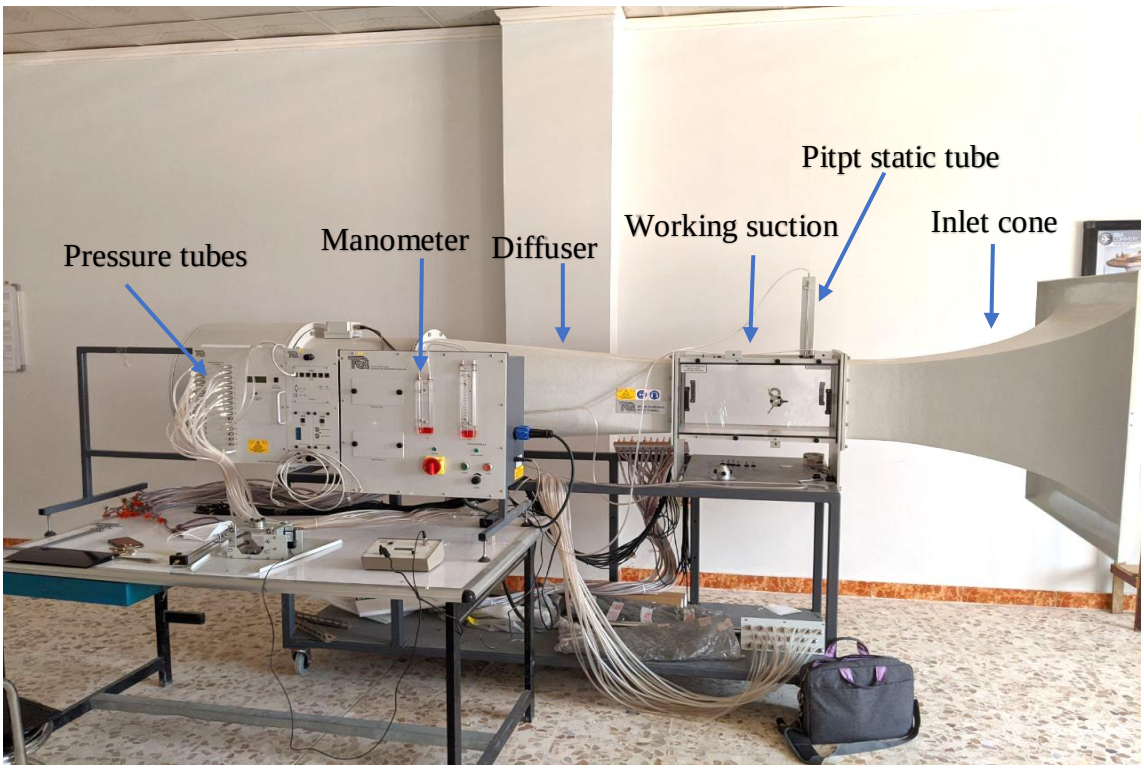

Figure (3.2) Actual diagram of Wind Tunnel

3.1.2 Airfoil Test Model

The NACA0012 airfoil with 150 mm chord and 300mm span and 2 kg weight is used in the current test. The Airfoil Model is a symmetrical NACA0012 segment airfoil that spans the entire width of the wind tunnel, Fig (3.4). There are 20 pressure-tapping locations on the airfoil. see table (3.1), Ten points are above the chord line, and ten points are below it. Tapping was spaced, so that those on the bottom are positioned at differing locations relative to those on the top. They are attached to the airfoil inside of small metal tubes that emerge from the airfoil and attach to flexible labelled pipes with adaptors to join a larger pipe. Included in the package is a manifold plate that makes it possible to make the smaller tubes into the larger pipes. Pressure taps of (1mm) diameter were mounted on the upper (10 tap) and lower surface (10 tap) of airfoil in the midspan through models to provide measurements of static pressure. figure (3.5)

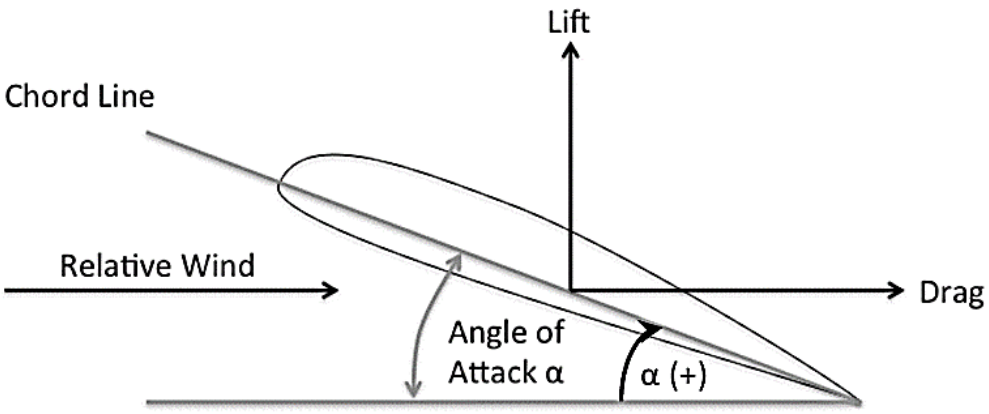

Figure (3.3) lift and drag force on Airfoil

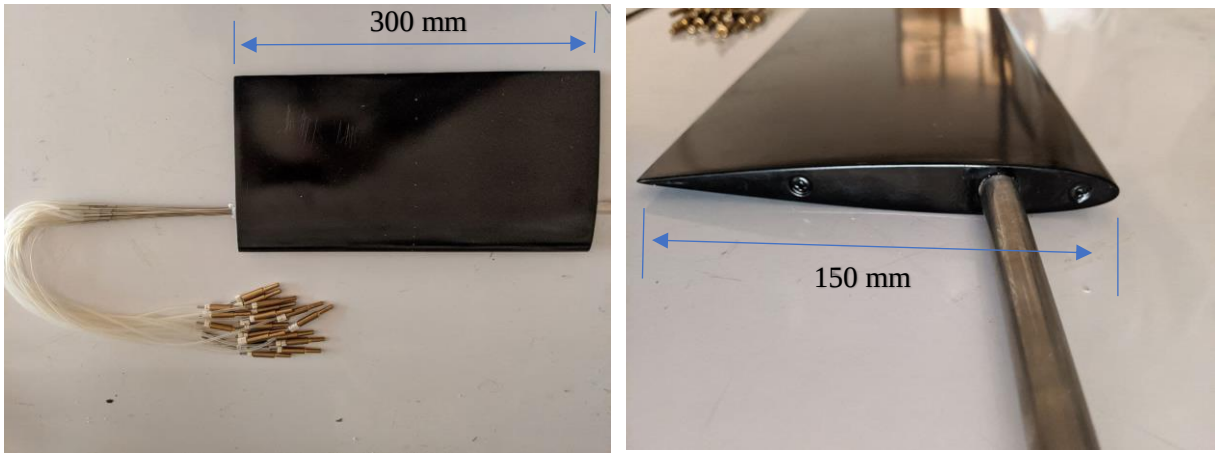

Figure (3.4) Test model airfoil (NACA0012)

Table (3.1) Tapping position on NACA 0012 Airfoil

Lower Surface Tapping	Distance From Leading Edge
2	1.52
4	7.62
6	15.24
8	22.86
10	41.15
12	59.44
14	77.73
16	96.02
18	114.30
20	129.54

Upper Surface Tapping	Distance From Leading Edge
1	0.76
3	3.81
5	11.43
7	19.05
9	38.00
11	62.0
13	80.77
15	101.35
17	121.92
19	137.16

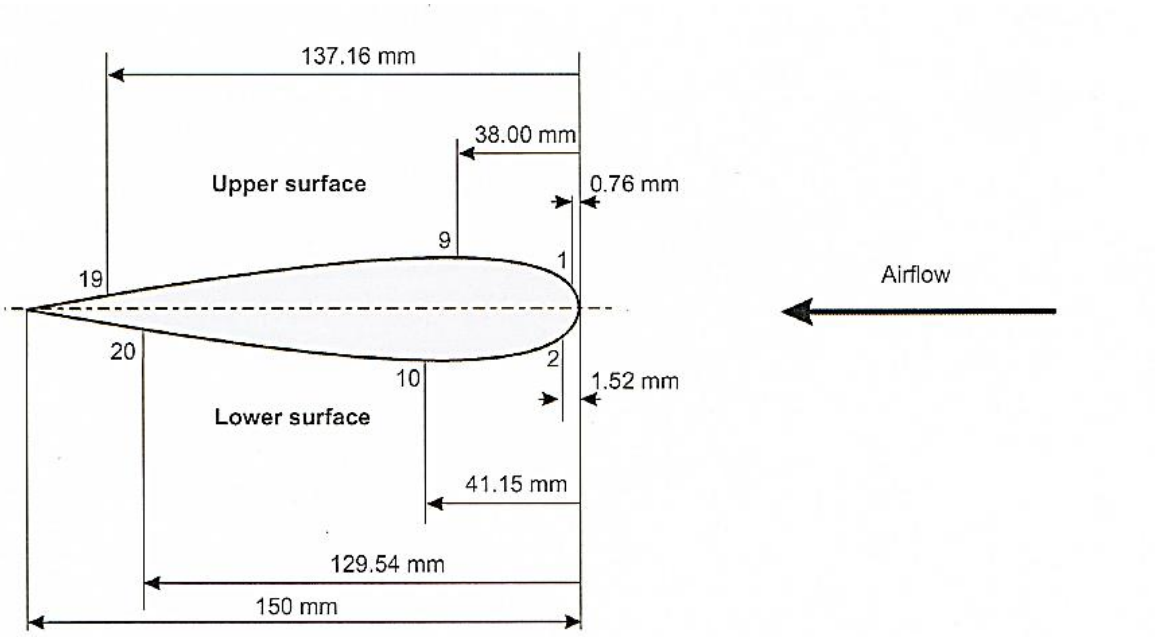

Figure (3.5) Airfoil Tapping distribution

3.1.3 Rough Surfaces Models

Before starting the experiment, the rough surface is prepared. Stainless steel 304L woven wire is applied to introduce surface roughness. A wide selection of grades of woven wire are used for this experiment. The size of the mesh of a rough surface is dependent on the relative amount of rough woven wire that is being used. The surface roughness increases as the number of holes (mesh per in) of the woven wire decreases. 40 Grades of surface roughness have more roughness than (60, 80, 100,120 and 200 Grade) Fig (3.6). Table (3.2) using the (300*150 mm) sizes of woven wire to cover the airfoil surface. Rough surfaces were applied on 50% of the airfoil area, for the purpose of pasting rough surface (woven wire) to the airfoil surface, the surfaces are fixed by using double sided adhesive tape. Figure (3.7)

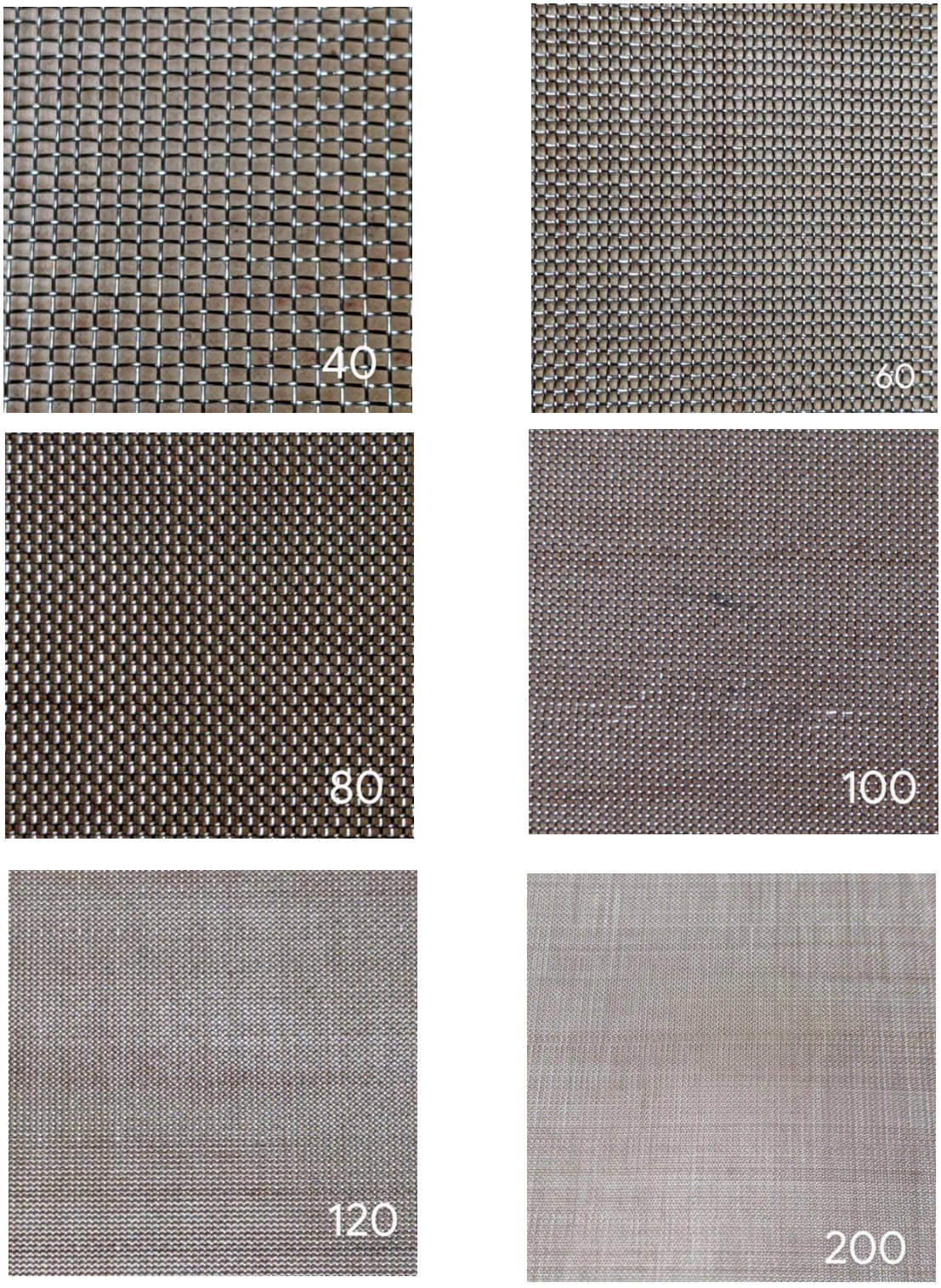

Figure (3.6) rough surfaces models

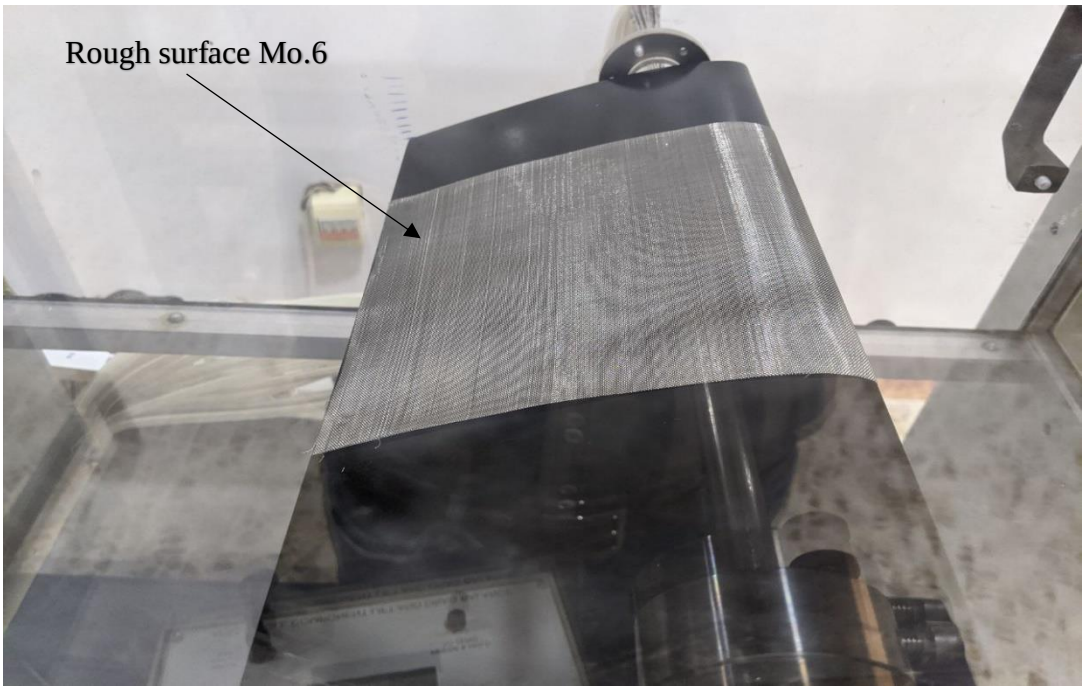

Figure (3.7) airfoil with rough surfaces were applied on surface

Different grades of roughness are being used in my experiment to demonstrate the effects of roughness on the boundary layer. These are some characteristics of the rough surface. Table (3.2)

Table (3.2) Rough surfaces dimensions

no.	mesh per in.	size (mm)	hole	wire dime.
Mo.1	40	300*150	0.425 mm	0.190 mm
Mo.2	60	300*150	0.169 mm	0.25 mm
Mo.3	80	300*150	0.18 mm	0.120 mm
Mo.4	100	300*150	0.1 mm	0.150 mm
Mo.5	120	300*150	0.125 mm	0.06 mm
Mo.6	200	300*150	0.075 mm	0.08 mm

3.2 Measurement Devices

3.2.1 Pitot Static Tube

The pitot-static probe or pitot-static tube is one of the most devises used for calculate the local velocity of air. It also used for airspeed measuring in aircraft. The principal of operation is very simple based on Bernoulli's equation to determine the dynamic pressure (pressure difference) which given by:

$$P_{dynamic} = \frac{1}{2} \rho v^2 = p_{stagnation} - p_{static} \quad \text{.....(1)}$$

The tunnel reference velocity was determined using a typical ellipsoidal nosed Pitot-static tube with a curved junction. A 4 mm OD stainless steel tube has a collet style mounting chuck (bush) mounted on the upper side of the working section to allow for full motion through the working section, as shown in figure (3.8). It has five measuring holes, the center (forward-facing) hole of 1mm diameter indicates stagnation (total) pressure and the four (side–facing) holes of 1 mm diameter indicate static pressure. The pitot-static tube can determine the difference between total and static pressure and thus velocities, from dynamic pressure and fluid velocity relation. Total pressure is equal to static pressure plus dynamic pressure.

Figure (3.8) Pitot – static Tube.

3.2.2 Pressure Display Unit

The pressure display module is part of wind tunnel. The module fits into the control and instrumentation frame of the wind tunnels. It provides a means to measure and display 32 different pressures from models. The module contains 32 calibrated pressure transducers rated at a maximum of +7 kPa. The module has an integral liquid crystal display with a scroll control that allows the user to read all 32 channels at any time. All pressures are measured with respect to atmosphere. The 32-Way Pressure Display can be interfaced to a PC that allows pressure measurements to be displayed, captured, conveniently tabulated, graphed, and exported to a spread sheet package for further processing. Figure (3.9)

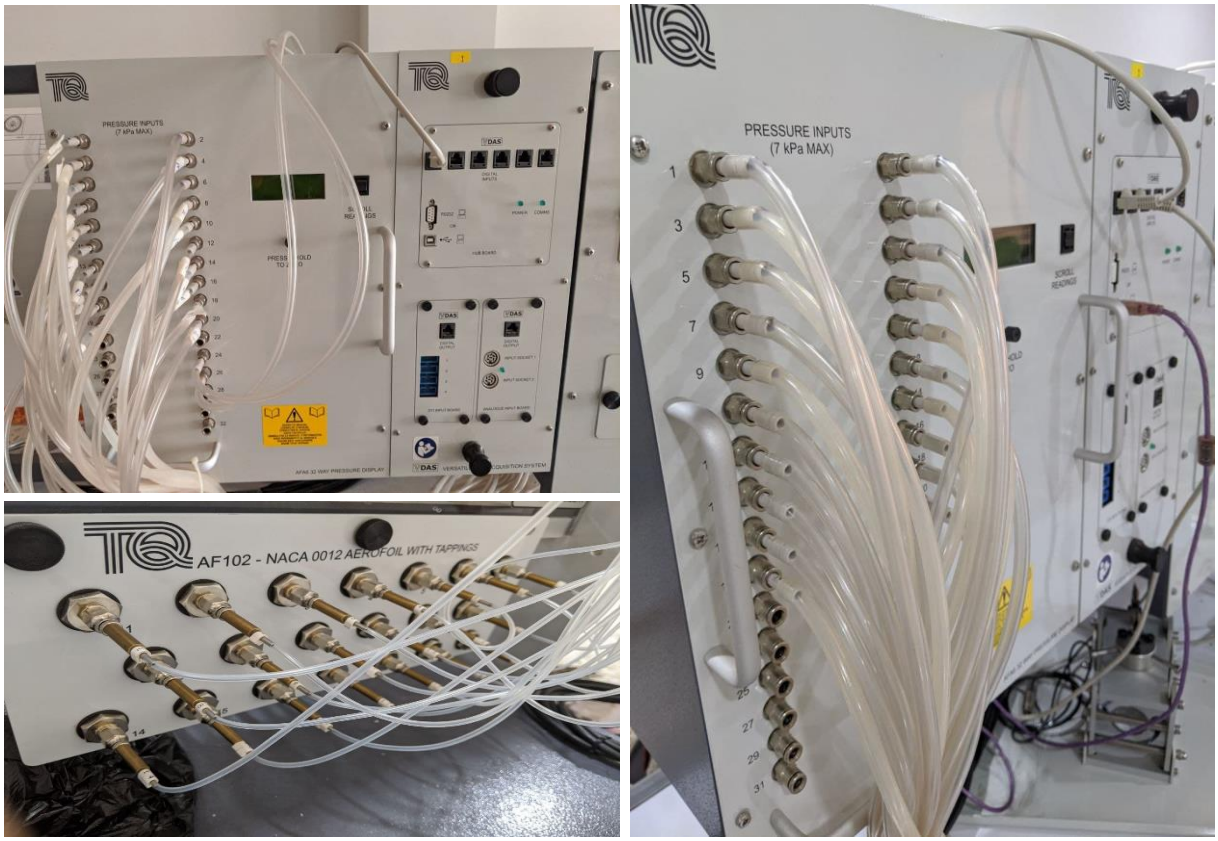

Figure (3.9) 32-Way Pressure Display units

3.2.3 Lift and Drag Component Balance

For studying the forces on airfoils and similar objects in wind tunnel, it is important to use equipment for measuring the different forces which the airfoil is subjected. The single-component balance was used to give a means to calculate the lift and drag forces on the airfoil fixed in the subsonic wind tunnel. The balance is mainly constricted from aluminum alloy and the general framework is secured to the side of the working section of the wind tunnel. The models which are used with the balance should be provided with a mounting stem of a 12 mm diameter which is inserted inside the module and used to support the module by tightened it by model clamp. The forces acting on the module are transmitted to the force plate which is transfer the forces to strain gauge load cell through a flexible cable, the load cell measures the lift and drag force and shows the result on the display units, see figure (3.10).

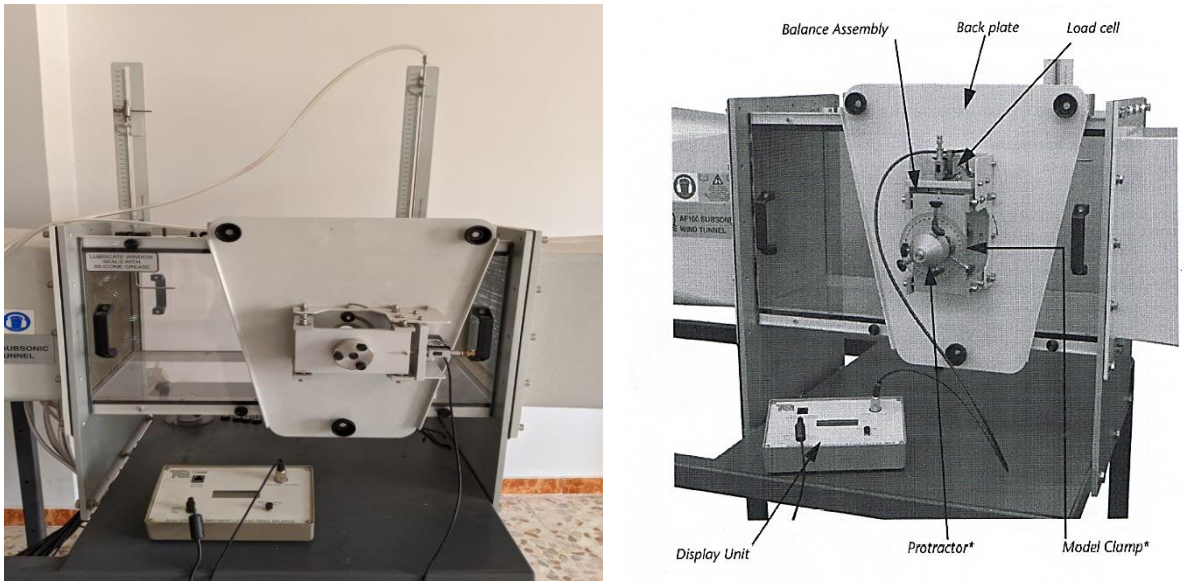

Figure (3.10) Lift and Drag Component Balance

3.3 Principle of Operation

As pointed out in the preceding discussion, the experimental work was employed in this study to investigate the effect of rough surfaces on aerodynamics characteristic on NACA0012 at open loop wind tunnel. For the wind tunnel tests the experiments were conducted to measure the pressure distribution at (10) tap on upper surface and (10) tap on lower surface for smooth and rough surface model of NACA.

There are two main testing conditions:

(1) Smooth airfoils.

(2) Rough model surfaces airfoils.

For the above two testing conditions, tests were carried out at Reynolds numbers (1.39×10^5, 1.67×10^5 and 1.86×10^5) based on chord length at the angles of attack (0,2,4,6,8,10,12,14 and 16). Measurement are done for smooth and rough models surface on NACA0012. Repeatability of the pressure readings ensured by repeating the first reading at each measuring group until the readings difference is not more than (3%).

3.4 Procedure of Experimental Work

Before each test, the following procedure must be done:

1. Measuring the ambient temperature to calculate the air density. These values are summarized in Table (3.3), together with other experimental parameters.
2. Checking whether the velocity in the tunnel is constant.
3. Fixing the model in the test section of the wind tunnel. Figure (3.11)
4. Checking the pressure probes and connecting the tubes to the mainfold plate wish transfer pressure to pressure display unit.
5. Operating the wind tunnel and waiting sometime about 3 minute to reach steady state then recording the reading of pressure when they reach steadiness.
6. Repeating steps (2–5) by changing the rough surface dimensions. see figure (3.14)

Table (3.3) Experimental Parameters

Description	Symbol	Amount	Units
Freestream velocity	U_s	15-18-20	**m/s**
Air density	ρ	1.164	**Kg/m^3**
Air dynamic viscosity	μ	1.872×10^{-5}	**Kg/m. s**
Reynolds number	Re	____	____
Air Temperature	T_a	30	**C^o**
Atmosphere pressure	P_{atm}	101.325	**kN/m^2**

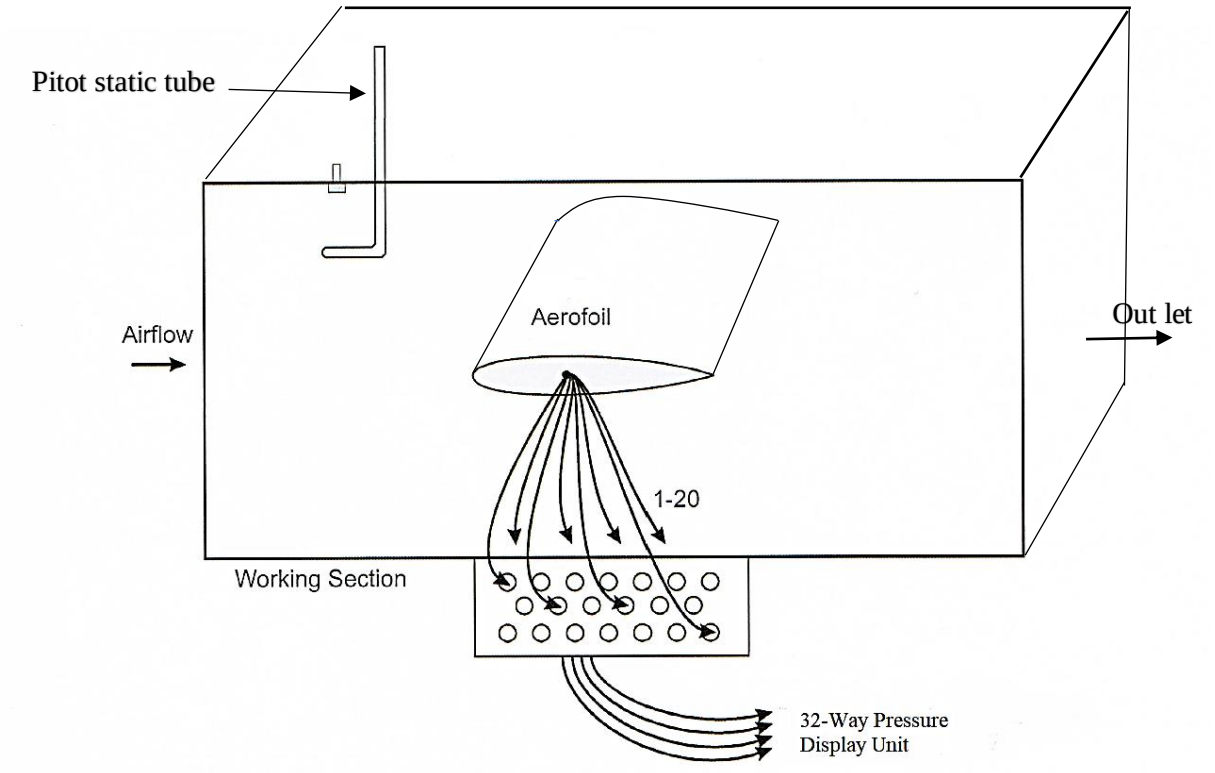

Figure (3.11) Fit the Airfoil inside working suction and connect the pipes to the manifold plate

3.5 Theoretical Calculations for Experimental Work

As it is known, when fluid flows over a solid surface, a layer is formed at the surface at which the velocity gradient is very high. The fluid is retarded in this layer on an account of viscous resistance. This layer is known as boundary layer. In this layer, velocity increase rapidly from zero at the boundary surface (i.e. no slip) to that equal to the main stream velocity at the outer edge of the boundary layer. The thickness of the boundary layer (δ) is usually taken as the normal distance between the plate and the point where the velocity is 0.99 times the velocity of main flow.

Air Density:

From a combination of the atmospheric pressure, the gas constant, and the ambient temperature, determine the density of the air in the wind tunnel:

$$\rho = p/RT \qquad \text{……. (2)}$$

Two Dimensions Assumption:

As the airfoil fully spans the working section of the wind tunnel, the air cannot flow around the wing edges or 'wing tips', as in a real airfoil. The air flow is only over the upper and lower surface of the wing. This is two dimensional airflow. Flow around wing tips adds the third dimension, but creates additional drag and other complications.

Wing Area s :

This is simply the plan view of the airfoil, which is the product of the span and the chord.

$$\text{Wing Area} = \text{chord} \times \text{span} \qquad \text{……. (3)}$$

Pressure Coefficient C_p

the pressure coefficient is given as:

$$Cp = \frac{P - Pw}{\frac{1}{2}\rho u_\infty^{\,2}} \qquad \text{..... (4)}$$

Coefficient of Lift C_L and drag C_D

A larger wing of a certain design can offer more real or simple lift or drag than a smaller wing of the same design, so to compare wings of different sizes, there must be an account for the difference in size, engineers calculate this by using a non-dimensional value that is called the lift or drag coefficient.

$$C_L = L / (\tfrac{1}{2}\rho\ u_\infty^2\ s) \qquad \text{..... (5)}$$

$$C_D = D / (\tfrac{1}{2}\rho\ u_\infty^2\ s) \qquad \text{..... (6)}$$

The equation shows that you can use the coefficient of lift or drag with the air and airfoil properties to calculate basic lift or drag.

$$L = C_L (\tfrac{1}{2}\ \rho\ u_\infty^2\ s) \qquad \text{.....(7)}$$

$$D = C_D (\tfrac{1}{2}\ \rho\ u_\infty^2\ s) \qquad \text{.....(8)}$$

Finding Coefficient of Lift

When graphing the coefficient of pressure against the distance along the airfoil, the coefficient of lift is plotted underneath the line. In order to make the distance along the airfoil non-dimensional, it must be divided by the chord length to yield a fraction x/c, with values between 0 and 1.

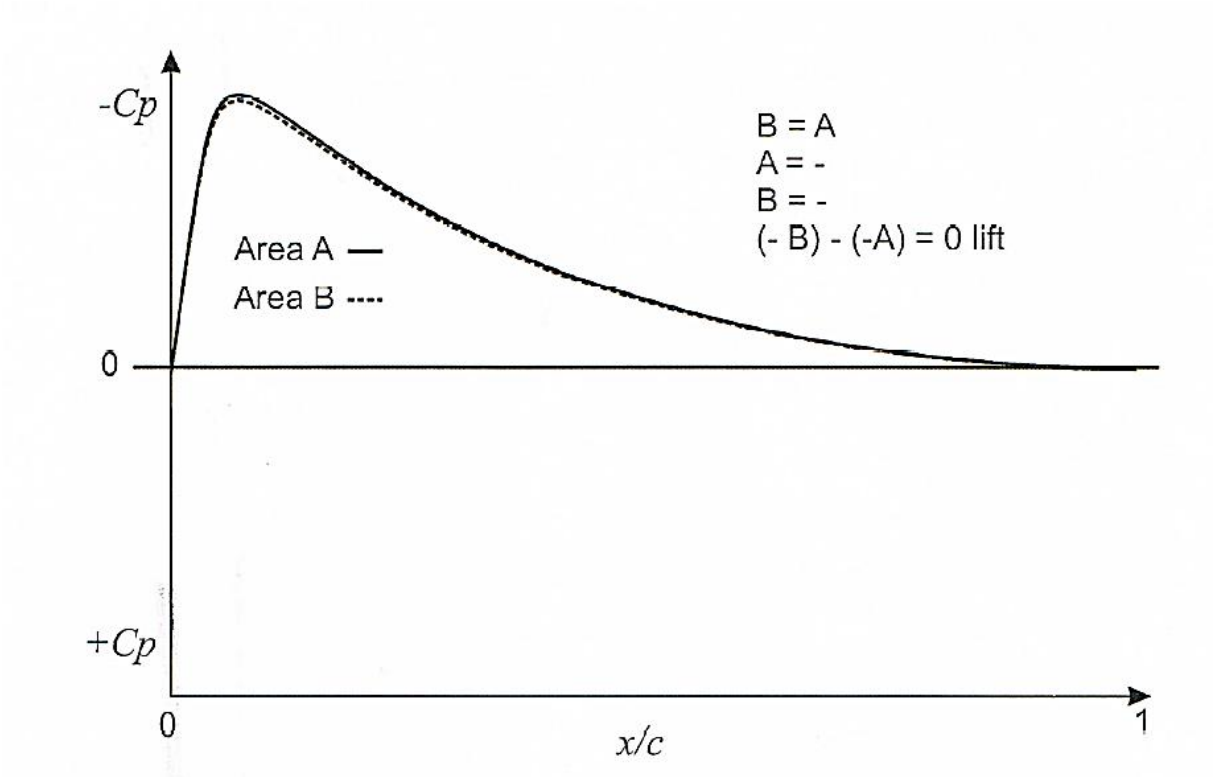

Figure (3.12) Finding Coefficient of Lift [33]

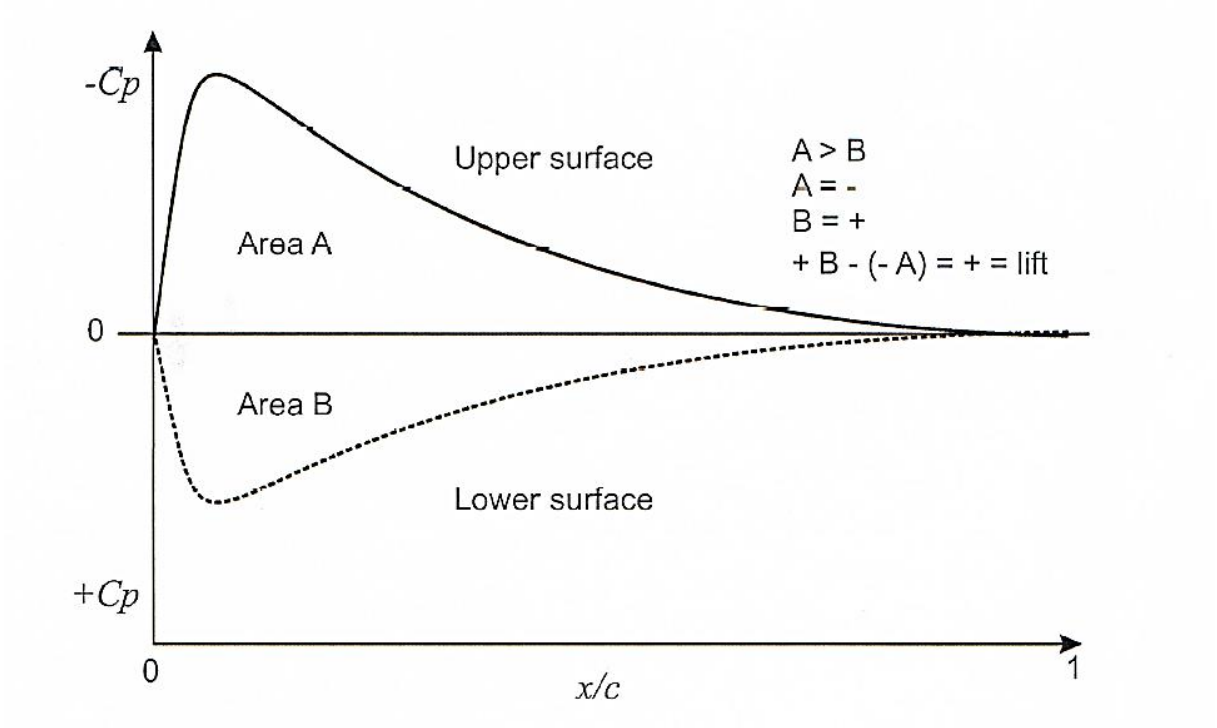

Figure (3.13) Finding Coefficient of Lift [33]

$$C_L = \text{Area B} - \text{Area A} \qquad \text{…….(9)}$$

The difference between the two areas (B-A) is the lift coefficient. At 0 degrees incidence, for a symmetrical airfoil both areas would be equal and negative, giving a lift of 0. Figure (3.12)

If the area under the upper surface curve is greater and negative, while the lower surface gives positive pressure coefficients, then you have a net positive lift coefficient. Figure (3.13)

Velocity Measurement:

To calculate the local velocities from measurements devices, for incompressible flow Bernoulli's equation used as follows:

$$P_s + P_d = P_t = \text{Constant} \quad \ldots\ldots\ldots\ldots\ldots (10)$$

$$\Delta P = P_d = P_t - P_s$$

$$P_d = \frac{1}{2} \rho \, u_{\infty}^2 \quad \ldots\ldots\ldots\ldots\ldots (11)$$

Dynamic pressure can be expressed in terms of:

$$P_d = (\Delta H \, \rho)_{water} \, g \quad \ldots\ldots\ldots\ldots\ldots (12)$$

From equations (11) and (12):

$$u_{\infty} = [2g \, \frac{(\Delta H \rho) water}{\rho \, air}]^{1/2} \quad \ldots\ldots\ldots\ldots\ldots (13)$$

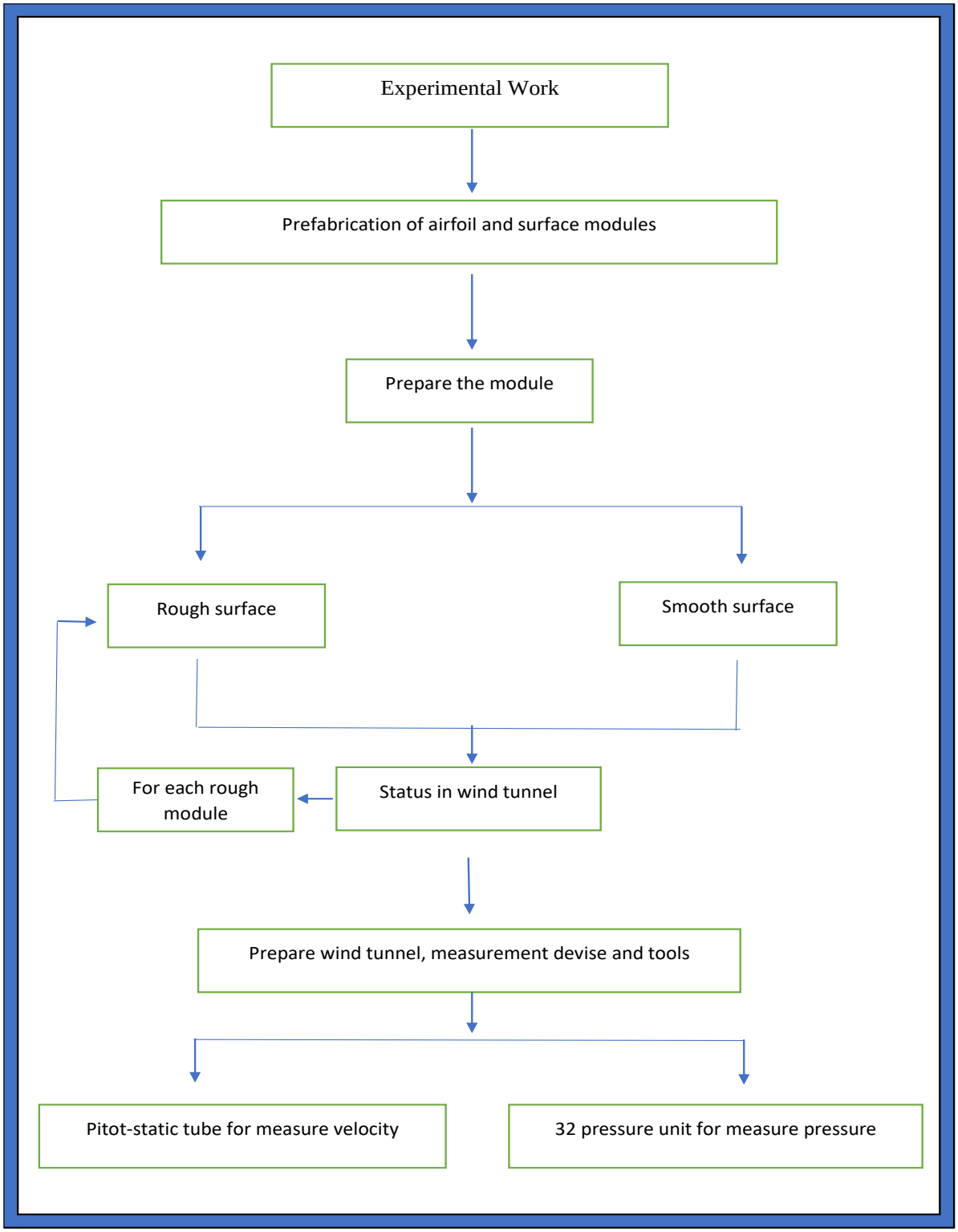

Figure (3.14) procedure of experiment work

CHAPTER FOUR

RESULTS AND DISCUSSION

CHAPTER FOUR

RESULTS AND DISCUSSION

4.1 Introduction

Experiments were carried out using stainless steel wire mesh as six different rough surfaces (Mo.1, Mo.2, Mo.3, Mo.4, Mo.5 and Mo.6) and a smooth surface of airfoil for comparison. The tests have been achieved for two dimensional, steady, turbulent, incompressible, viscous flow. All cases were used for the pressure measurement in the low-speed wind tunnel at Reynolds numbers (1.39×10^5, 1.67×10^5 and 1.86×10^5) based on the mean velocity and airfoil chord length. Rough surfaces were applied on 50% of the airfoil area, and pitot tube was utilized to measure the dynamic pressure in the working suction of wind tunnel. The experimental results included pressure, mean velocity profile, lift, drag coefficients curves for the airfoil.

4.2 Experimental Results

Experiments were carried out using airfoil model (NACA 0012) in a subsonic wind tunnel. The experimental results included pressure, velocity profile and lift, drag coefficients curves for the airfoil with and without rough surfaces at different angles of attack (0,2,4,6,8,10,12,14 and 16) for rough models (Mo.1, Mo.2, Mo.3, Mo.4, Mo.5 and Mo.6) at Reynolds numbers (1.39×10^5, 1.67×10^5 and 1.86×10^5) based on chord. Tables (4.1) and (4.2).

Table (4.1) rough surfaces cases for C_p, C_L, C_D

Case study	**Surface module**	**Air velocity**	**Angle of attack**	**Measurement**
Case 1	Smooth	15,18 and 20	0,2,4,6,8,10,12,14 and 16	C_p, C_L, C_D
Case 2	40 holes per in (Mo.1)	15,18 and 20	0,2,4,6,8,10,12,14 and 16	C_p, C_L, C_D
Case 3	60 holes per in (Mo.2)	15,18 and 20	0,2,4,6,8,10,12,14 and 16	C_p, C_L, C_D
Case 4	80 holes per in (Mo.3)	15,18 and 20	0,2,4,6,8,10,12,14 and 16	C_p, C_L, C_D
Case 5	100 holes per in (Mo.4)	15,18 and 20	0,2,4,6,8,10,12,14 and 16	C_p, C_L, C_D
Case 6	120 holes per in (Mo.5)	15,18 and 20	0,2,4,6,8,10,12,14 and 16	C_p, C_L, C_D
Case 7	200 holes per in (Mo.6)	15,18 and 20	0,2,4,6,8,10,12,14 and 16	C_p, C_L, C_D

Table (4.2) Rough surfaces cases for velocity profile measurement

Case study	**Surface module**	**Air velocity**	**Angle of attack**	**Measurement**
Case 1	Smooth	15,18 and 20	zero	Velocity profile
Case 2	40 holes per in	15,18 and 20	zero	Velocity profile
Case 3	60 holes per in	15,18 and 20	zero	Velocity profile
Case 4	80 holes per in	15,18 and 20	zero	Velocity profile
Case 5	100 holes per in	15,18 and 20	zero	Velocity profile
Case 6	120 holes per in	15,18 and 20	zero	Velocity profile
Case 7	200 holes per in	15,18 and 20	zero	Velocity profile

4.2.1 Effect of Roughness on Velocity Profile

Streamwise mean velocity profiles were measured in the longitudinal (y) plane with respect to the airfoil centerline for both with and without rough surfaces at positions x=0.20L, where L is length of working suction, as shown in figures (4.1 – 4.3) for Reynolds numbers (1.39×10^5, 1.67×10^5 and 1.86×10^5) respectively. All measurement of velocity profile was done at a constant angle of attack (0 degree). Presence of the rough surface will strongly influence the velocity profile near the wall of the airfoil, indicating a reduction in the momentum transferred from the fluid to the wall. For most rough surface cases in the present investigation, the velocity profiles shift slightly downward compared with the smooth surface. This happens because of the reduction in the vorticity of the fluid or the smallest size of turbulent eddies in the boundary layer. This effect shifts the profiles in this direction. Similar results were obtained at different Reynolds numbers so they are not influent on velocity profile.

4.2.2 Effect of Roughness on Pressure Distribution

NACA 0012 chordwise pressure distribution measured at various angles of attack (0°, 2°, 4°, 6°, 8°, 10°, 12°, 14°, and 16°), for smooth and rough surfaces (Mo.1, Mo.2, Mo.3, Mo.4, Mo.5 and Mo.6). Pressure coefficients distribution along airfoil chord for NACA 0012 are presented in figures (4.4 - 4.8), figures (4.9 - 4.13) and figures (4.14 - 4.18) for Reynolds numbers (1.39×10^5, 1.67×10^5 and 1.86×10^5) respectively. In this model (Mo.6, 200 holes per inch), the chordwise pressure distribution on the rough surface is very different from other surfaces. Pressure distribution with rough surface has a greater pressure area than a pressure distribution area with smooth surface and other modules (Mo.1, Mo.2,

Mo.3, Mo.4, and Mo.5) due to inflows towards the wall carry high streamwise momentum and, when reaching smooth wall, spread laterally. This creates an extended area of the surface with high streamwise velocity gradient. If there is inflow, there will be a rise in pressure at the smooth wall, on the rough surface which can disrupt the lateral motion of the inrush directly below the inflow. As a result, the size of region with high streamwise velocity gradient is then decreased. The larger area with rough surface will result in model (Mo.6) which has larger area for all measurement.

4.2.3 Roughness Effect on Lift and Drag

It is known that the pressure distribution is sensitive to the effect of rough surfaces. Figure (4.19), Figures (4.21) and Figures (4.23), show the variations of the lift coefficient verses angle of attack for both smooth and rough surfaces at Reynolds numbers (1.39×10^5, 1.67×10^5 and 1.86×10^5) respectively. Figures (4.20), Figures (4.22) and Figures (4.24), show the variations of the drag coefficient verses angle of attack for both smooth and rough surfaces at Reynolds numbers (1.39×10^5, 1.67×10^5 and 1.86×10^5) respectively. Figure (4.25), Figure (4.26) and Figure (4.27), show the variations of the lift/drag ratio verses angle of attack for both smooth and rough surfaces at Reynolds numbers (1.39×10^5, 1.67×10^5 and 1.86×10^5) respectively.

The result shows a small increase in lift curve slope about (8-17%) and a decrease in drag about (12-18%) for NACA 0012 over an angle of attack range from (0° to 16°), when the flow is modified within the rough surface model

(Mo.6). The slope of (*Cl*) increases and decreases in (*Cd*) obviously results from reducing the thicknesses in boundary layer caused by rough surface; essentially rough surface leads to a lower viscous effect on the airfoil.

The results also showed that stall angle of attack at (α=12°) are unaffected by rough surfaces, so the (*Cl*/*Cd*) ratio increases to maximum value (*Cl*/*Cd*=13, 14.5, 25) for Reynold numbers (1.39×10^5, 1.67×10^5 and 1.86×10^5) respectively as seen in figures (4.25 to 4.27). The rough surface model (Mo.6) has shown the greatest potential for drag reduction, with maximum recorded reduction of (18%) at Reynold number (1.86×10^5), also it gives highest value enhancement in lift coefficient of (17%) for NACA 0012 at Reynold number (1.39×10^5).

4.2.4 Lift Performance with Angle of Attack

Results of lift increase for rough surface model (Mo.6) for Reynold number (1.86×10^5) at each angle of attack are shown in figure (4.39 b) for NACA0012. This implies that roughness on the surface increases lift but at an angle of attack up to 10°, and then decreases at a higher angle of attack, Surface model (Mo.6) has proved the greatest lift increase. The lift increase for Surface model (Mo.6) on NACA0012 increased initially with angle of attack about at (a=10°) then decrease to at (a=16°).

4.3 Comparison of the present work with others researches

Comparisons between the results of the present experimental work for the rough surfaces models (Mo.1, Mo.2, Mo.3, Mo.4, Mo.5 and Mo.6) and others researches are presented in this paragraph. It is found that the results for rough module (Mo.6) of computational work agree well with the results obtained by **[18] Nibras Mohammed** wish is investigated experimentally the effect of longitudinal riblet surface models on NACA0012. For other surfaces module (Mo.1, Mo.2, Mo.3, Mo.4 and Mo.5) the results obtained agree with **[13] W. Chakroun, and [14] A.A. Abdel-Rahman** which is show that the smooth surface is more efficient than other modules (Mo.1, Mo.2, Mo.3, Mo.4 and Mo.5).

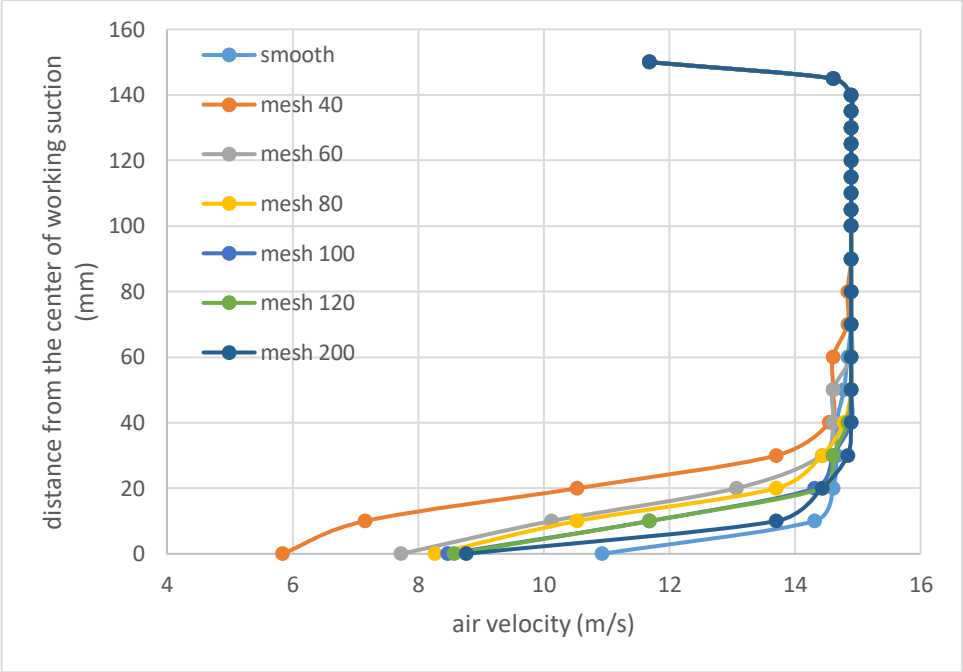

Figure (4.1) Velocity profile Distribution For smooth and Rough Surfaces with constant Angles of Attack at Re =1.39×10^5

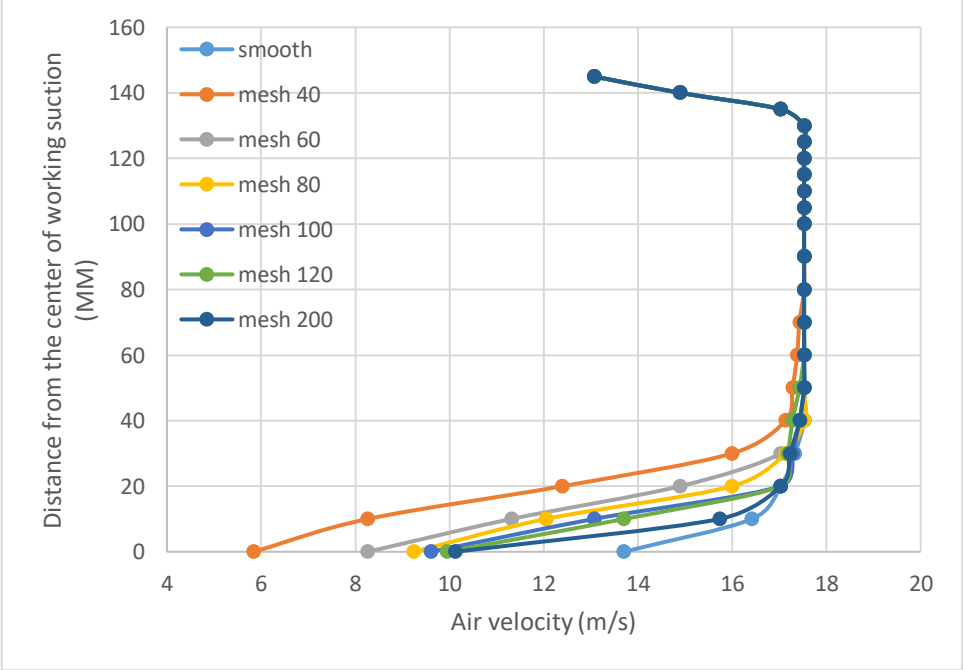

Figure (4.2) Velocity profile Distribution For smooth and Rough Surfaces with constant Angles of Attack at Re = 1.67×10^5

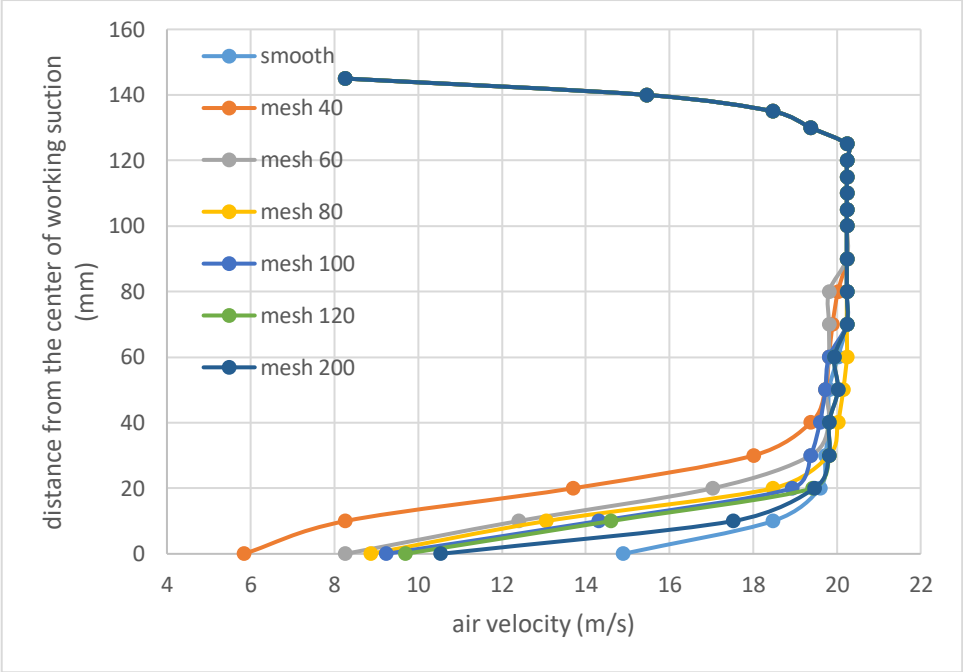

Figure (4.3) Velocity profile Distribution For smooth and Rough Surfaces with constant Angles of Attack at Re = 1.86×10^5

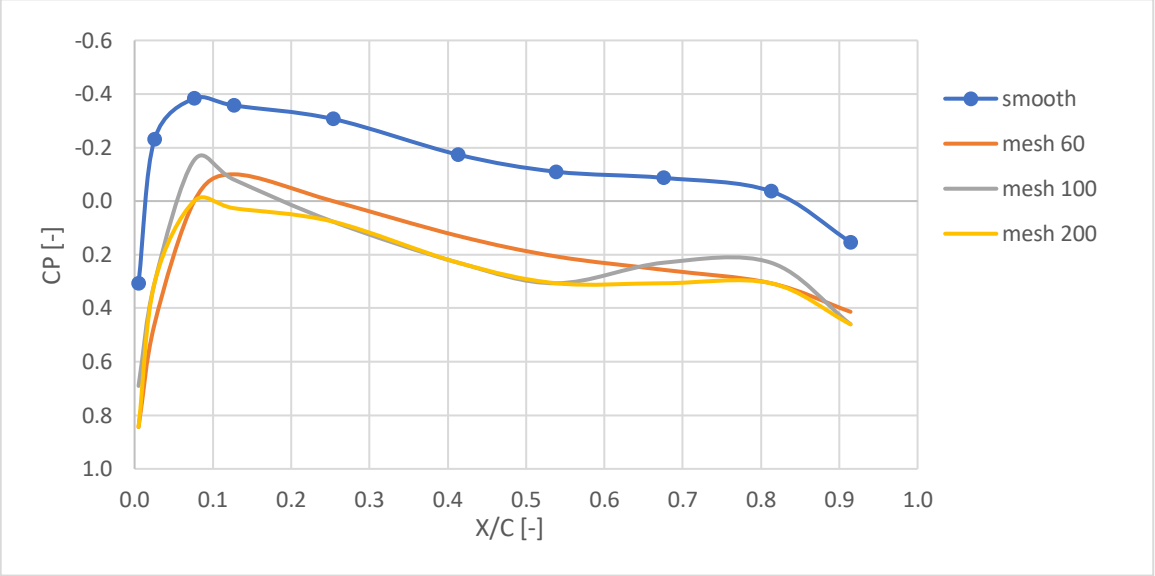

(a)

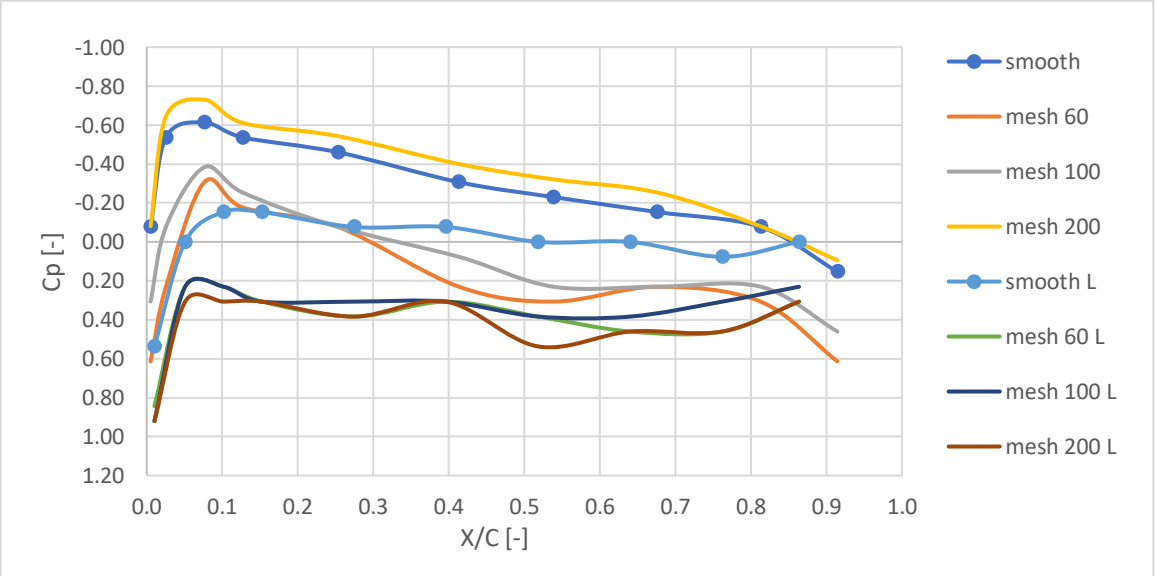

(b)

Figure (4.4) Pressure Coefficients Distribution Along Airfoil Chord For NACA 0012 at *Re* = 1.39×10^5 and Angle of Attack a) α=0 b) α=2

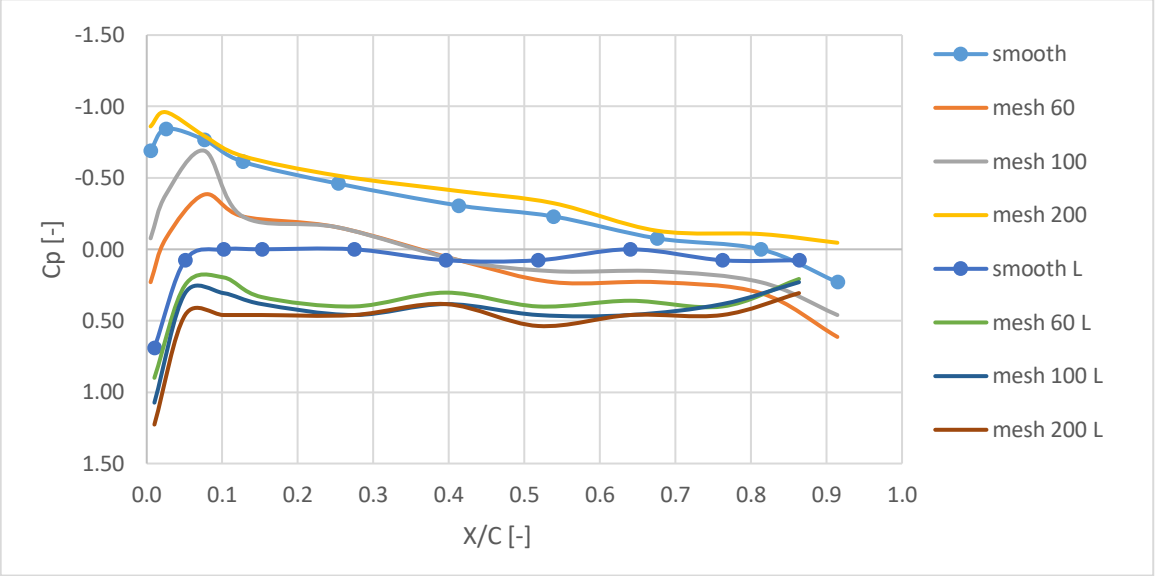

(a)

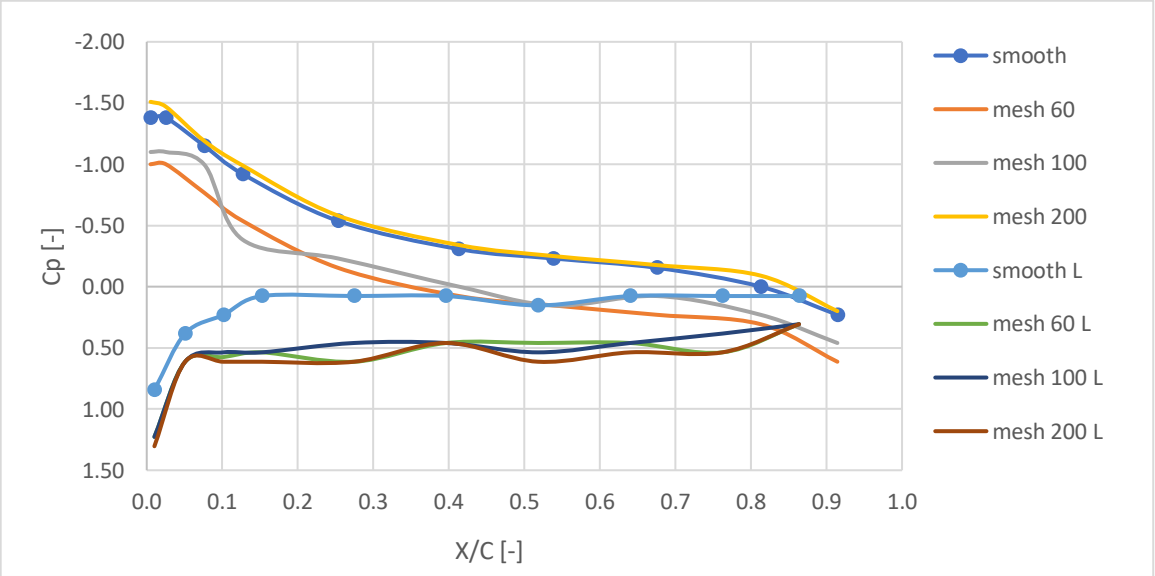

(b)

Figure (4.5) Pressure Coefficients Distribution Along Airfoil Chord For NACA 0012 at *Re* = 1.39×10^5 and Angle of Attack a) $\alpha = 4$ b) $\alpha = 6$

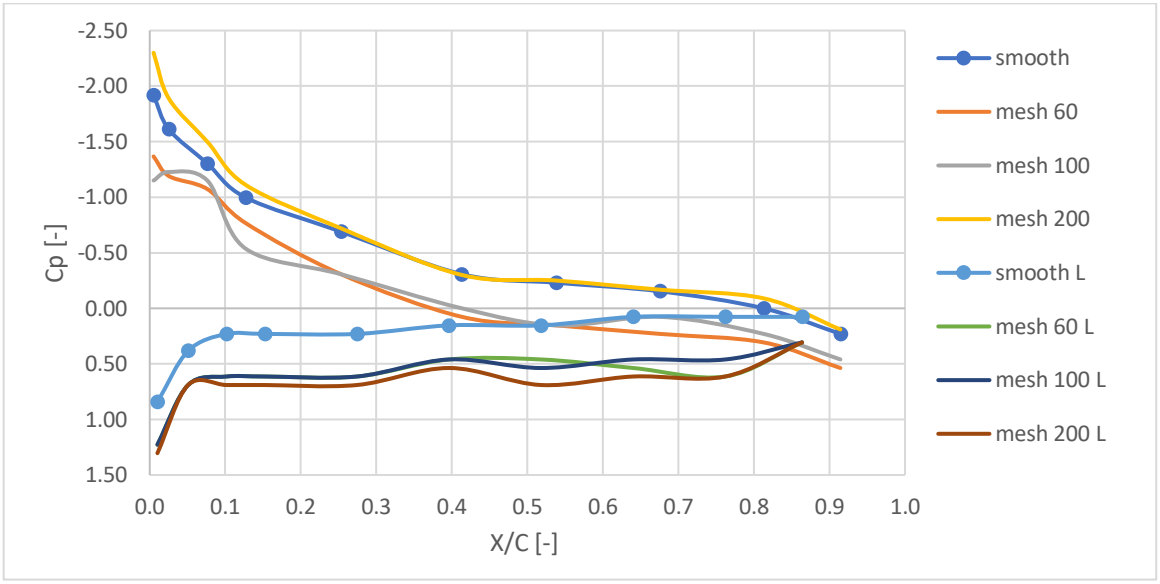

(a)

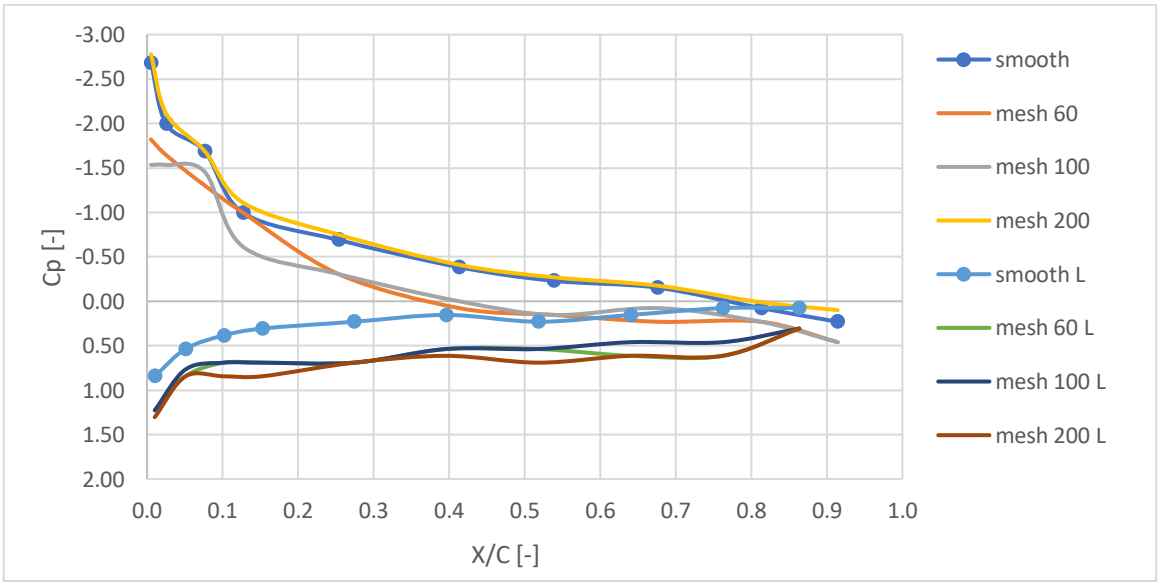

(b)

Figure (4.6) Pressure Coefficients Distribution Along Airfoil Chord For NACA 0012 at *Re* = 1.39×10^5 and Angle of Attack a) $\alpha = 8$ b) $\alpha = 10$

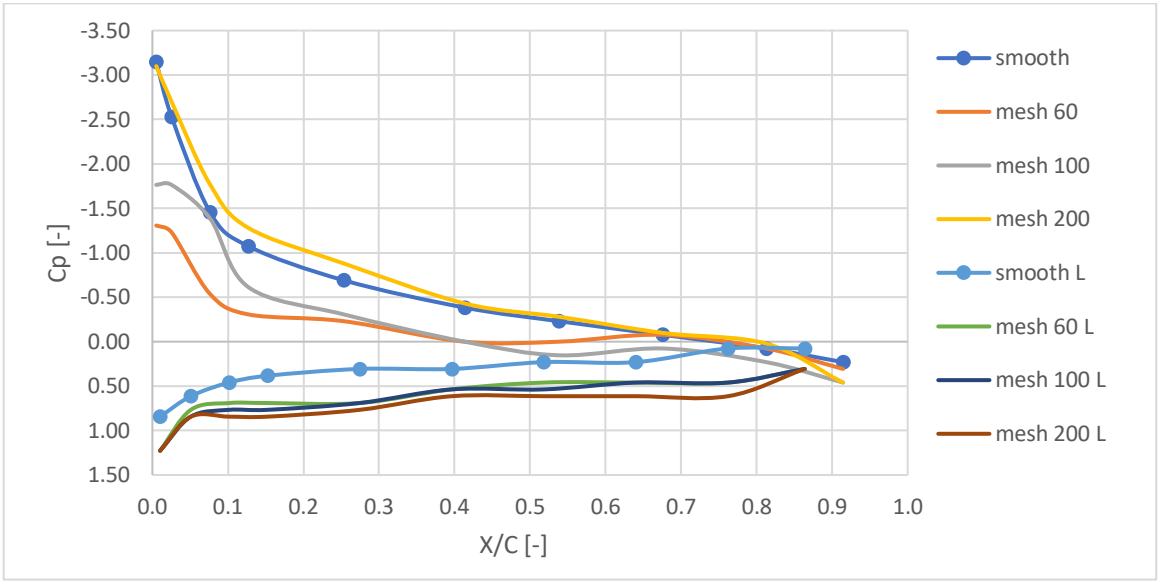

(a)

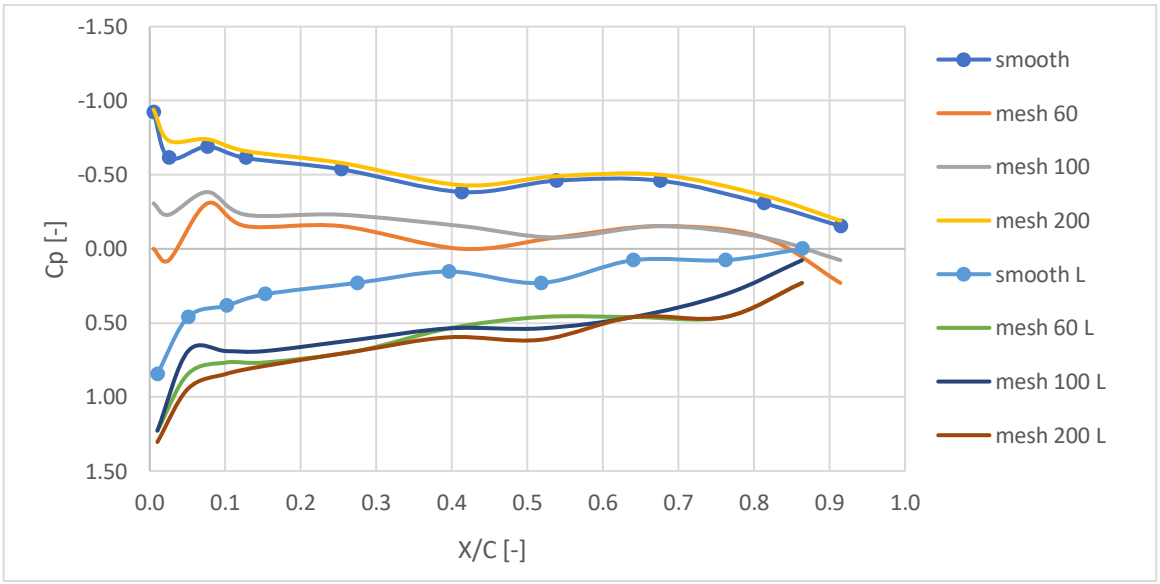

(b)

Figure (4.7) Pressure Coefficients Distribution Along Airfoil Chord For NACA 0012 at *Re* = 1.39×10^5 and Angle of Attack a) α =12 b) α =14

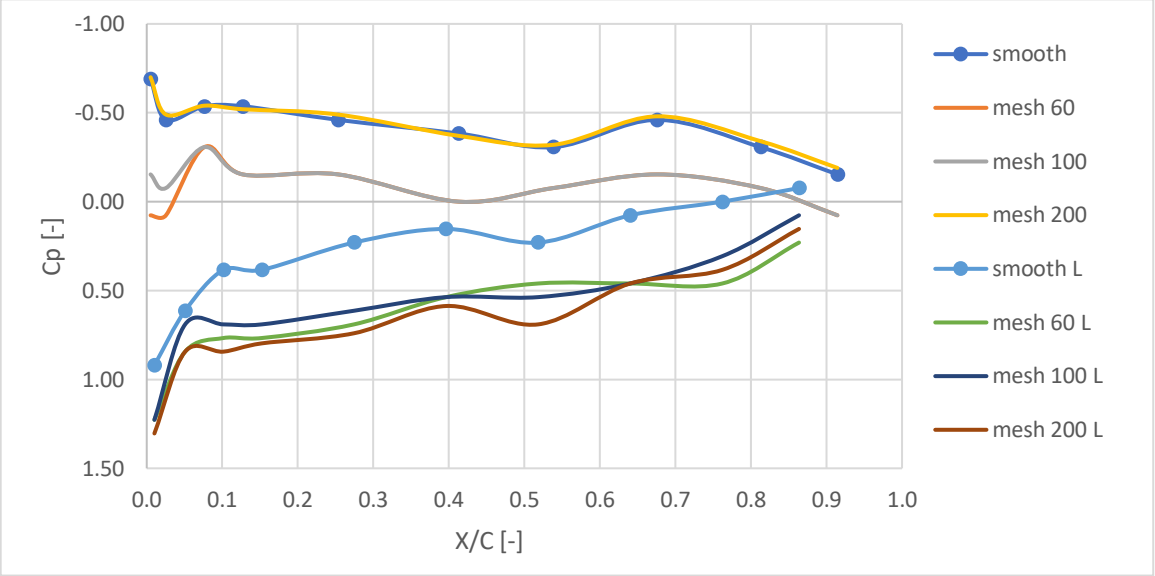

Figure (4.8) Pressure Coefficients Distribution Along Airfoil Chord For NACA 0012 at *Re* = 1.39×10^5 and Angle of Attack α =16

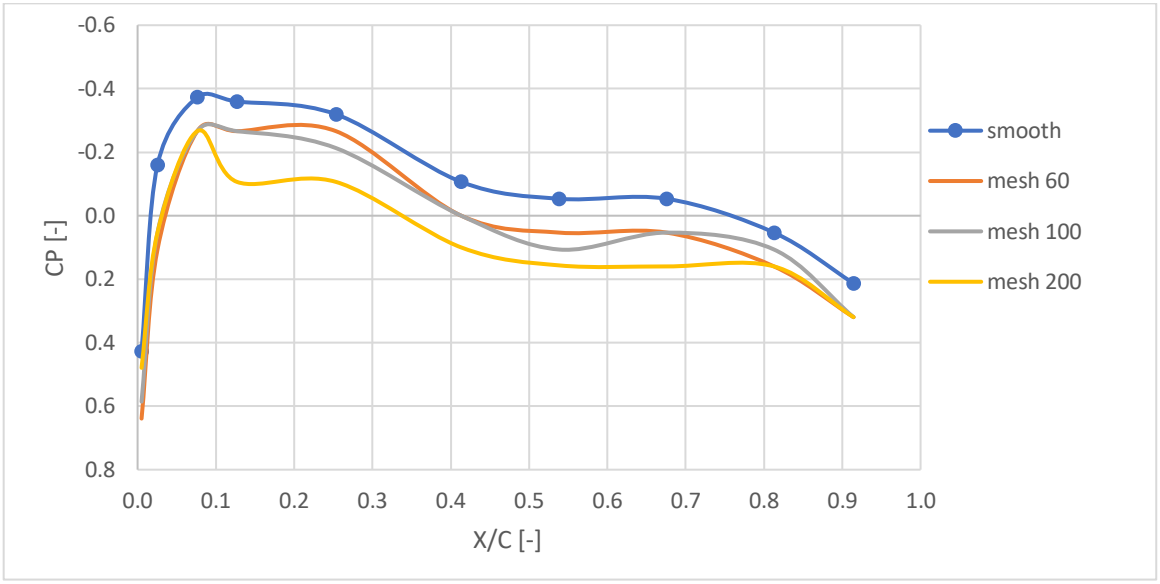

(a)

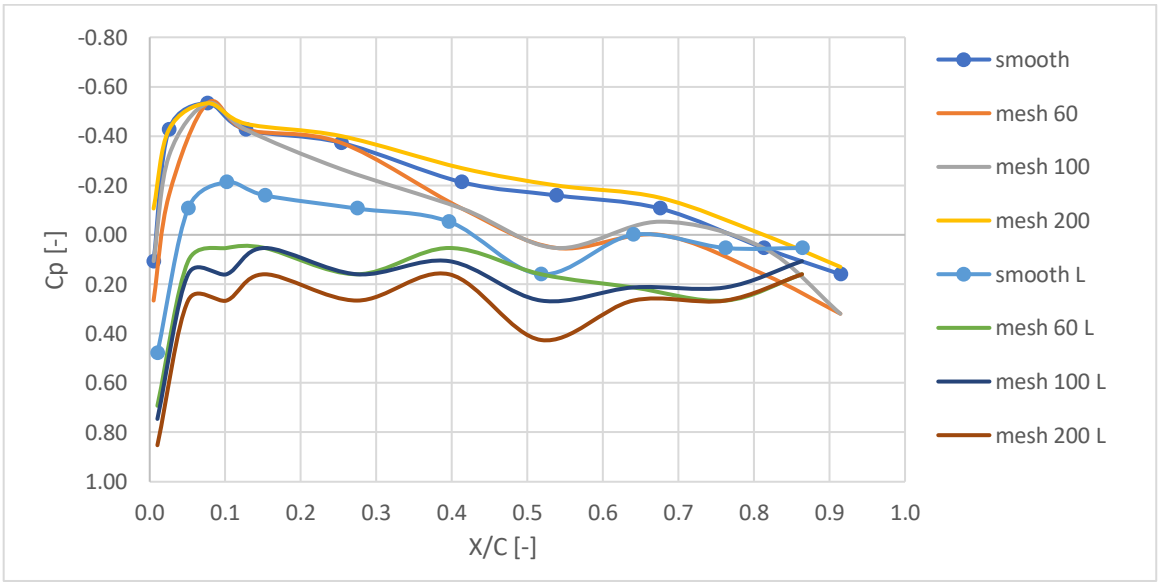

(b)

Figure (4.9) Pressure Coefficients Distribution Along Airfoil Chord For NACA 0012 at *Re* = 1.67×10^5 and Angle of Attack a) $\alpha = 0$ b) $\alpha = 2$

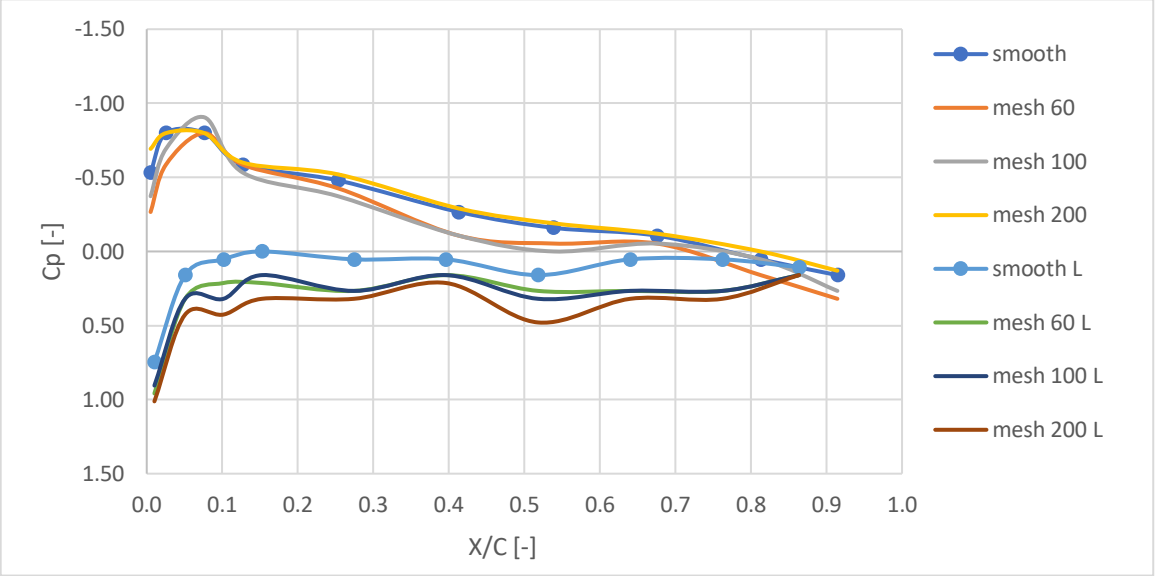

(a)

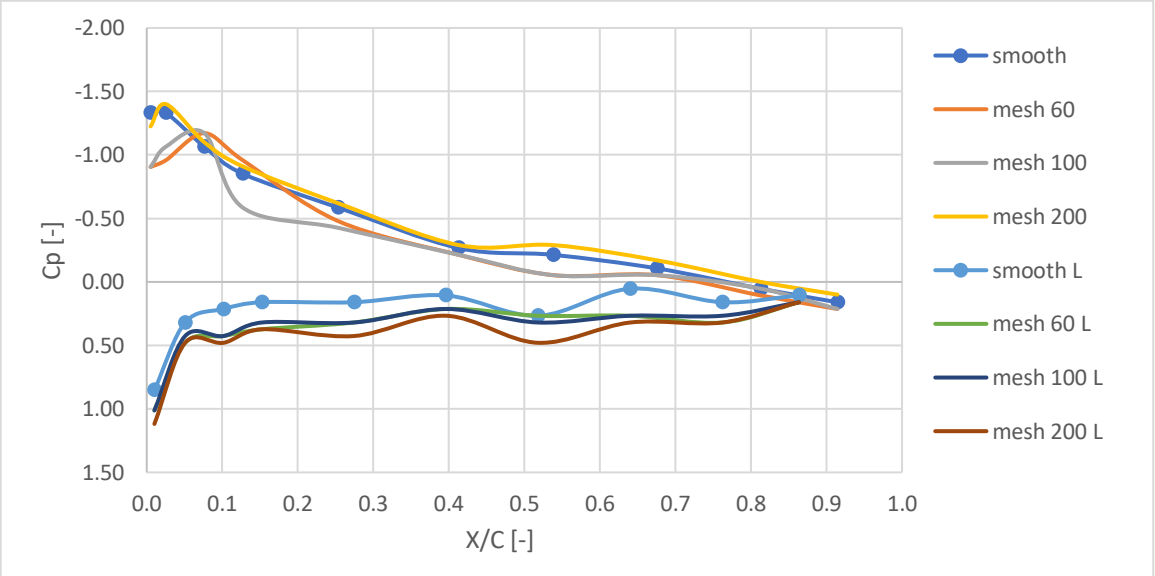

(b)

Figure (4.10) Pressure Coefficients Distribution Along Airfoil Chord For NACA 0012 at *Re* = 1.67×10^5 and Angle of Attack a) $\alpha = 4$ b) $\alpha = 6$

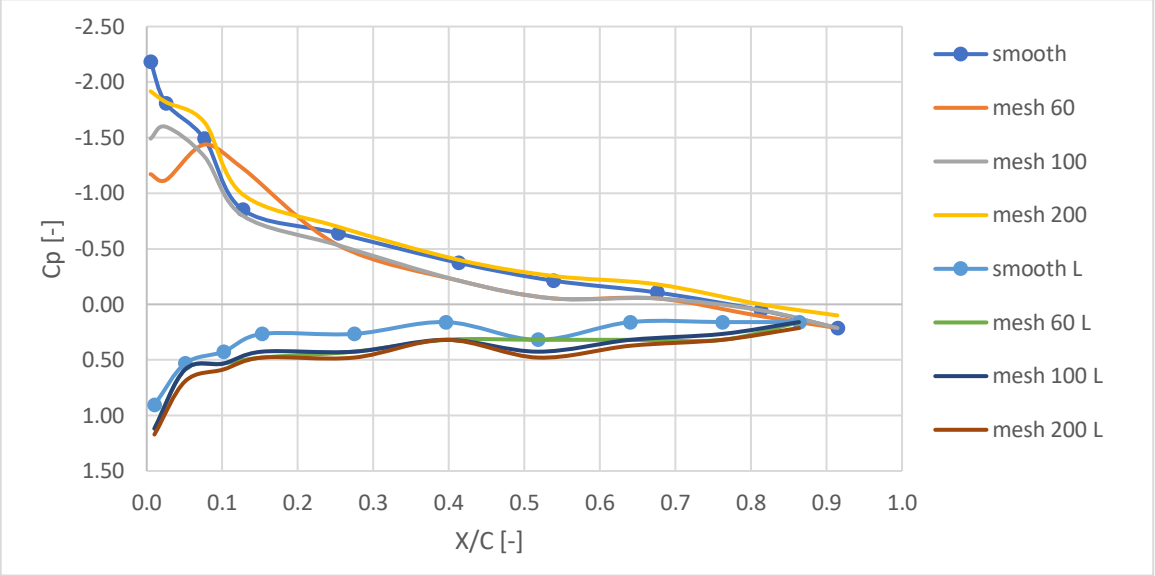

(a)

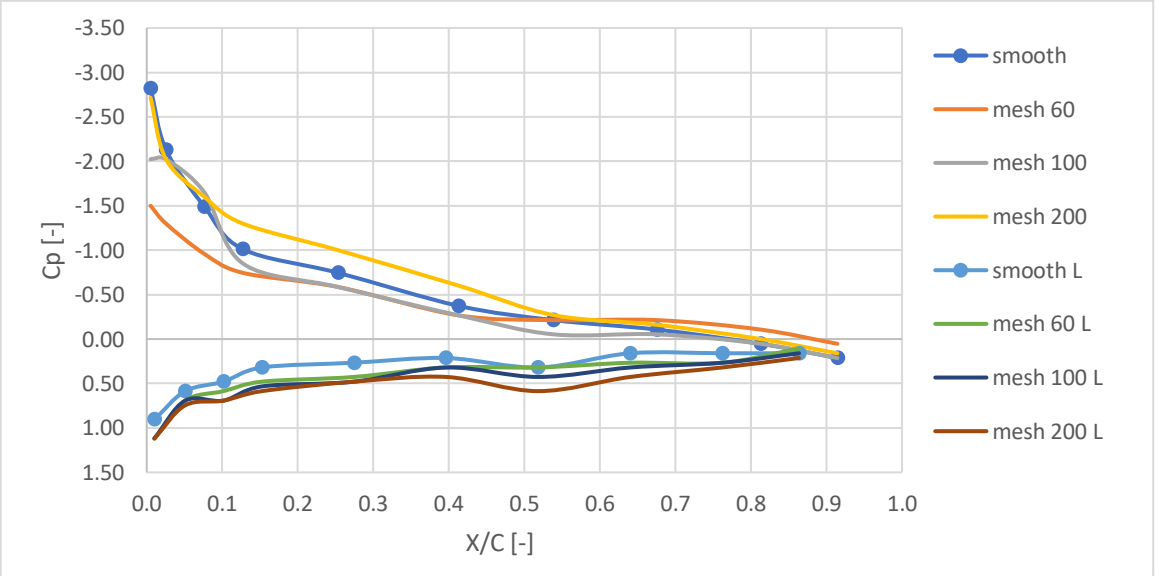

(b)

Figure (4.11) Pressure Coefficients Distribution Along Airfoil Chord For NACA 0012 at *Re* = 1.67×10^5 and Angle of Attack a) α =8 b) α =10

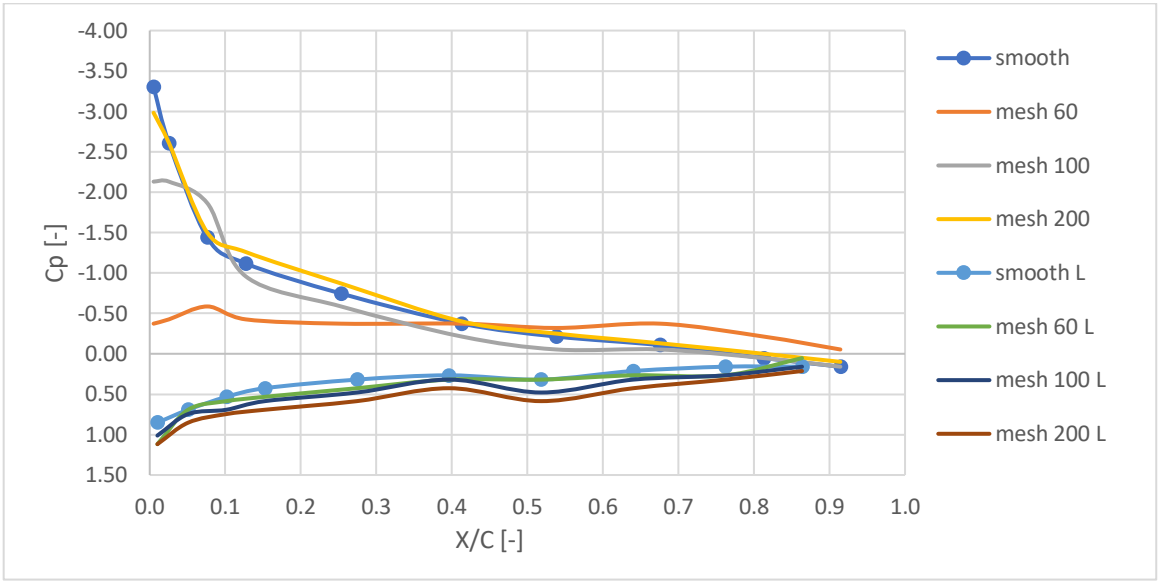

(a)

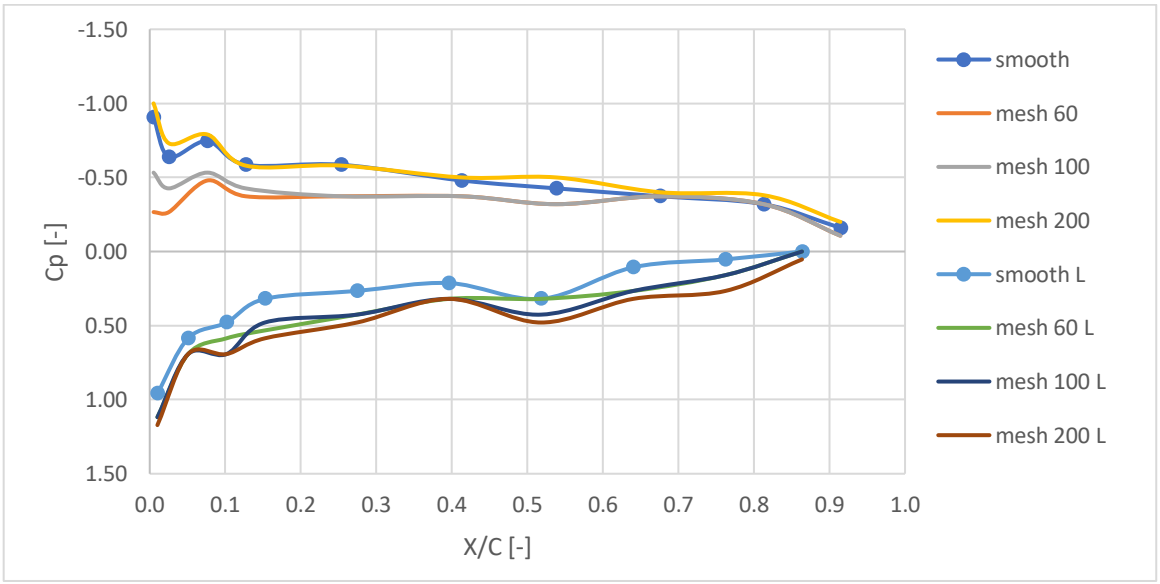

(b)

Figure (4.12) Pressure Coefficients Distribution Along Airfoil Chord For NACA 0012 at *Re* = 1.67×10^5 and Angle of Attack a) α =12 b) α =14

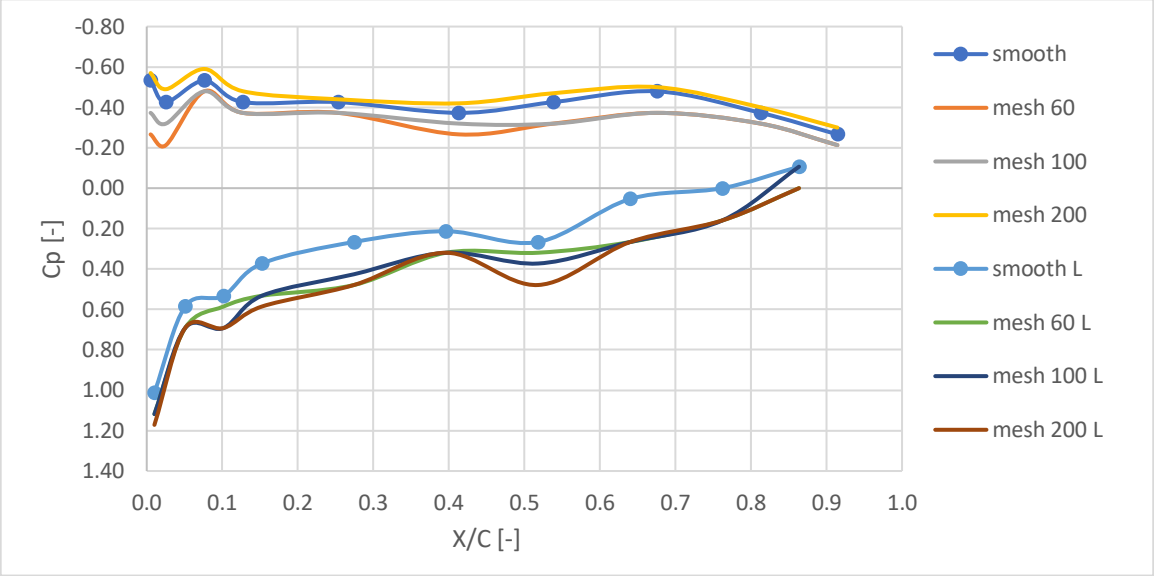

Figure (4.13) Pressure Coefficients Distribution Along Airfoil Chord For NACA 0012 at *Re* = 1.67×10^5 and Angle of Attack α =16

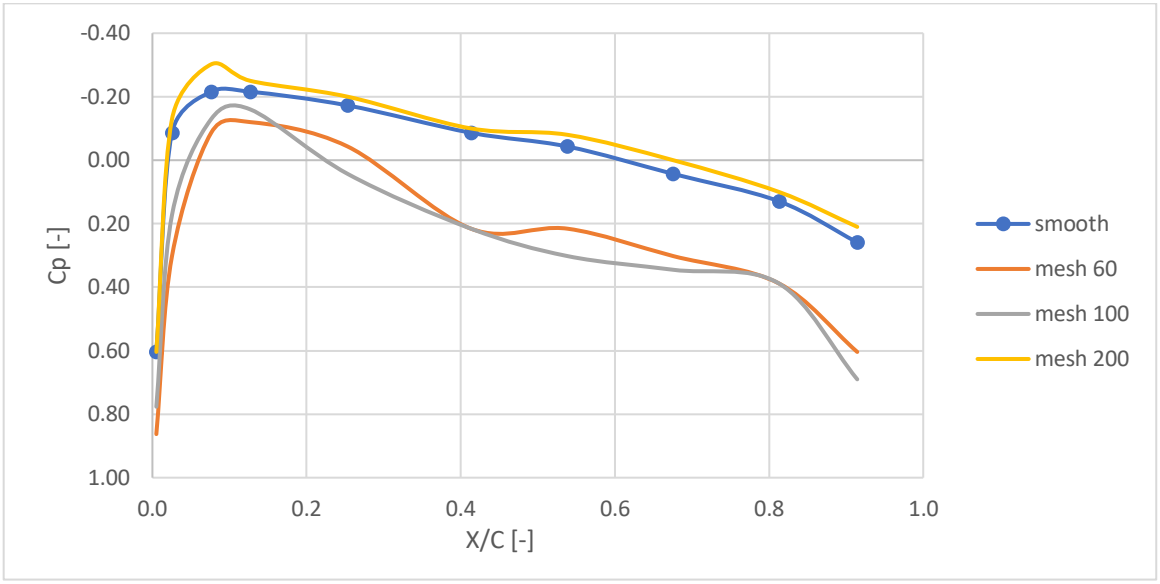

(a)

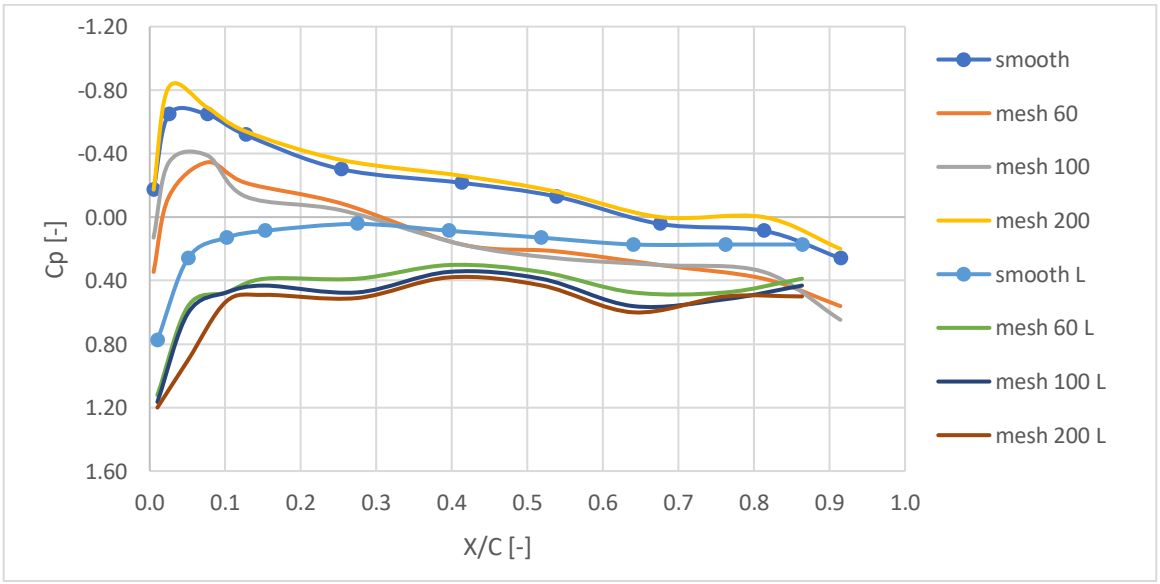

(b)

Figure (4.14) Pressure Coefficients Distribution Along Airfoil Chord For NACA 0012 at *Re* = $1.86\times10^5$and Angle of Attack a) α =0 b) α =2

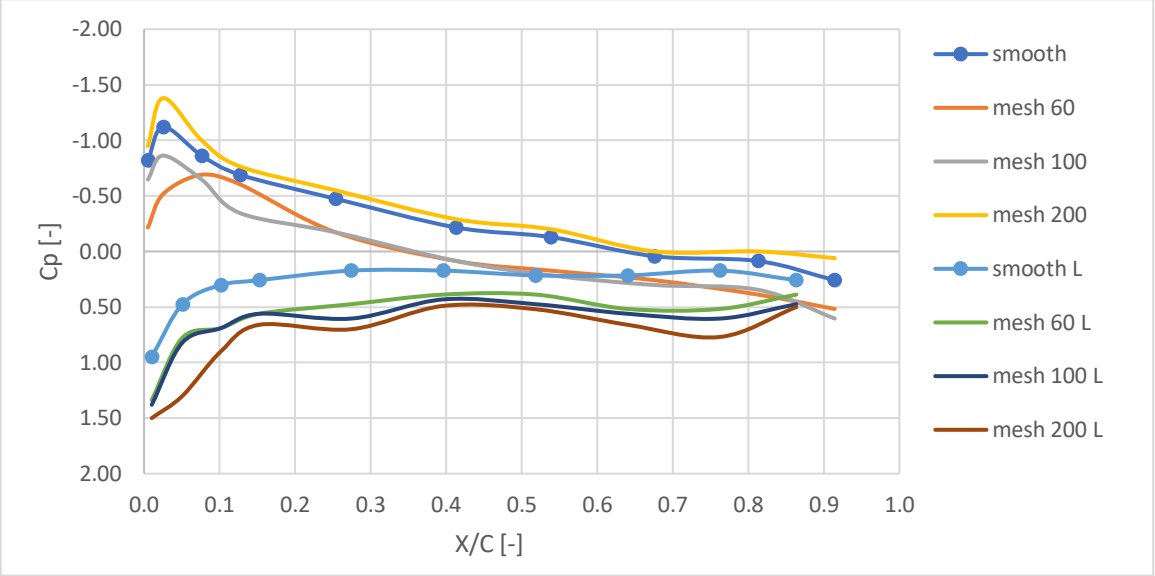

(a)

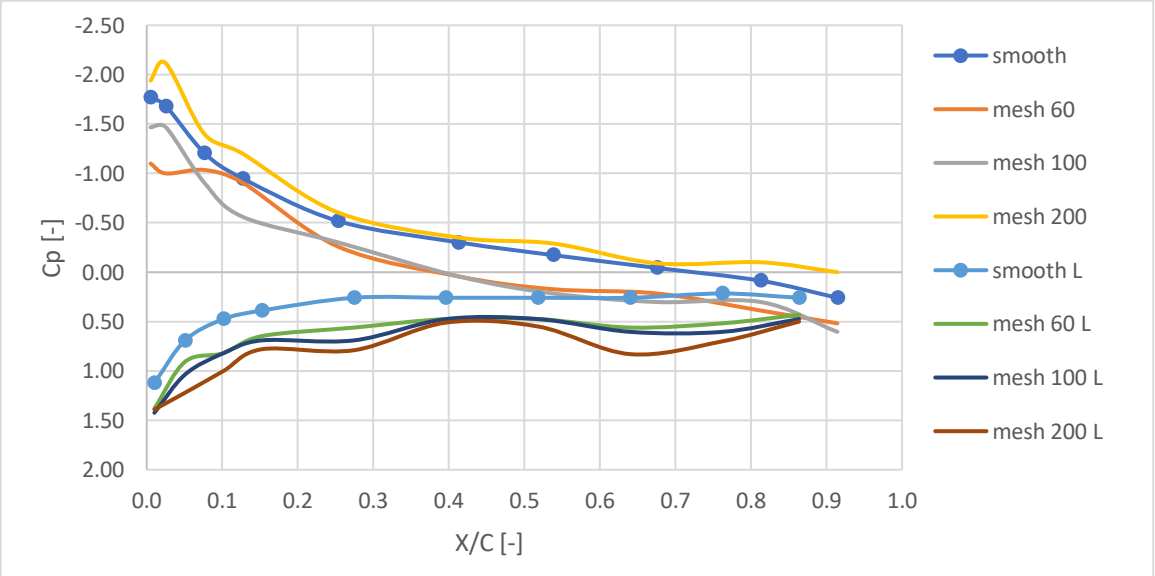

(b)

Figure (4.15) Pressure Coefficients Distribution Along Airfoil Chord For NACA 0012 at *Re* = $1.86\times10^5$and Angle of Attack a) α =4 b) α =6

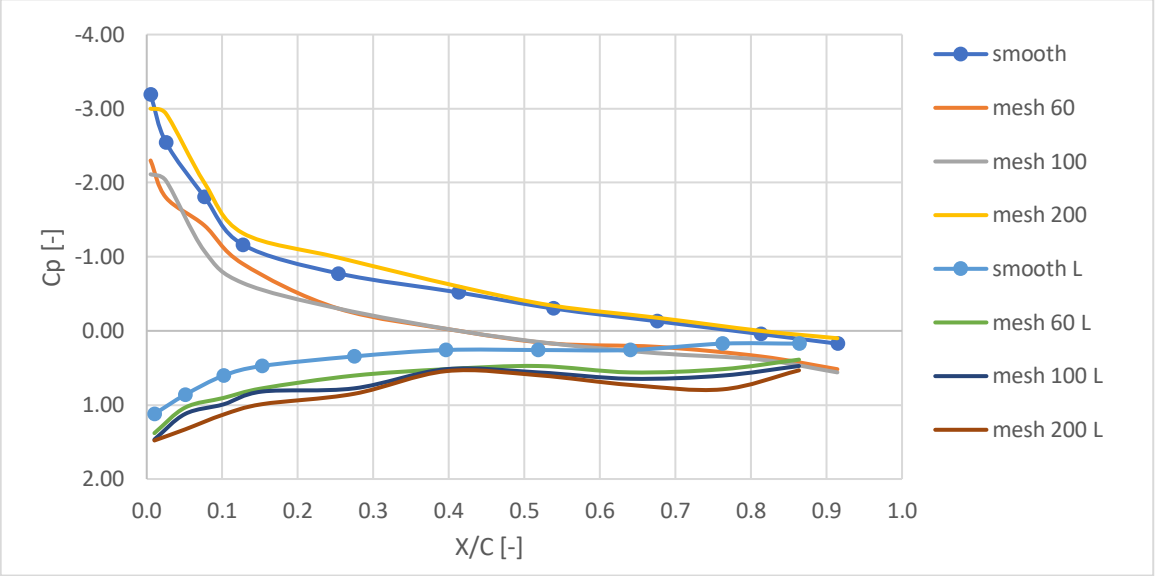

(a)

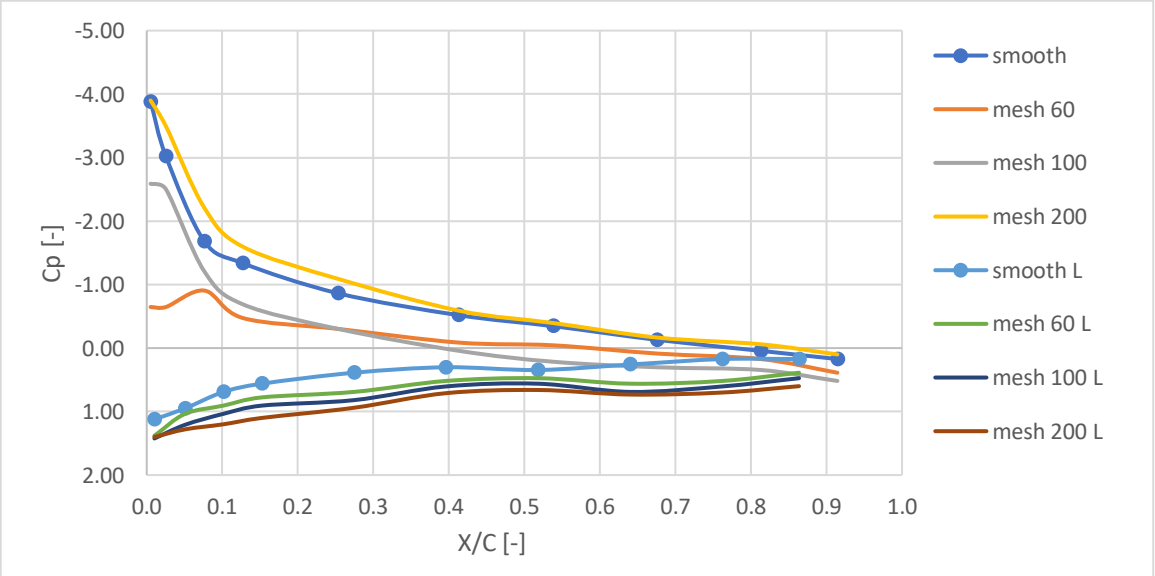

(b)

Figure (4.16) Pressure Coefficients Distribution Along Airfoil Chord For NACA 0012 at *Re* = 1.86×10^5 and Angle of Attack a) α =8 b) α =10

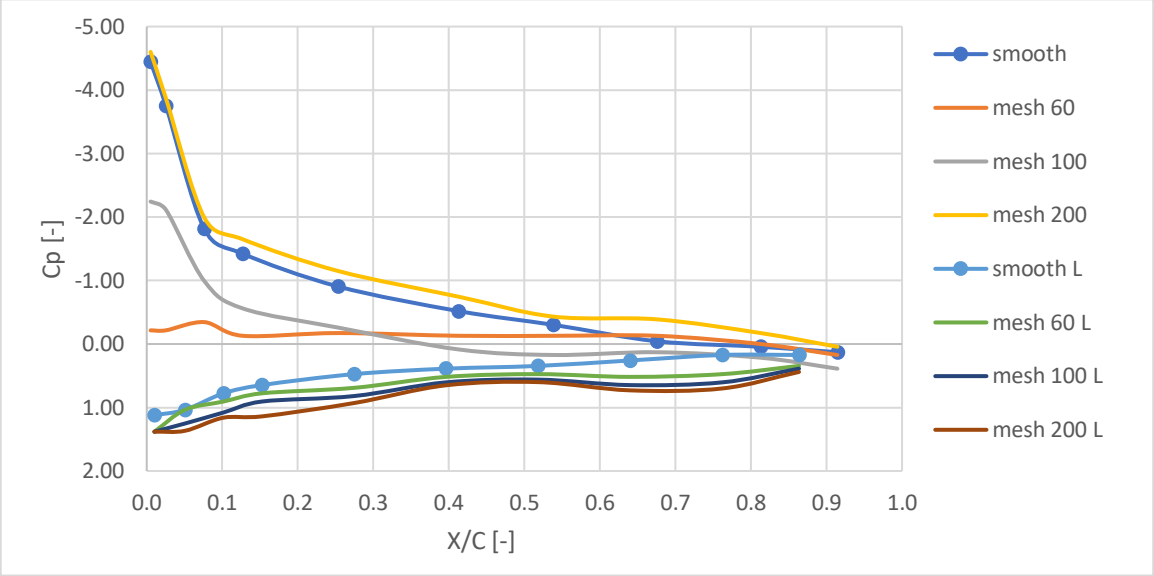

(a)

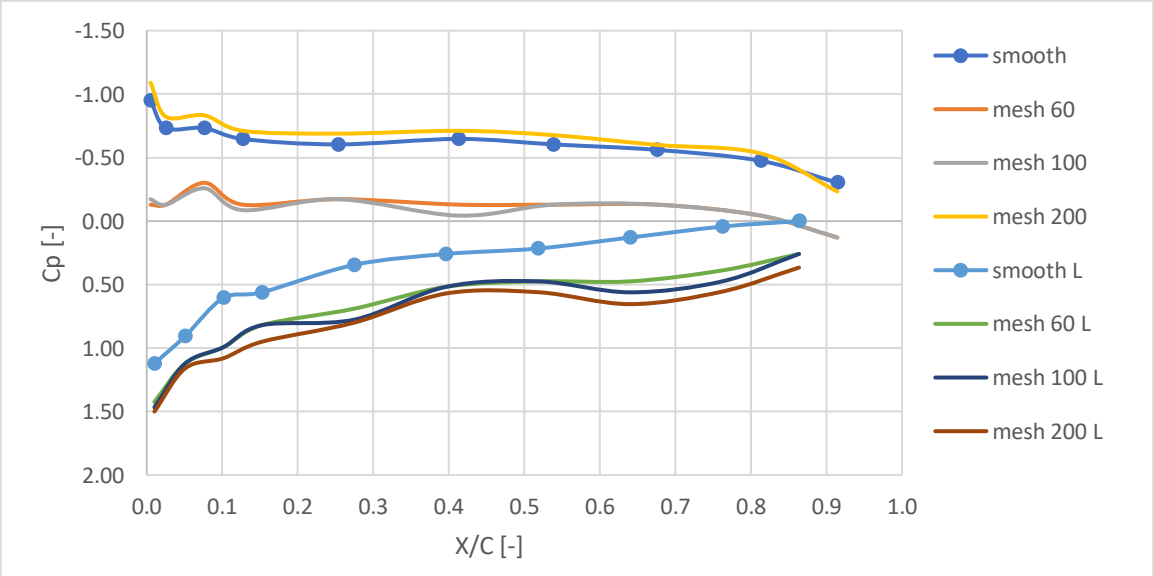

(b)

Figure (4.17) Pressure Coefficients Distribution Along Airfoil Chord For NACA 0012 at *Re* = 1.86×10^5 and Angle of Attack a) α =12 b) α =14

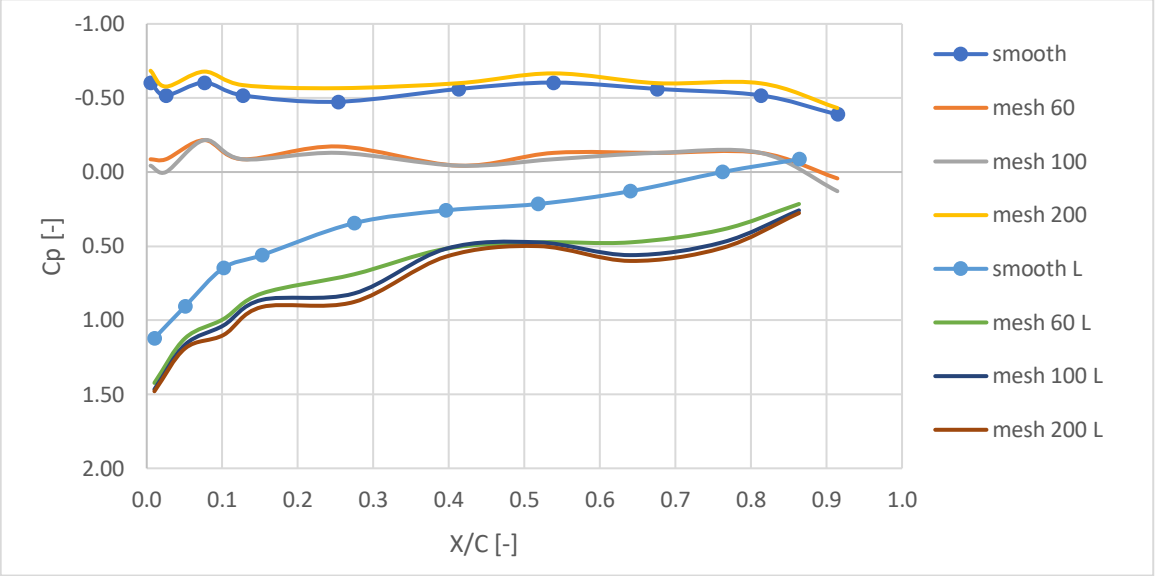

Figure (4.18) Pressure Coefficients Distribution Along Airfoil Chord For NACA 0012 at *Re* = 1.86×10^5 and Angle of Attack α =16

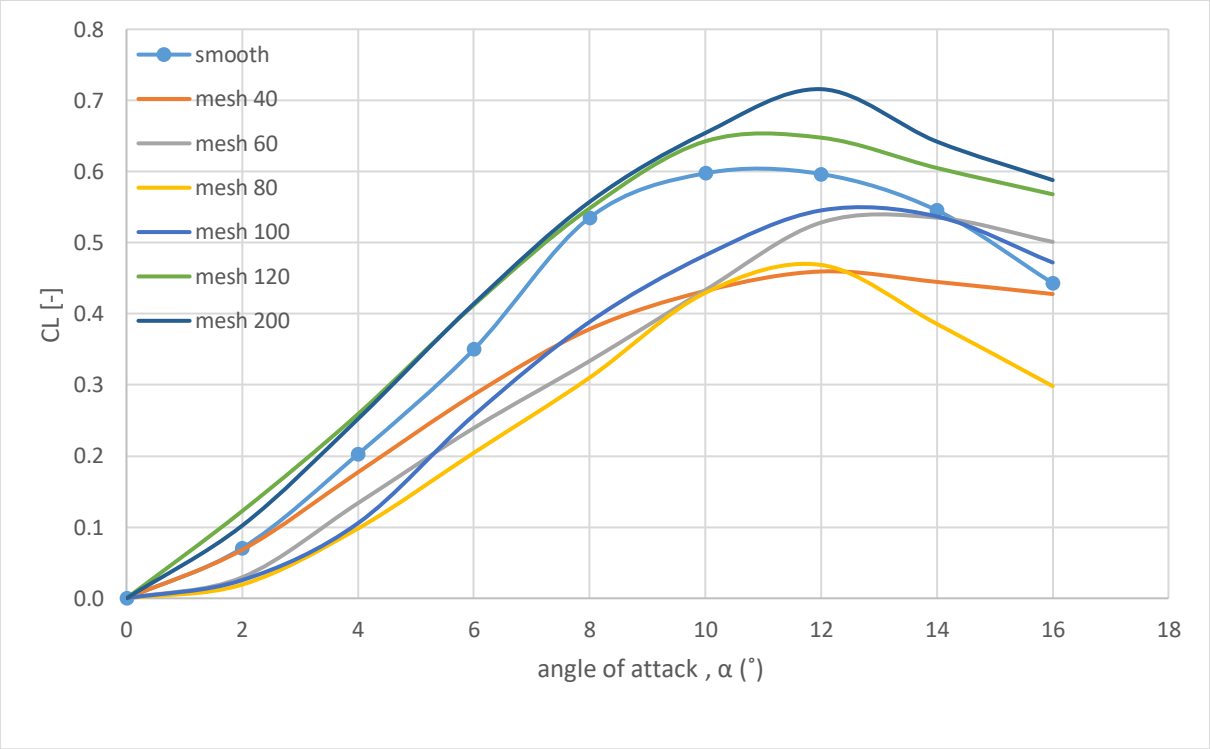

Figure (4.19) Lift Coefficients Verses Angle of Attack for smooth and rough surfaces at $Re = 1.39\times10^5$

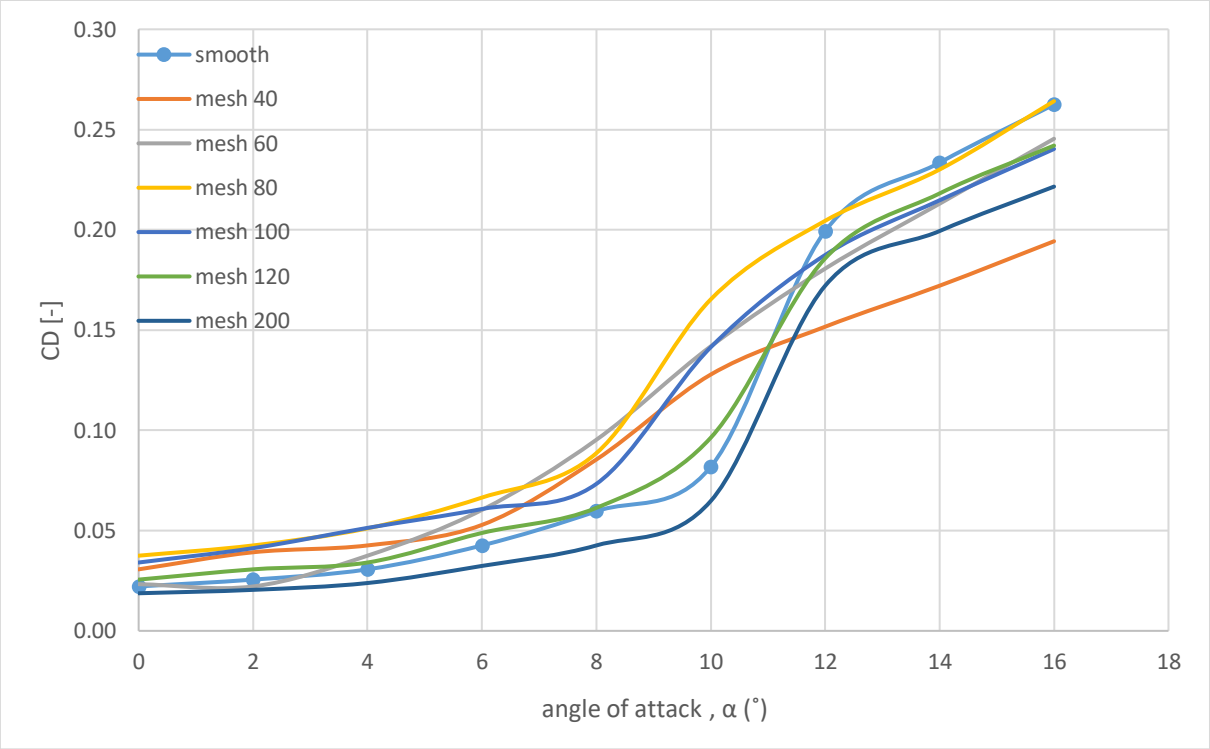

Figure (4.20) Drag Coefficients Verses Angle of Attack for smooth and rough surfaces at $Re = 1.39\times10^5$

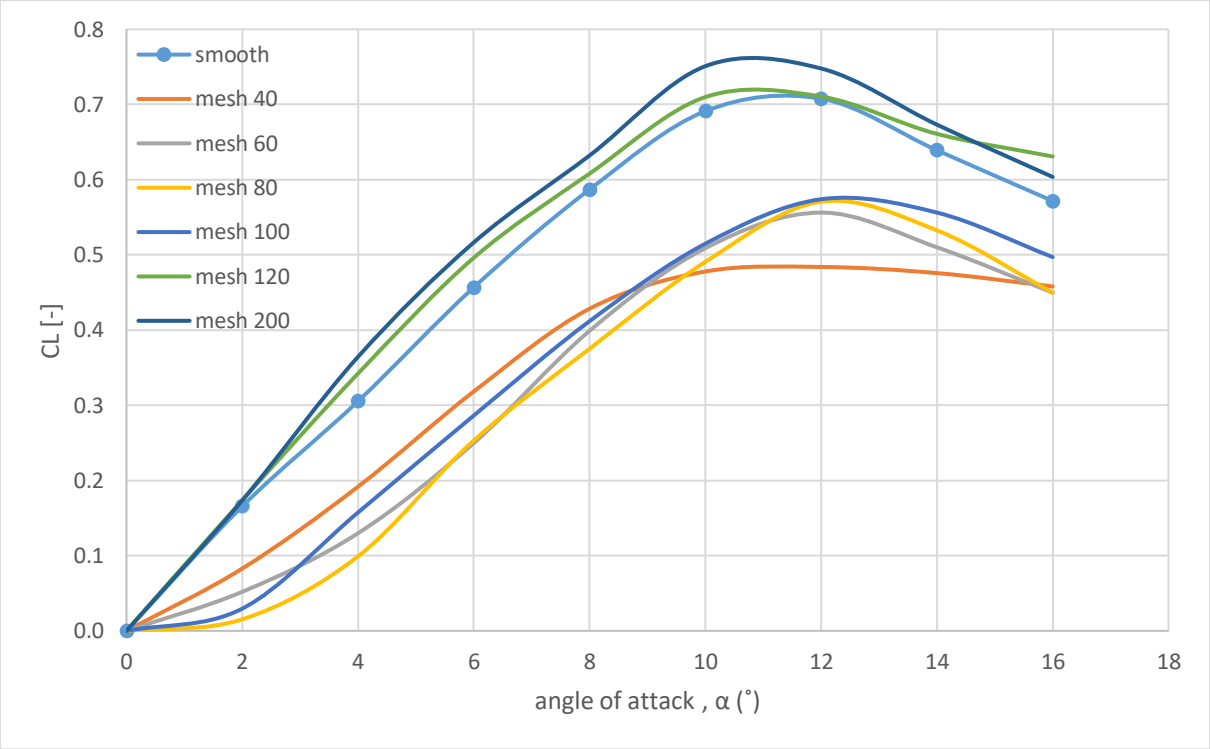

Figure (4.21) Lift Coefficients Verses Angle of Attack for smooth and rough surfaces at $Re = 1.67\times10^5$

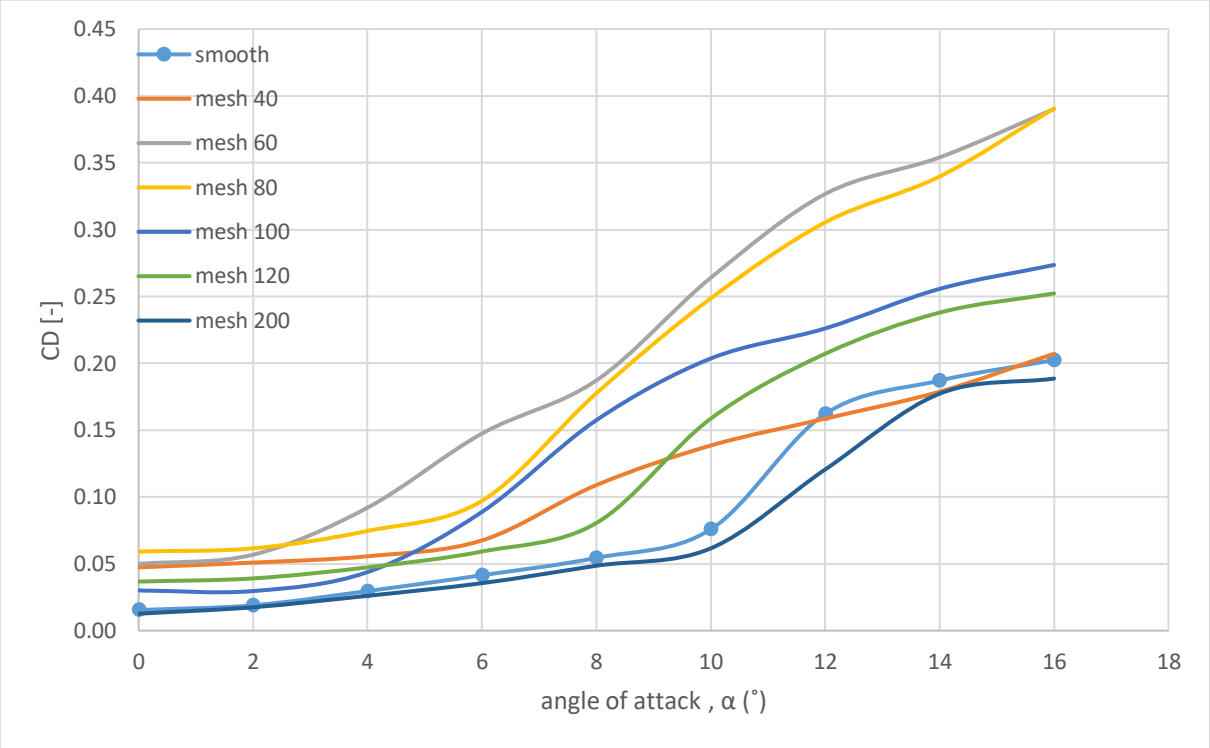

Figure (4.22) Drag Coefficients Verses Angle of Attack for smooth and rough surfaces at $Re = 1.67\times10^5$

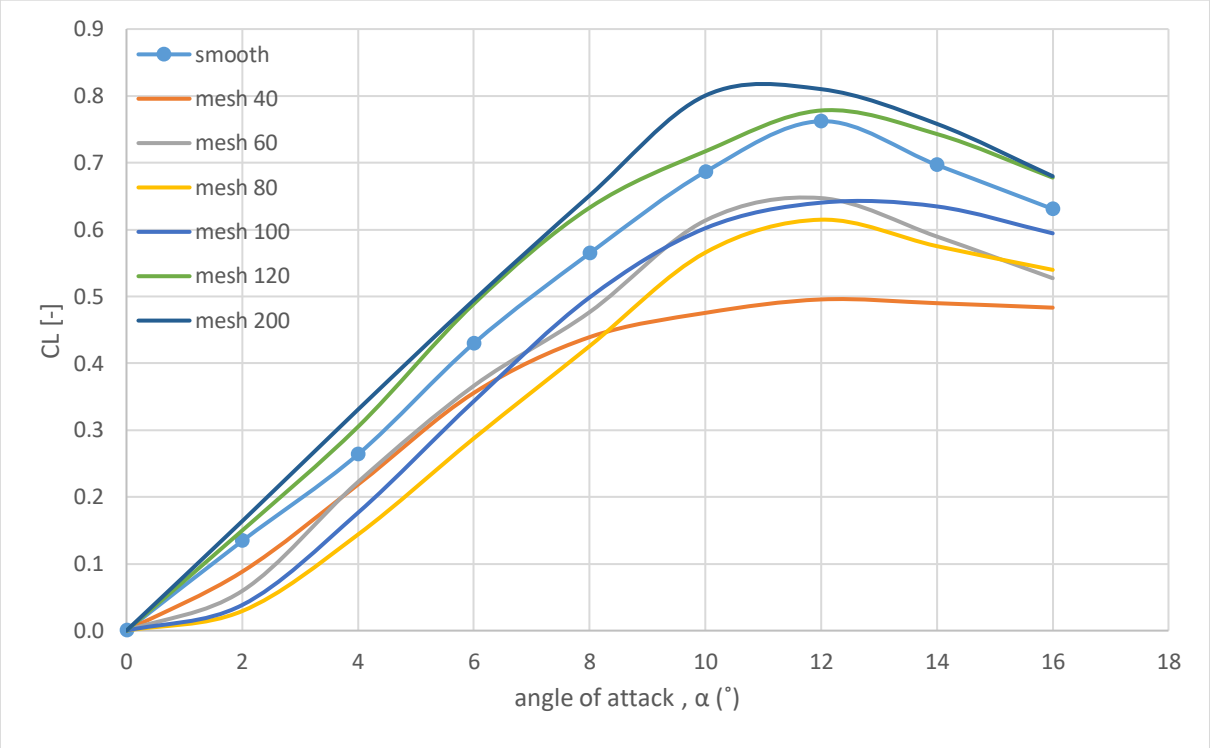

Figure (4.23) Lift Coefficients Verses Angle of Attack for Smooth and Rough Surfaces at $Re = 1.86\times10^5$

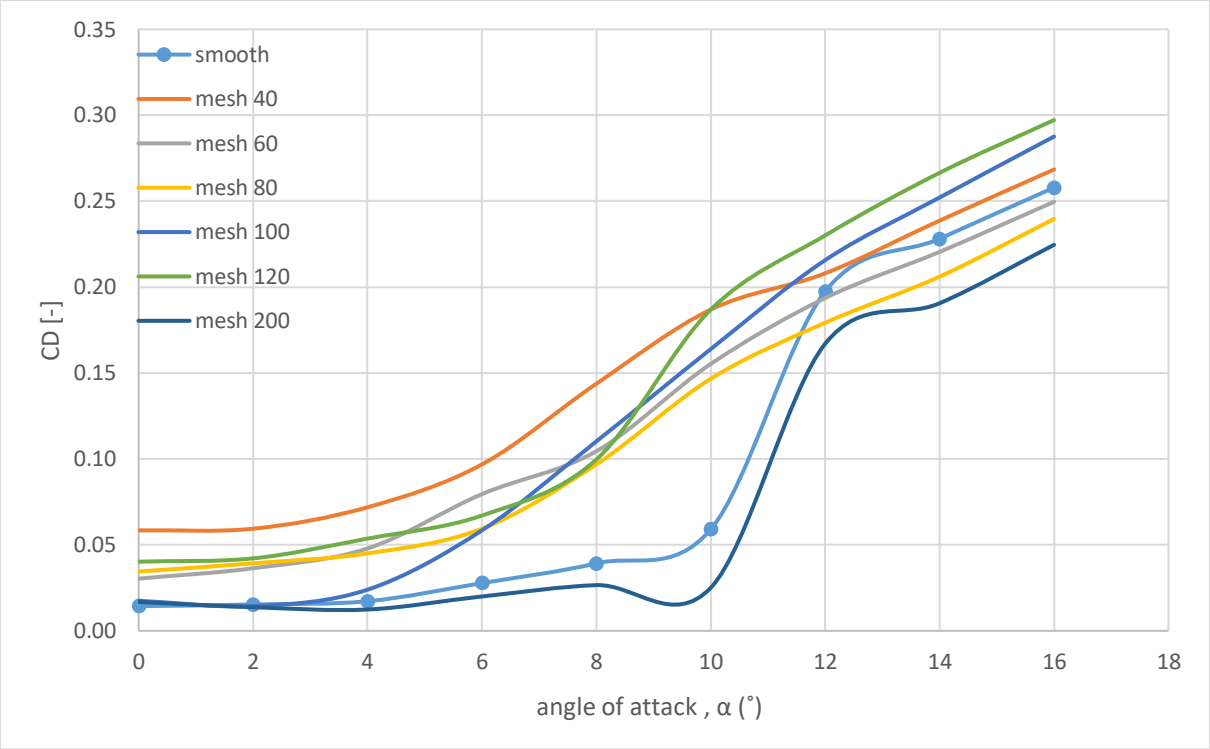

Figure (4.24) Drag Coefficients Verses Angle of Attack for smooth and rough surfaces at $Re = 1.86\times10^5$

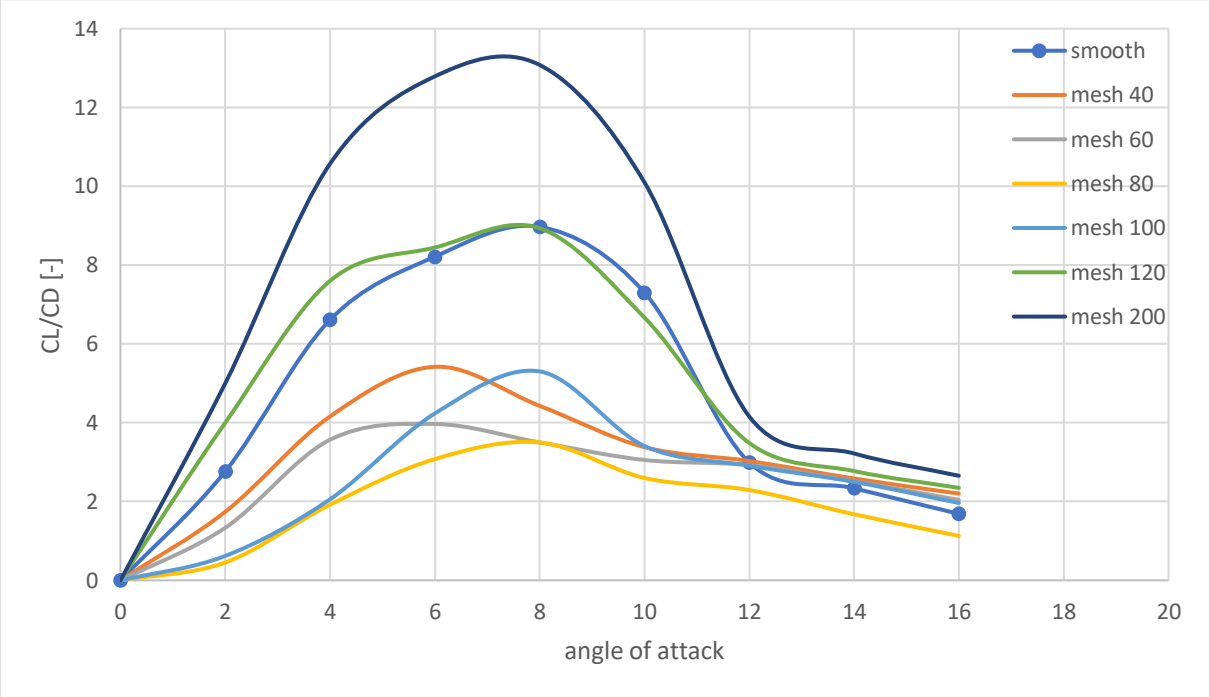

Figure (4.25) Experimental *Cl* /*Cd* Ratio Verses Angle of Attack For NACA 0012 at *Re* = 1.39×10^5

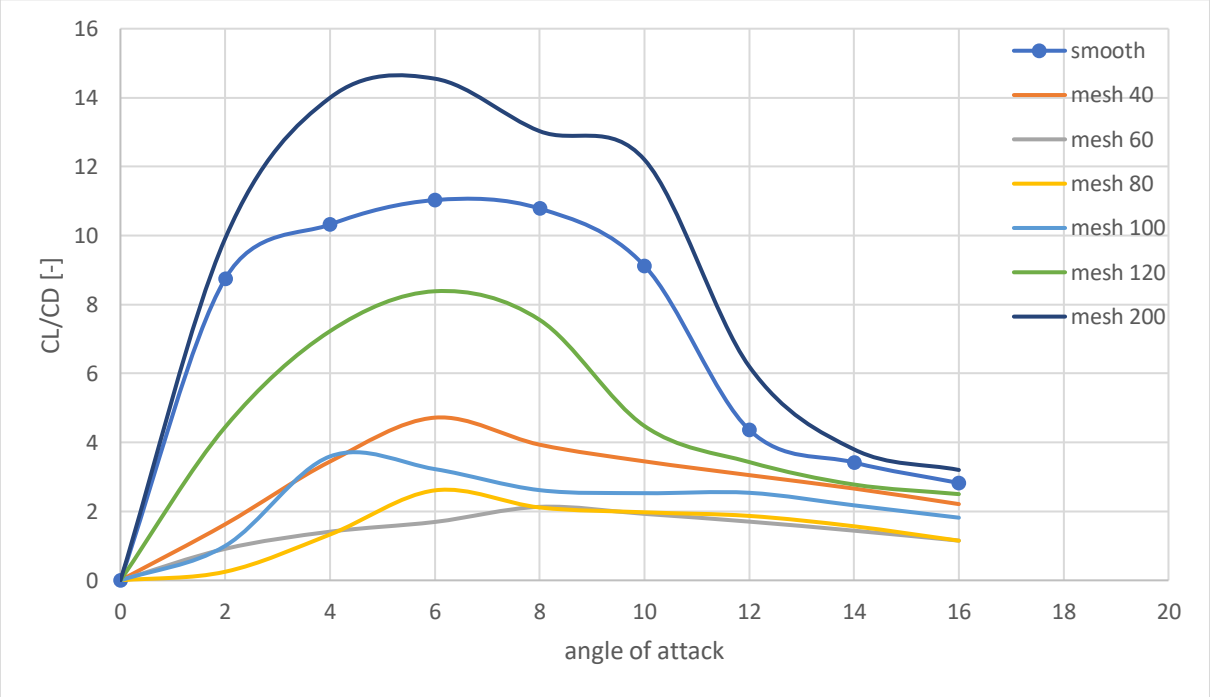

Figure (4.26) Experimental *Cl* /*Cd* Ratio Verses Angle of Attack For NACA 0012 at *Re* = 1.67×10^5

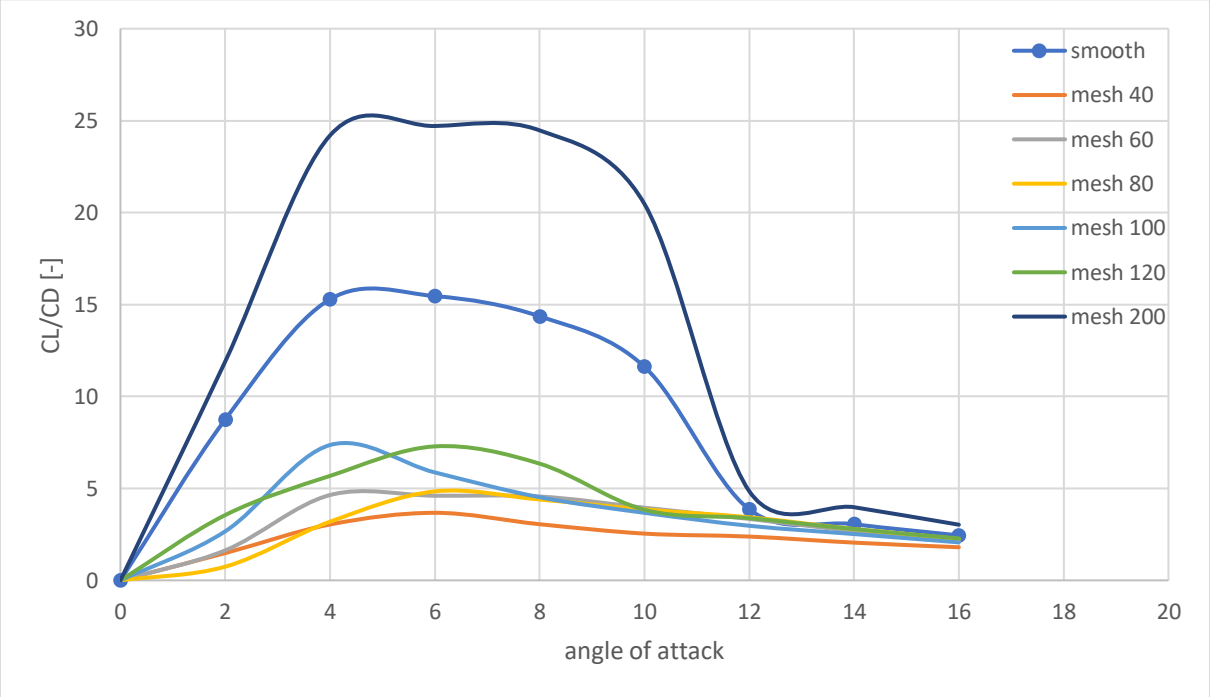

Figure (4.27) Experimental *Cl* /*Cd* Ratio Verses Angle of Attack For NACA 0012 at *Re* = 1.86×10^5

CHAPTER FIVE

CONCLUSIONS

AND

RECOMMENDATIONS

CHAPTER FIVE

CONCLUSIONS AND RECOMMENDATIONS

From the discussion of the experimental results for the present work, the following conclusions may be drawn:

5.1 Conclusions

1) The distribution of pressure area with a rough surface is greater than a smooth surface. Surface model (Mo.6) has a greater total surface area for all measurements.
2) The results show clear evidence of a small increase in lift and a decrease in drag for NACA 0012 over different angles of attack, when the flow is modified within the rough surface models (Mo.6). Model (Mo.6) has a maximum drag coefficient recorded reduction of (18%), also it gives the highest value of enhancement in lift coefficient of (12%) for NACA 0012.

3) Stall angle of attack is unaffected by roughness, so the (Cl/Cd) ratio increases to maximum value (Cl/Cd=25) for NACA 0012 at Reynold number 1.86×10^5

4) The rough surface flow velocity gradient was lower than the smooth surface gradient, thus meaning a decrease in the momentum, energy, and displacement thicknesses.

5.2 Recommendations for Future Work

The increase in lift and decrease in drag of wing is importance to the aircraft performance involving fluid flow. Controlling boundary layer (active or passive) leads to drag reduction and lift enhancement on airfoil. For future work, the following points can be recommended:

1) Repeating the previous experiments for the same conditions by using flow visualizations to recognize the flow structure qualitative on the smooth and modified surface.
2) Studying experimentally the distribution of skin friction coefficient and shear stress on the rough surface models.
3) For studying the effect of heat and rough surface on boundary layer characteristics, we can add a heat source function on the airfoil model with rough surfaces.
4) Mathematical model to estimate the lift and drag theoretically and to compare with the experimental work.
5) Repeating the use of wind tunnel for the same conditions of the previous experiments and the same rough surface models on the flat plate to estimate the lift and drag behavior.
6) Influence of rough surface models on the wake area being tested experimentally and theoretically.

REFERENCE

REFERENCE

[1] Matthew McCarty "The Measurement of the Pressure Distribution over the Wing of an Aircraft in Flight "University of New South Wales, 2008.

[1] Bechert D. W., Bartenwerfer M., Hoppe G., Reif W. E, "*Drag Reduction Mechanisms Derived from Shark Skin*", Presented at the 15th ICAS Congress, London, 86-1.8.3, distributed as AIAA paper, 1986.

[2] Gupta B., Goodman R., Fukang-Jiang, Yu-Chong-Tai, Tung, S., and Chih-Ming Ho, "Analog VLSI system for active drag reduction", IEEE-Micro. Vol. 16, PP(53-59), 1996.

[3] Stefan A, "The Shark Coating ", SOFTPEDIA, 16 Dec 2006.

[4] Szodruch J, "Viscous Drag Reduction on Transport Aircraft", AIAA Paper 91-0685, 1991.

[5] Report of the Group of Personalities. European Aeronautics: A vision for 2020. January 2001.

[6] https://aerospaceengineeringblog.com/boundary-layers/

[7] Hussain Abed Ali Shinan "Numerical and Experimental Study of the Boundary Layer Separation Control on the NACA 0012 Airfoil using Triangular Rib"

[8] Green J. E, "Civil Aviation and the Environment Challenge", The Aeronautical Journal, June 2003.

[9] "Airfoil Boundary-Layer Control through Pulsating Jets"

[10] Vivek Gupta " Boundary Layer Studies on Rough Flat Plates Under Negative Pressure Gradient"

[11] Vivek Gupta" Boundary Layer Studies on Rough Flat Plates Under Negative Pressure Gradient" Department of Civil Engineering National Institute of Technology Rourkela Orissa (2014)

[12] Imad S. Ali and Noor H. Al-Fatlawie" Drag Reduction In Turbulent Flow using Different Kinds of Riblets" University of Babylon Hilla- Iraq (2011).

[13] Rzuqe M. H, "Drag reduction in fluid flow by using longitudinal ribs", Mechanical Engineering Department, University of Technology, M. SC Thesis, 1988.

[14] Walsh M. J, "Riblets as a Viscous Drag Reduction Technique", AIAA Journal, Vol. 21, PP(485–486), 1983**.**

[15] Debisschop J. R., Nieuwstadt F. M, "Turbulent Boundary Layer in an Adverse Pressure Gradient: Effectiveness of Riblets", AIAA Journal, 34(5), PP(932–937), 1996.

[16] Parker K., Sayers A.T, "The Effect of Longitudinal Microstriations and their profiles in the Drag of Flat Plate", Department of Mechanical Engineering, University of Cope Town, South Africa, Proc Instn Mech Engrs Vol. 213, 1999.

[17] Yan Zhang, Takafumi Igarashi and Hui Hu" Experimental Investigations on the Performance Degradation of a Low-Reynolds-Number Airfoil with Distributed Leading Edge Roughness" Iowa State University,(2011).

[18] Michael F. Kerho and Michael B. Bragg "Airfoil Boundary-Layer Development and Transition with Large Leading-Edge Roughness**"** University of Illinois (1997).

[19] Diane R. Bloch and Thomas J. Mueller" Effects of Distributed Grit Roughness on Separation And Transition on An Airfoil At Low Reynolds Numbers" Department o f Aerospace and Mechanical Engineering University of Notre Dame.(1986).

[20] Walid Chakroun, Issa Al-Mesri and Sami Al-Fahad" Effect of Surface Roughness on the Aerodynamic Characteristics of a Symmetrical Airfoil" Kuwait University, Mechanical Engineering Department(2004).

[21] Adel Ahmed Abdel-Rahman and W. Chakroun" Surface roughness effects on flow over aerofoils"(1997)

[22] Mahbubur Rahman, Md. Amzad Hossain, Md. Nizam Uddin and Mohammad Mashud" Experimental Study of Passive Flow Separation Control Over A NACA 0012 Airfoil" (2015)

[23] Nibras Mohammed Mahdi "Effect of Riblets Geometry on Drag Reduction and Its Application on Airfoils" the Mechanical Engineering Department,

University of Technology(2000)

[24] Md. Mahbub Alam . Y. Zhou . H. X. Yang . H. Guo . J. Mi "The ultra-low Reynolds number airfoil wake" (2009).

[25] Zambri Harun, Ashraf Amer Abbas, Eslam Reda Lotfy and Morteza Khashehchi "Turbulent structure effects due to ordered surface roughness" Alexandria University (2020)

[26] K. Freudenreich, K. Kaiser "Reynolds Number and Roughness Effects on Thick Airfoils for Wind Turbines" (2004)

[27] Coustols E., Cousteix J, "Experimental Investigation of Turbulent Boundary Layers Manipulated with Internal Devises: Riblet", In: Gry A, editor.

Proceedings of the IUTAM Symposium on Structure of Turbulent and Drag Reduction. Berlin: Springer, pp(577–584), 1990.

[28] Viswanath "Aircraft viscous drag reduction using riblets", Experimental Aerodynamics Division, National Aerospace Laboratories, India.

[29] Viswanath P. R, "Aircraft Viscous Drag Reduction using Riblets", Progress in Aerospace Sciences, Vol. 38, PP(571–600), 2002.

[30] Mclean J. D., George–Falvy D. N., Sullivan P. P, "Flight–Test of Turbulent Skin Friction Reduction by Riblets", Proceedings of International Conference on Turbulent Drag Reduction by Passive Means, Section 16, London: Royal Aeronautical society, PP(1–17), 1987.

[31] Squire L. C., Savill A. M, "Drag Measurements on Planar Riblet Surfaces at high Subsonic Speeds" APPL Sci Res. 46, PP(229–243), 1989.

[32] D. Luo, D. Huang, and X. Sun, “Passive flow control of a stalled airfoil using a microcylinder,” J. Wind Eng. Ind. Aerodyn., vol. 170, no. March, pp. 256–273, 2017.

[33] A. K. Saraf, M. P. Singh, and T. S. Chouhan, “Effect of Dimple on Aerodynamic Behaviour of Airfoil,” vol. 9, no. 3, pp. 2268–2277, 2017.

[34] V. del Campo, D. Ragni, D. Micallef, J. Diez, and C. J. Simão Ferreira, “Estimation of loads on a horizontal axis wind turbine,” Wind Energy, vol. 18, no. 11, pp. 1875–1891, 2015.

[35] S. Gildersleeve, D. Clingman, and M. Amitay, “Separation Control over a Flapped NACA 0012 Model using an Array of Low Aspect Ratio Cylindrical Pins,” no. June, pp. 1–19, 2016.

[36] A. G. Domel, K. Bertoldi, M. Saadat, G. V. Lauder, J. C. Weaver, and H. Haj-Hariri, "Shark skin-inspired designs that improve aerodynamic performance," J. R. Soc. Interface, vol. 15, no. 139, pp. 1–9, 2018.

[37] S. K. Rasal and R. R. Katwate, "EXPERIMENTAL INVESTIGATION OF LIFT & DRAG PERFORMANCE OF NACA0012 WIND TURBINE AEROFOIL," pp. 265–270.

[38] R. R. Leknys, M. Arjomandi, R. M. Kelso, and C. H. Birzer, "Journal of Wind Engineering & Industrial Aerodynamics Thin airfoil load control during post-stall and large pitch angles using leading-edge trips," vol. 179, no. May, pp. 80–91, 2018.

[33] TecQuipment Ltd 2013 "Af102" User Guide

APPENDIX A

The Experimental Data

Table A.1 Smooth Surface Data(pressure) at Re=1.39×10^5

	x/c	Pt a=16	Pt a=14	Pt a=12	Pt a=10	Pt a=8	Pt a=6	Pt a=4	Pt a=2	Pt a=0
Upper surface	0.005	-0.20	-0.23	-0.52	-0.46	-0.36	-0.29	-0.20	-0.12	-0.07
	0.025	-0.17	-0.19	-0.44	-0.37	-0.32	-0.29	-0.22	-0.18	-0.14
	0.076	-0.18	-0.20	-0.30	-0.33	-0.28	-0.26	-0.21	-0.19	-0.16
	0.127	-0.18	-0.19	-0.25	-0.24	-0.24	-0.23	-0.19	-0.18	-0.15
	0.253	-0.17	-0.18	-0.20	-0.20	-0.20	-0.18	-0.17	-0.17	-0.15
	0.413	-0.16	-0.16	-0.16	-0.16	-0.15	-0.15	-0.15	-0.15	-0.13
	0.538	-0.15	-0.17	-0.14	-0.14	-0.14	-0.14	-0.14	-0.14	-0.12
	0.676	-0.17	-0.17	-0.12	-0.13	-0.13	-0.13	-0.12	-0.13	-0.12
	0.813	-0.15	-0.15	-0.10	-0.10	-0.11	-0.11	-0.11	-0.12	-0.12
	0.914	-0.13	-0.13	-0.08	-0.08	-0.08	-0.08	-0.08	-0.09	-0.09
Lower surface	0.010	0.01	0.00	0.00	0.00	0.00	0.00	-0.02	-0.04	-0.08
	0.051	-0.03	-0.05	-0.03	-0.04	-0.06	-0.06	-0.10	-0.11	-0.15
	0.102	-0.06	-0.06	-0.05	-0.06	-0.08	-0.08	-0.11	-0.13	-0.15
	0.152	-0.06	-0.07	-0.06	-0.07	-0.08	-0.10	-0.11	-0.13	-0.14
	0.274	-0.08	-0.08	-0.07	-0.08	-0.08	-0.10	-0.11	-0.12	-0.13
	0.396	-0.09	-0.09	-0.07	-0.09	-0.09	-0.10	-0.10	-0.12	-0.12
	0.518	-0.08	-0.08	-0.08	-0.08	-0.09	-0.09	-0.10	-0.11	-0.11
	0.640	-0.10	-0.10	-0.08	-0.09	-0.10	-0.10	-0.11	-0.11	-0.11
	0.762	-0.11	-0.10	-0.10	-0.10	-0.10	-0.10	-0.10	-0.10	-0.11
	0.864	-0.12	-0.11	-0.10	-0.10	-0.10	-0.10	-0.10	-0.11	-0.11

Table A.2 rough Surface (Mo.1) Data(pressure) at Re=1.39×10^5

	x/c	Pt a=16	Pt a=14	Pt a=12	Pt a=10	Pt a=8	Pt a=6	Pt a=4	Pt a=2	Pt a=0
Upper surface	0.005	-0.18	-0.20	-0.22	-0.29	-0.28	-0.21	-0.16	-0.10	-0.05
	0.025	-0.17	-0.20	-0.22	-0.31	-0.29	-0.24	-0.20	-0.17	-0.14
	0.076	-0.20	-0.21	-0.25	-0.34	-0.31	-0.26	-0.23	-0.20	-0.17
	0.127	-0.18	-0.19	-0.21	-0.26	-0.23	-0.23	-0.21	-0.18	-0.16
	0.253	-0.18	-0.19	-0.20	-0.19	-0.20	-0.18	-0.18	-0.17	-0.16
	0.413	-0.16	-0.17	-0.16	-0.15	-0.15	-0.15	-0.15	-0.14	-0.13
	0.538	-0.17	-0.17	-0.17	-0.14	-0.14	-0.14	-0.14	-0.14	-0.14
	0.676	-0.18	-0.17	-0.17	-0.13	-0.13	-0.13	-0.13	-0.13	-0.13
	0.813	-0.17	-0.15	-0.15	-0.12	-0.12	-0.12	-0.12	-0.12	-0.12
	0.914	-0.15	-0.13	-0.12	-0.10	-0.10	-0.08	-0.08	-0.08	-0.08
Lower surface	-0.08	0.02	0.02	0.02	0.02	0.02	0.00	-0.02	-0.05	-0.08
	-0.15	-0.03	-0.03	-0.03	-0.03	-0.05	-0.07	-0.10	-0.11	-0.15
	-0.15	-0.05	-0.04	-0.04	-0.05	-0.07	-0.08	-0.11	-0.13	-0.15
	-0.14	-0.06	-0.06	-0.06	-0.06	-0.08	-0.10	-0.11	-0.13	-0.14
	-0.13	-0.07	-0.07	-0.07	-0.07	-0.08	-0.10	-0.10	-0.11	-0.13
	-0.13	-0.08	-0.08	-0.08	-0.08	-0.09	-0.10	-0.11	-0.12	-0.13
	-0.12	-0.08	-0.08	-0.08	-0.08	-0.08	-0.09	-0.10	-0.11	-0.12
	-0.12	-0.10	-0.10	-0.10	-0.09	-0.10	-0.10	-0.11	-0.11	-0.12
	-0.11	-0.11	-0.10	-0.10	-0.10	-0.10	-0.10	-0.11	-0.11	-0.11
	-0.13	-0.13	-0.13	-0.11	-0.11	-0.11	-0.11	-0.11	-0.12	-0.13

Table A.3 rough Surface (Mo.2) Data(pressure) at Re=1.39×10^5

	x/c	Pt a=16	Pt a=14	Pt a=12	Pt a=10	Pt a=8	Pt a=6	Pt a=4	Pt a=2	Pt a=0
Upper surface	0.005	-0.10	-0.11	-0.15	-0.23	-0.21	-0.15	-0.08	-0.03	0.00
	0.025	-0.10	-0.10	-0.14	-0.22	-0.20	-0.17	-0.12	-0.08	-0.05
	0.076	-0.15	-0.15	-0.18	-0.28	-0.25	-0.21	-0.16	-0.15	-0.11
	0.127	-0.13	-0.13	-0.15	-0.24	-0.21	-0.18	-0.14	-0.12	-0.11
	0.253	-0.13	-0.13	-0.14	-0.15	-0.15	-0.13	-0.13	-0.12	-0.11
	0.413	-0.11	-0.11	-0.11	-0.10	-0.10	-0.10	-0.10	-0.08	-0.08
	0.538	-0.12	-0.12	-0.11	-0.09	-0.09	-0.09	-0.08	-0.07	-0.07
	0.676	-0.13	-0.13	-0.12	-0.08	-0.08	-0.08	-0.08	-0.08	-0.07
	0.813	-0.12	-0.12	-0.10	-0.08	-0.07	-0.07	-0.07	-0.07	-0.07
	0.914	-0.10	-0.08	-0.07	-0.05	-0.04	-0.03	-0.03	-0.03	-0.03
Lower surface	0.010	0.05	0.05	0.05	0.05	0.05	0.05	0.03	0.00	-0.03
	0.051	0.00	0.00	-0.01	0.00	-0.02	-0.03	-0.07	-0.08	-0.10
	0.102	-0.01	-0.01	-0.02	-0.02	-0.03	-0.04	-0.07	-0.08	-0.10
	0.152	-0.01	-0.01	-0.02	-0.02	-0.03	-0.04	-0.06	-0.07	-0.09
	0.274	-0.02	-0.02	-0.02	-0.02	-0.03	-0.03	-0.05	-0.06	-0.08
	0.396	-0.04	-0.04	-0.04	-0.04	-0.05	-0.05	-0.06	-0.07	-0.08
	0.518	-0.05	-0.05	-0.05	-0.04	-0.05	-0.05	-0.05	-0.06	-0.07
	0.640	-0.05	-0.05	-0.05	-0.03	-0.04	-0.05	-0.05	-0.05	-0.05
	0.762	-0.05	-0.05	-0.05	-0.03	-0.03	-0.04	-0.05	-0.05	-0.05
	0.864	-0.08	-0.08	-0.07	-0.07	-0.07	-0.07	-0.07	-0.07	-0.07

Table A.4 rough Surface (Mo.3) Data(pressure) at Re=1.39×10^5

	x/c	Pt a=16	Pt a=14	Pt a=12	Pt a=10	Pt a=8	Pt a=6	Pt a=4	Pt a=2	Pt a=0
Upper surface	0.005	-0.16	-0.18	-0.20	-0.29	-0.26	-0.21	-0.15	-0.10	-0.05
	0.025	-0.17	-0.17	-0.20	-0.31	-0.28	-0.25	-0.20	-0.17	-0.13
	0.076	-0.18	-0.18	-0.21	-0.33	-0.30	-0.26	-0.21	-0.18	-0.16
	0.127	-0.18	-0.18	-0.19	-0.29	-0.29	-0.27	-0.21	-0.18	-0.14
	0.253	-0.17	-0.17	-0.18	-0.18	-0.18	-0.17	-0.17	-0.16	-0.15
	0.413	-0.16	-0.16	-0.16	-0.15	-0.15	-0.15	-0.13	-0.13	-0.13
	0.538	-0.15	-0.15	-0.16	-0.14	-0.14	-0.14	-0.13	-0.12	-0.12
	0.676	-0.17	-0.17	-0.16	-0.12	-0.12	-0.12	-0.12	-0.12	-0.12
	0.813	-0.15	-0.15	-0.13	-0.11	-0.10	-0.10	-0.10	-0.10	-0.10
	0.914	-0.13	-0.13	-0.12	-0.08	-0.08	-0.08	-0.08	-0.08	-0.08
Lower surface	0.010	0.01	0.01	0.00	0.00	0.00	0.00	-0.02	-0.05	-0.09
	0.051	-0.04	-0.05	-0.05	-0.05	-0.06	-0.07	-0.10	-0.13	-0.15
	0.102	-0.06	-0.07	-0.07	-0.07	-0.07	-0.08	-0.11	-0.13	-0.15
	0.152	-0.06	-0.07	-0.07	-0.07	-0.07	-0.08	-0.11	-0.12	-0.14
	0.274	-0.07	-0.08	-0.08	-0.07	-0.08	-0.09	-0.10	-0.11	-0.13
	0.396	-0.08	-0.08	-0.08	-0.08	-0.08	-0.10	-0.10	-0.11	-0.12
	0.518	-0.08	-0.08	-0.08	-0.08	-0.08	-0.09	-0.10	-0.10	-0.11
	0.640	-0.10	-0.10	-0.10	-0.10	-0.10	-0.10	-0.11	-0.11	-0.11
	0.762	-0.10	-0.10	-0.10	-0.10	-0.10	-0.10	-0.10	-0.11	-0.11
	0.864	-0.12	-0.11	-0.11	-0.10	-0.10	-0.10	-0.10	-0.11	-0.11

Table A.5 rough Surface (Mo.4) Data(pressure) at Re=1.39×10^5

	x/c	Pt a=16	Pt a=14	Pt a=12	Pt a=10	Pt a=8	Pt a=6	Pt a=4	Pt a=2	Pt a=0
Upper surface	0.005	-0.13	-0.15	-0.34	-0.31	-0.26	-0.20	-0.12	-0.07	-0.02
	0.025	-0.12	-0.14	-0.34	-0.31	-0.27	-0.22	-0.16	-0.12	-0.07
	0.076	-0.15	-0.16	-0.33	-0.30	-0.26	-0.24	-0.20	-0.16	-0.13
	0.127	-0.13	-0.14	-0.19	-0.19	-0.18	-0.16	-0.14	-0.13	-0.11
	0.253	-0.13	-0.14	-0.15	-0.15	-0.15	-0.14	-0.13	-0.12	-0.10
	0.413	-0.11	-0.13	-0.11	-0.11	-0.11	-0.11	-0.10	-0.10	-0.08
	0.538	-0.12	-0.12	-0.09	-0.09	-0.09	-0.09	-0.09	-0.08	-0.07
	0.676	-0.13	-0.13	-0.10	-0.10	-0.10	-0.10	-0.09	-0.08	-0.08
	0.813	-0.12	-0.12	-0.08	-0.08	-0.08	-0.08	-0.08	-0.08	-0.08
	0.914	-0.10	-0.10	-0.05	-0.05	-0.05	-0.05	-0.05	-0.05	-0.05
Lower surface	0.010	0.05	0.05	0.05	0.05	0.05	0.05	0.03	0.01	-0.02
	0.051	-0.02	-0.02	0.00	-0.01	-0.02	-0.03	-0.07	-0.08	-0.11
	0.102	-0.02	-0.02	-0.01	-0.02	-0.03	-0.04	-0.07	-0.08	-0.11
	0.152	-0.02	-0.02	-0.01	-0.02	-0.03	-0.04	-0.06	-0.07	-0.10
	0.274	-0.03	-0.03	-0.02	-0.02	-0.03	-0.05	-0.05	-0.07	-0.08
	0.396	-0.04	-0.04	-0.04	-0.04	-0.05	-0.05	-0.06	-0.07	-0.08
	0.518	-0.04	-0.04	-0.04	-0.04	-0.04	-0.04	-0.05	-0.06	-0.07
	0.640	-0.05	-0.05	-0.05	-0.05	-0.05	-0.05	-0.05	-0.06	-0.07
	0.762	-0.07	-0.07	-0.05	-0.05	-0.05	-0.06	-0.06	-0.07	-0.07
	0.864	-0.10	-0.10	-0.07	-0.07	-0.07	-0.07	-0.08	-0.08	-0.08

Table A.6 rough Surface (Mo.5) Data(pressure) at Re=1.39×10^5

	x/c	Pt a=16	Pt a=14	Pt a=12	Pt a=10	Pt a=8	Pt a=6	Pt a=4	Pt a=2	Pt a=0
Upper surface	0.005	-0.11	-0.16	-0.39	-0.35	-0.28	-0.20	-0.11	-0.07	0.00
	0.025	-0.10	-0.14	-0.35	-0.31	-0.26	-0.20	-0.15	-0.10	-0.07
	0.076	-0.15	-0.16	-0.31	-0.30	-0.28	-0.25	-0.20	-0.16	-0.13
	0.127	-0.13	-0.14	-0.19	-0.19	-0.18	-0.16	-0.14	-0.12	-0.10
	0.253	-0.13	-0.14	-0.17	-0.16	-0.15	-0.14	-0.13	-0.12	-0.10
	0.413	-0.11	-0.13	-0.11	-0.11	-0.11	-0.10	-0.10	-0.10	-0.08
	0.538	-0.12	-0.12	-0.10	-0.10	-0.10	-0.09	-0.09	-0.08	-0.07
	0.676	-0.13	-0.13	-0.09	-0.09	-0.09	-0.08	-0.08	-0.08	-0.08
	0.813	-0.12	-0.12	-0.08	-0.07	-0.07	-0.07	-0.07	-0.07	-0.07
	0.914	-0.10	-0.08	-0.05	-0.05	-0.05	-0.05	-0.04	-0.04	-0.03
Lower surface	0.010	0.06	0.06	0.05	0.06	0.06	0.05	0.03	0.01	-0.02
	0.051	0.00	0.00	0.00	0.00	-0.02	-0.03	-0.06	-0.08	-0.10
	0.102	0.00	0.00	0.00	0.00	-0.02	-0.03	-0.05	-0.07	-0.09
	0.152	0.00	0.00	0.00	0.00	-0.02	-0.03	-0.05	-0.07	-0.08
	0.274	-0.02	-0.02	-0.02	-0.02	-0.03	-0.03	-0.05	-0.05	-0.07
	0.396	-0.04	-0.04	-0.03	-0.03	-0.04	-0.04	-0.06	-0.06	-0.07
	0.518	-0.04	-0.04	-0.03	-0.03	-0.03	-0.04	-0.04	-0.05	-0.05
	0.640	-0.05	-0.05	-0.03	-0.03	-0.03	-0.05	-0.05	-0.05	-0.05
	0.762	-0.06	-0.05	-0.03	-0.03	-0.03	-0.04	-0.05	-0.05	-0.05
	0.864	-0.08	-0.08	-0.07	-0.07	-0.07	-0.07	-0.07	-0.07	-0.07

Table A.7 rough Surface (Mo.6) Data(pressure) at Re=1.39×10^5

	x/c	Pt a=16	Pt a=14	Pt a=12	Pt a=10	Pt a=8	Pt a=6	Pt a=4	Pt a=2	Pt a=0
Upper surface	0.005	-0.12	-0.15	-0.43	-0.41	-0.33	-0.21	-0.15	-0.07	0.00
	0.025	-0.10	-0.12	-0.36	-0.32	-0.27	-0.20	-0.17	-0.10	-0.07
	0.076	-0.15	-0.16	-0.26	-0.25	-0.26	-0.21	-0.18	-0.15	-0.11
	0.127	-0.12	-0.13	-0.19	-0.19	-0.18	-0.16	-0.14	-0.12	-0.10
	0.253	-0.13	-0.13	-0.15	-0.16	-0.15	-0.13	-0.13	-0.12	-0.10
	0.413	-0.11	-0.12	-0.11	-0.11	-0.11	-0.10	-0.10	-0.09	-0.08
	0.538	-0.12	-0.12	-0.09	-0.09	-0.09	-0.09	-0.08	-0.07	-0.07
	0.676	-0.13	-0.12	-0.08	-0.08	-0.09	-0.08	-0.08	-0.08	-0.07
	0.813	-0.12	-0.12	-0.08	-0.07	-0.08	-0.07	-0.07	-0.07	-0.07
	0.914	-0.10	-0.08	-0.05	-0.05	-0.05	-0.05	-0.05	-0.05	-0.05
Lower surface	0.010	0.06	0.06	0.05	0.06	0.06	0.06	0.05	0.01	-0.02
	0.051	0.00	0.00	0.00	0.00	-0.02	-0.03	-0.05	-0.07	-0.10
	0.102	0.00	0.00	0.00	0.00	-0.02	-0.03	-0.05	-0.07	-0.09
	0.152	-0.01	-0.02	0.00	0.00	-0.02	-0.03	-0.05	-0.07	-0.09
	0.274	-0.02	-0.02	-0.01	-0.02	-0.02	-0.03	-0.05	-0.06	-0.08
	0.396	-0.04	-0.04	-0.03	-0.03	-0.04	-0.05	-0.06	-0.07	-0.08
	0.518	-0.02	-0.03	-0.03	-0.02	-0.02	-0.03	-0.04	-0.04	-0.05
	0.640	-0.05	-0.05	-0.03	-0.03	-0.03	-0.04	-0.05	-0.05	-0.05
	0.762	-0.06	-0.05	-0.03	-0.03	-0.03	-0.04	-0.05	-0.05	-0.05
	0.864	-0.09	-0.08	-0.07	-0.07	-0.07	-0.07	-0.07	-0.07	-0.07

Table A.8 Experiment Data(velocity) at Re=1.39×10^5

Position y	Velocity m/s						
	smooth	**Mo.1**	**Mo.2**	**Mo.3**	**Mo.4**	**Mo.5**	**Mo.6**
0	10.93	5.84	7.73	8.26	8.46	8.57	8.76
10	14.31	7.15	10.12	10.53	11.68	11.68	13.70
20	14.60	10.53	13.06	13.70	14.31	14.43	14.43
30	14.66	13.70	14.43	14.43	14.60	14.60	14.84
40	14.66	14.54	14.60	14.78	14.89	14.84	14.89
50	14.78	14.60	14.60	14.89	14.89	14.89	14.89
60	14.84	14.60	14.89	14.89	14.89	14.89	14.89
70	14.89	14.84	14.89	14.89	14.89	14.89	14.89
80	14.89	14.84	14.89	14.89	14.89	14.89	14.89
90	14.89	14.89	14.89	14.89	14.89	14.89	14.89
100	14.89	14.89	14.89	14.89	14.89	14.89	14.89
105	14.89	14.89	14.89	14.89	14.89	14.89	14.89
110	14.89	14.89	14.89	14.89	14.89	14.89	14.89
115	14.89	14.89	14.89	14.89	14.89	14.89	14.89
120	14.89	14.89	14.89	14.89	14.89	14.89	14.89
125	14.89	14.89	14.89	14.89	14.89	14.89	14.89
130	14.89	14.89	14.89	14.89	14.89	14.89	14.89
135	14.89	14.89	14.89	14.89	14.89	14.89	14.89
140	14.60	14.60	14.60	14.60	14.60	14.60	14.60
145	11.68	11.68	11.68	11.68	11.68	11.68	11.68

Table A.9 Experiment Data(velocity) at Re=1.67×10^5

Position y	Velocity m/s						
	smooth	**Mo.1**	**Mo.2**	**Mo.3**	**Mo.4**	**Mo.5**	**Mo.6**
0	13.70	5.84	8.26	9.24	9.60	9.95	10.12
10	16.42	8.26	11.31	12.04	13.06	13.70	15.73
20	17.03	12.39	14.89	16.00	17.03	17.03	17.03
30	17.33	16.00	17.03	17.13	17.28	17.18	17.23
40	17.52	17.13	17.52	17.52	17.43	17.28	17.43
50	17.52	17.28	17.52	17.52	17.52	17.43	17.52
60	17.52	17.38	17.52	17.52	17.52	17.52	17.52
70	17.52	17.43	17.52	17.52	17.52	17.52	17.52
80	17.52	17.52	17.52	17.52	17.52	17.52	17.52
90	17.52	17.52	17.52	17.52	17.52	17.52	17.52
100	17.52	17.52	17.52	17.52	17.52	17.52	17.52
105	17.52	17.52	17.52	17.52	17.52	17.52	17.52
110	17.52	17.52	17.52	17.52	17.52	17.52	17.52
115	17.52	17.52	17.52	17.52	17.52	17.52	17.52
120	17.52	17.52	17.52	17.52	17.52	17.52	17.52
125	17.52	17.52	17.52	17.52	17.52	17.52	17.52
130	17.52	17.52	17.52	17.52	17.52	17.52	17.52
135	17.03	17.03	17.03	17.03	17.03	17.03	17.03
140	14.89	14.89	14.89	14.89	14.89	14.89	14.89
145	13.06	13.06	13.06	13.06	13.06	13.06	13.06

Table A.10 Experiment Data(velocity) at Re=1.86×10^5

Position y	Velocity m/s						
	smooth	Mo.1	Mo.2	Mo.3	Mo.4	Mo.5	Mo.6
0	14.89	5.84	8.26	8.86	9.24	9.69	10.53
10	18.47	8.26	12.39	13.06	14.31	14.60	17.52
20	19.59	13.70	17.03	18.47	18.93	19.42	19.46
30	19.72	18.00	19.37	19.81	19.37	19.81	19.81
40	19.81	19.37	19.81	20.02	19.59	19.81	19.81
50	19.81	19.72	19.72	20.15	19,72	20.02	19.94
60	20.02	19.81	19.81	20.24	19.81	19.94	20.02
70	20.24	19.90	19.81	20.24	20.24	20.24	20.24
80	20.24	20.02	19.81	20.24	20.24	20.24	20.24
90	20.24	20.24	20.24	20.24	20.24	20.24	20.24
100	20.24	20.24	20.24	20.24	20.24	20.24	20.24
105	20.24	20.24	20.24	20.24	20.24	20.24	20.24
110	20.24	20.24	20.24	20.24	20.24	20.24	20.24
115	20.24	20.24	20.24	20.24	20.24	20.24	20.24
120	20.24	20.24	20.24	20.24	20.24	20.24	20.24
125	20.24	20.24	20.24	20.24	20.24	20.24	20.24
130	19.37	19.37	19.37	19.37	19.37	19.37	19.37
135	18.47	18.47	18.47	18.47	18.47	18.47	18.47
140	15.45	15.45	15.45	15.45	15.45	15.45	15.45
145	8.26	8.26	8.26	8.26	8.26	8.26	8.26

APPENDIX B
WIND TUNNEL DATA

Table B.1 Technical data for wind tunnel

Item	Specification
Dimensions and weight	3700 mm long x 1900 mm high x 1065 mm depth Combined assembled weight 293 kg
Operating Environment	Altitude up to 2000 m Temperature range 5°C to 40°C Maximum relative humidity 80% for temperatures up to 31°C, decreasing linearly to 50% relative humidity at 40°C Overvoltage category 2 (as specified in EN61010-1). Pollution degree 2 (as specified in EN61010-1).
Working Section	305 mm x 305 mm x 600 mm
Nominal Air Velocity	0 to 36 $m.s^{-1}$
Fan Motor	AC Three-Phase Axial Variable Speed
Electrical Supply	
Type	Three-Phase AC
Voltage (depends on order)	415 V or 220 V
Supply Current	16 A (415 V)/20 A (220 V) 50 Hz to 60Hz
External connections	2 x 4 way IEC type sockets to back of Instrumentation Frame. Output value is the same as the supply phase to neutral value.
Circuit Protection	
Drive Unit	(415 V) Three phase 16 A MCB (Miniature Circuit Breakers) (220 V) Three phase 20 A MCB
IEC Outlets	10 A MCB
Low Voltage Instrumentation Supply	2 A MCB

Table B.2 wind tunnel reference data at v=20 m/s and 8 angle of incidence

	Tapping Number	Distance From Leading Edge x (mm)	x/c	Reading of manometer h_T (mm H_2O) or pressure display p_T (kPa)	Local Relative Static Head h_T-h_w (mm H_2O)	Local Relative Static Pressure p_T-p_w (kPa)	C_p
Upper Surface	START	0	0	0		0	0
	1	0.76	0.005	-1.18		-0.89	-3.43
	3	3.81	0.025	-0.76		-0.47	-1.81
	5	11.43	0.076	-0.77		-0.48	-1.85
	7	19.05	0.127	-0.65		-0.36	-1.39
	9	38.00	0.253	-0.53		-0.24	-0.92
	11	62.00	0.413	-0.45		-0.16	-0.62
	13	80.77	0.538	-0.40		-0.11	-0.42
	15	101.35	0.676	-0.37		-0.08	-0.31
	17	121.92	0.813	-0.33		-0.04	-0.15
	19	137.16	0.914	-0.29		0	0
	END	150	1.00	0			0
Lower Surface	START	0	0	0		0	0
	2	1.52	0.010	-0.03		0.26	1.001
	4	7.62	0.051	-0.09		0.2	0.77
	6	15.24	0.102	-0.16		0.13	0.501
	8	22.86	0.152	-0.19		0.1	0.385
	10	41.15	0.274	-0.24		0.05	0.193
	12	59.44	0.396	-0.22		0.07	0.27
	14	77.73	0.518	-0.27		0.02	0.077
	16	96.02	0.640	-0.27		0.02	0.077
	18	114.30	0.762	-0.27		0.02	0.077
	20	129.54	0.864	-0.29		0	0
	END	150	1.00	0			0

APPENDIX C
CALIBRATION

There is error percentage in most readings of the measuring devices. In this section, the error percentage for all devices has been determine as follow:

Pressure Measurement:

The error percentage in pressure readings of 32-Way Pressure Display units which result from the reading of pressure probe is taken by comparing the experiment reading with the reference reading of the model, figure (c-1) the test was done at wind tunnel air velocity (20.72 m/s) and angle of attack (8 degree). error percentage for mean pressure is estimated from calibration to be (±7 %).

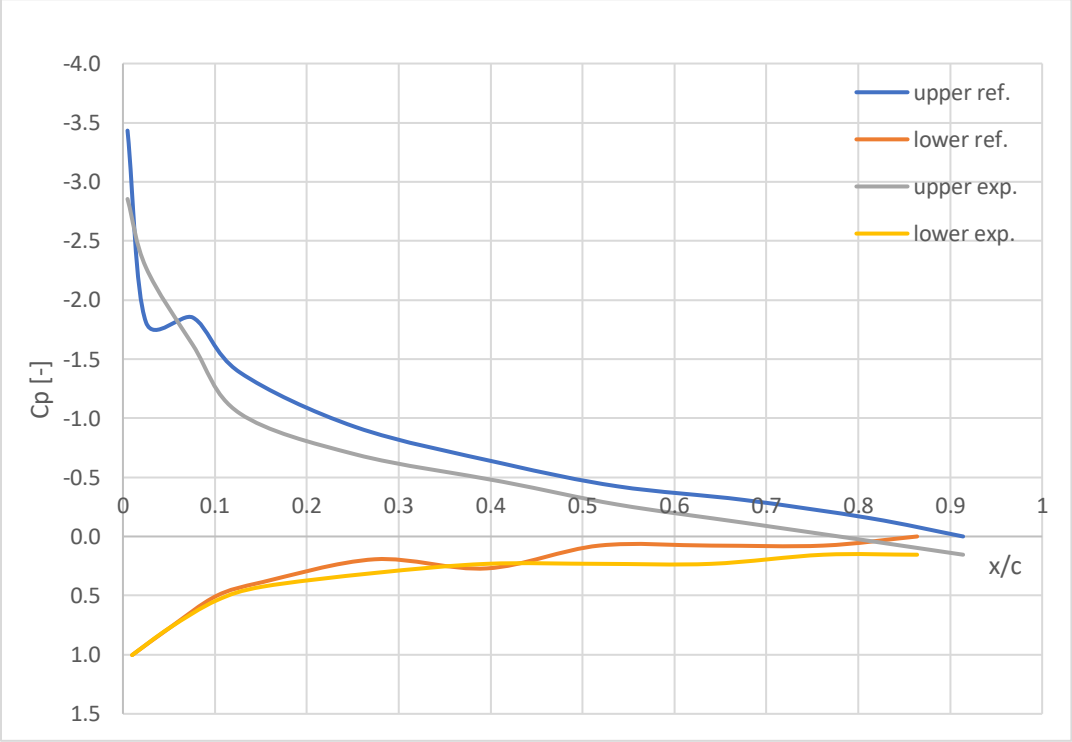

Figure (c-1) coefficient of pressure reference reading with experiment reading at angle of attack (8 degree) and air velocity (20.72 m/s)

الخلاصة

تتناول هذه الرسالة اجراء دراسة تجريبية مختبرية لتأثير استخدام اسطح ذات خشونة منتظمة على المواصفات الايروديناميكية لجسم هوائي.

الاختبارات اجريت في مختبر الايروديناميك في الكلية التقنية الهندسية النجف على نموذج جناح متناظر يحمل الرمز (NACA 0012). تم استخدام مشبك معدني صوفي ذو ابعاد مختلفة للحصول على الخشونة المطلوبة؛ حيث تم استخدام ستة نماذج من الصوف المعدني اشير اليها بالرموز (Mo.1, 2, 3, 4, 5, 6) و التي يقابلها (40, 60, 80, 100, 120, 200 فتحة في البوصة المربعة) على التوالي. النماذج اختبرت عند زوايا هجوم هوائية مختلفة (0°, 2°, 4°, 6°, 8°, 10°, 12°, 14°, and 16°) و لثلاث اعداد رينولد (1.39×10^5,1.67×10^5 and 1.86×10^5) . الضغط ، منحني متوسط السرعة، منحني معاملات الرفع و الكبح للشكل الهوائي تم رسمها من خلال النتائج.

التجارب العملية اجريت في نفق هوائي تحت صوتي من النوع المفتوح و مواصفات الجريان كانت عند رقم رنولد (1.39×10^5, 1.67×10^5 and 1.86×10^5). النتائج اظهرت بان شكل خشونة السطح هو احد مفاتيح التحكم بخصائص الجسم الهوائي. ان تقنية خشونة السطح قادرة على تعديل خصائص الجريان و بالتالي تحسين الخواص الهواء الدينامية . اكثر النماذج فعالية خلال التجارب كان النموذج رقم 6 و الذي يمثل سطح بخشونة 200 ثقب في البوصة المربعة مقارنة مع السطح الاملس. النتائج اظهرت زيادة في منحني الرفع تراوح بين 8-17% و نقصان في الكبح بمقدار 12-18% للجناح NACA0012 بالاعتماد على زوايا هجوم هوائية بين (0° to 16°).

دراسة تحقيقية عملية لتوزيع الضغط على سطح جنيح طائرة نوع NACA 0012

رسالة مقدمة الى
قسم هندسة تقنيات ميكانيك القوى
كجزء من متطلبات نيل درجة ماجستير تقني في هندسة الحراريات

تقدم بها

يوسف فايز يوسف

إشراف

أ.م.د. زيد معن حسن

أ.م.د. محمد عبد الرضا حسين

اكتوبر / 2021